Progress in Materials Science 94 (2018) 114–173

Contents lists available at ScienceDirect

Progress in Materials Science

journal homepage: www.elsevier.com/locate/pmatsci

Mechanical metamaterials associated with stiffness, rigidity and compressibility: A brief review

Xianglong Yu [a,b], Ji Zhou [a,*], Haiyi Liang [b], Zhengyi Jiang [c], Lingling Wu [a]

[a] State Key Laboratory of New Ceramics and Fine Processing, School of Materials Science and Engineering, Tsinghua University, Beijing 100084, China
[b] CAS Key Laboratory of Mechanical Behavior and Design of Materials, University of Science and Technology of China, Hefei 230026, Anhui, China
[c] School of Mechanical, Materials and Mechatronic Engineering, University of Wollongong, Wollongong, NSW 2522, Australia

ARTICLE INFO

Article history:
Received 10 November 2015
Received in revised form 3 December 2017
Accepted 20 December 2017
Available online 21 December 2017

Keywords:
Mechanical metamaterials
Microlattice
Tunable stiffness
Negative compressibility
Metafluid
Negative Poisson's ratio

ABSTRACT

Mechanical metamaterials are man-made structures with counterintuitive mechanical properties that originate in the geometry of their unit cell instead of the properties of each component. The typical mechanical metamaterials are generally associated with the four elastic constants, the Young's modulus E, shear modulus G, bulk modulus K and Poisson's ratio υ, the former three of which correspond to the stiffness, rigidity, and compressibility of a material from an engineering point of view. Here we review the important advancements in structural topology optimisation of the underlying design principles, coupled with experimental fabrication, thereby to obtain various counterintuitive mechanical properties. Further, a clear classification of mechanical metamaterials have been established based on the fundamental material mechanics. Consequently, mechanical metamaterials can be divide into strong-lightweight (E/ρ), pattern transformation with tunable stiffness, negative compressibility ($-4G/3 < K < 0$), Pentamode metamaterials ($G \ll K$) and auxetic metamaterials ($G \gg K$), simultaneously using topology optimisation to share various fancy but feasible mechanical properties, ultralight, ultra-stiffness, well-controllable stiffness, vanishing shear modulus, negative compressibility and negative Poisson's ratio. We provide here a broad overview of significant potential mechanical metamaterials together with the upcoming challenges in the intriguing and promising research field.

Contents

1. Introduction . . . 116
2. Historical perspectives of metamaterials . . . 117
3. Fundamentals of stiffness, rigidity and compressibility . . . 118
4. Basic classification of mechanical metamaterials . . . 120
5. Structural design and properties of mechanical metamaterials associated with stiffness . . . 122
   5.1. Mechanical metamaterials associated with strength and lightweight (E/ρ) . . . 122
      5.1.1. Micro-/nanolattices metamaterials . . . 123
      5.1.2. Chiral, anti-chiral, and hierarchical metamaterials . . . 129
      5.1.3. Origami-inspired metamaterials . . . 131
      5.1.4. Cellular origami metamaterials . . . 137
      5.1.5. Pattern transformation: controllable stiffness . . . 138

* Corresponding author.
E-mail address: zhouji@tsinghua.edu.cn (J. Zhou).

https://doi.org/10.1016/j.pmatsci.2017.12.003
0079-6425/

Nomenclature

Acronyms

2D	two-dimensional
3D	three-dimensional
AM	additive manufacturing
BCC	body-centred cubic
CDC	complex diamond cubic
DMLS	direct metal laser sintering
EBM	electron beam melting
FCC	face-centred cubic
MOFs	metal–organic frameworks
NAC	negative area compressibility
NLC	negative linear compressibility
NPR	negative Poisson's ratio
NTE	negative thermal expansion
SLA	stereolithography
SLM	selective laser melting
SLS	selective laser sintering
SEM	scanning electron microscope
XRD	X-ray diffraction

Symbols

A	constant parameter
a	gap of adjoining hexagonal faces
b_1, b_2	change in the interlock gap perpendicular to the adjoining hexagonal faces
c	heat capacity
c_m	specific heat after phase change
C	specific heat
a, b, c, d	ordering of sector angles in single origami four-vertex geometry
E	Young's modulus
G	Gibbs free energy
G	shear modulus
H	length of the vertical struts
h	Planck's constant
K	bulk modulus
k	spring constant
k_h	spring constant of connected stiffness in an interlocking structure
L	length of the oblique struts
l	the edge lengths of each hexagon in an interlocking structure
n	power index
N	Avogadro's number
p	hydrostatic pressure
P	pressure
R_i	rod diameter of the crossing rod
R_o	rod diameter of FCC unit
S_{ij}, s_{ij}, s_{ijkl}	elastic compliances
S	buckling strength
T	temperature
t	the strut thickness
v, V	specific volume, volume
α	linear thermal expansion coefficient; the angle between two edges
β	volume thermal expansion coefficient
γ, γ_j	shear strain, components of Gruneisen function
ε	unit elongation
θ	re-entrant angle
υ	Poisson's ratio
ρ	mass density, folding angles or radius of a curve
ρ_s	relative materials density
σ	normal stress

σ_y	yield strength
σ_{ys}	relative yield strength
τ	shear stress

5.2. Design principles behind structures . . . 141
5.2.1. Maxwell's criterion and material mechanics . . . 142
5.2.2. Topological optimisation . . . 142
5.2.3. Folding features . . . 143
5.2.4. Geometrical frustration and elastic instability . . . 144
5.3. Enhanced mechanical properties . . . 146
5.3.1. Ultra-stiffness and low density . . . 146
5.3.2. Tunable stiffness . . . 146
5.3.3. Failure mode . . . 147
6. Structure and properties of mechanical metamaterials associated with shear/bulk moduli . . . 148
6.1. Mathematical classification . . . 148
6.2. Vanishing shear modulus ($G \ll K$) . . . 148
6.2.1. Pentamode structural design . . . 148
6.2.2. Kagome lattice . . . 150
6.3. Negative compressibility ($-4G/3<K<0$) . . . 152
6.3.1. Negative linear compressibility . . . 152
6.3.2. Negative area compressibility . . . 153
6.3.3. Negative thermal expansion metamaterials . . . 154
6.3.4. Recently proposed mechanisms behind negative compressibility . . . 155
7. Recent advances in mechanical metamaterials associated with Poisson's ratio . . . 156
7.1. Classification of cubic auxetic metamaterials . . . 156
7.2. Zero or negative Poisson's ratio ($G \gg K$) . . . 158
7.3. Negative/positive programmable Poisson's ratio . . . 158
8. Research translation and potential applications . . . 160
8.1. Established fabrication techniques . . . 160
8.1.1. Additive manufacturing . . . 160
8.1.2. Interlocking assembly . . . 160
8.1.3. Melt-electrospinning techniques . . . 161
8.2. Research translation . . . 161
8.3. Potential applications . . . 162
9. Conclusions and future directions . . . 164
9.1. Implications of metal-organic frameworks . . . 164
9.2. Structural optimisation . . . 164
Acknowledgements . . . 166
References . . . 166

1. Introduction

Metamaterials are not materials in the usual sense. They are products of human ingenuity, not observable in nature. These manmade materials enable us to design our own atoms-like units [1,2], and thereby create materials with unprecedented effective properties [3–5]. These unusual material properties are derived from their microstructural geometry, rather than from their material composition. A mechanical metamaterial or structural metamaterial refers to a sort of metamaterial with a unique mechanical property based on its structure. An ongoing challenge for modern materials science is to create these artificial structures with an unconventional response, programmed by a suitable geometrical or topological design. The fabrication and testing of rationally designed metamaterial microstructures in three dimensions is just emerging.

The influential concept of metamaterials originates in a paper by Bose [6], where a manmade twisted structure was subjected to the polarisation of an electromagnetic wave [7–9]. Experimental research in metamaterials first emerged in optics [3–5,10,11] but progressed soon after to acoustics and mechanics [12,13]. Optical metamaterials are artificially structured materials with nanoscale inclusions and unconventional properties observed for optical frequencies [10,14]. There are also opportunities in other fields such as thermodynamics and mechanics [15–17]. Acoustic metamaterials, showing vanishing shear [18], can in essence be classified as an individual series of metafluid mechanical metamaterials [19]. Specific metamaterials for imperceptibility cloaks can also be considered metafluids, i.e., pentamode metamaterials [20]. Initially, rationally designed mechanical metamaterials were developed to control wave propagation in acoustic media [21,22], thin elastic sheets, curved shells [23] and harness elastic instabilities to generate auxetic behaviour [24–27].

With this in mind, these newly developed mechanical metamaterials [16,17] have a variety of counterintuitive mechanical properties, and thereby they are not limited just to switching between two pattern states as before. These mechanical metamaterials can therefore be considered a counterpart to the well-known family of optical or acoustics metamaterial. So far they include auxetic (negative Poisson's ratio) metamaterials [28–32], metamaterials with vanishing shear modulus, such as pentamode structures [20,33,34], metamaterials with negative compressibility [35–37], singularly nonlinear materials [38,39], and topological metamaterials [40–42]. Fabrication of an ultra-strong glassy carbon nanolattice with a strut diameter of around 200 nm could lead to the realisation of advanced nanoscale-structured materials [16,43]. These explorations are concurrently making mechanical metamaterials much smaller and stronger. Understanding and identifying the key features of mechanical metamaterials is a precondition to their realisation. It is necessary to elucidate feasible blueprints for three-dimensional microstructures to achieve specific counterintuitive mechanical properties. A clear classification based on the mechanics for various emerging mechanical metamaterials needs to be established before we progress in this research field.

One word has been defined to describe the difference between composites and mechanical metamaterials. In contrast to conventional composite engineering, wherein methods generally rely on designing a response based on the interaction between the constituent parts composing the material, structural features in metamaterial design inject novelty at much larger than the atomic level. Most meta-atoms for optical metamaterials have dimensions of at least 50 nm. Acoustic meta-atoms are even larger, as acoustic wavelengths are larger than optical wavelengths. But the emerging mechanical metamaterials beyond wavelengths are expected into the atomic level. Some types provide novel functionality, such as complicated bistability, tunable stiffness, vanishing shear modulus, negative compressibility, negative thermal expansion, and auxetic behaviour. Therefore, metamaterials are a type of composite, but the difference is that they can achieve at least one abnormal property not observed in nature, due to the topographical optimisation rather than the composition of materials themselves. Just as in optical and acoustic metamaterials [2,44–46], the corresponding structural design and fabrication in mechanical metamaterials [47–49] are prompted by many of same factors as in any other field: new and puzzling observations, new techniques and new theories. Progress here would greatly enhance the possibilities.

The main purpose of this review is to make a clearly classify mechanical metamaterials, according to essential material mechanics, i.e., the relationships between three elastic moduli and the Poisson's ratio. We will also provide a critical review of the developments at the frontier of mechanical metamaterials, ranging from structural topological optimisation, design principles and fabrication, and various enhanced mechanical properties. Anyone who attempts to write an overview of the development from natural materials to mechanical metamaterials is bound to be heavily indebted to the work of others. In such a brief review their contributions will inevitably be compressed to the main points. This paper is intended for readers who seek a concise outline of mechanical metamaterials and the related terminology.

This review contains, apart from this introductory section, a historical perspective of metamaterials (Section 2), theoretical fundamentals (Section 3), basic classifications (Section 4), three separate critical assessments of the corresponding group sets (Sections 5–7), the potential applications (Section 8), and conclusions with future directions (Section 9). Section 2 provides a historical analysis encompassing more than mechanical metamaterials, including optical, acoustic and thermal metamaterials, as well as the five general dominant trends in these smart metamaterials. Section 3 discusses some general theoretical considerations, in particular the relevant basic concepts and equations. Section 4 establishes three group of mechanical metamaterials according to the Milton map (i.e., correlation between shear modulus and bulk modulus) and the materials density. Section 5 considers the first group set: mechanical metamaterials associated with stiffness. These strong and lightweight metamaterials (a scaling relationship between Young's modulus E and density ρ, E/ρ) may consist of micro-/nanolattices, chiral/anti-chiral hierarchical metamaterials, origami-inspired metamaterials, cellular origami metamaterials, and the last one for that the pattern can yield tunable stiffness. The second group set, mechanical metamaterials associated with shear/bulk moduli, G, K, will be introduced in Section 6. This group includes vanishing shear modulus ($G \ll K$), and negative compressibility ($-4G/3 < K < 0$). The third group set is presented in Section 7, and concerns auxetic metamaterials with negative Poisson's ratio ($G \gg K$). Fabrication techniques and application conditions for mechanical metamaterials will be addressed in Section 8. General dominant trends in the design of mechanical metamaterials have been highlighted in Section 9, as well as some implications for metal-organic frameworks (MOFs). Our systematic analysis aims to draw a clear overview of the current challenges for the science and technology associated with mechanical metamaterials. We answer many fundamental questions, while raising largely unaddressed questions. For instance, what are the design principles behind these structured metamaterials and what are some achievable counterintuitive mechanical properties?

2. Historical perspectives of metamaterials

This section gives a broad historical perspective in optical, acoustic and thermal metamaterials, and their corresponding structural design. The aims are to explore the rationale behind the theory, to summarise trends to target the role of mechanical metamaterials in various types of metamaterials, and finally to state the gaps in this research field. It is important to state the difference between metamaterials and photonic crystals [50]. The period and the size of a unit cell in photonic crystals are comparable to the wavelength of light, whereas the size of the meta-atom is much smaller than the wavelength of light. More importantly, photonic crystals scatter light, whereas metamaterials bend light due to the electromagnetic field generated by the material. Thus, metamaterials can be considered as effective media, whereas photonic crystals are not [46]. Photonic crystals are a special case of metamaterials indeed, which is not included in this review.

Optical and acoustic metamaterials have developed rapidly. The emergence of homogenised acoustic metamaterials [50,51] with a negative modulus analogous to negative permittivity has opened the field of mechanical metamaterials. Recently smart metamaterials have emerged in this field. These metamaterials intelligently respond to changes in the external environments, while simultaneously responding to thermal and mechanical stimuli. The classification of a smart metamaterial is similar in all types of optical, acoustic, mechanical, and thermal metamaterials. In addition to the four types of metamaterial, a special case is coupled smart metamaterials which are tailored for their application.

Five fundamental research fields can be proposed for these smart metamaterials. (i) Research on coupled mechanisms in the field of multi-physics: The classical direction of optical metamaterials may be combined with other physical fields to create a smart metamaterial, including acoustically, mechanically and thermally dynamic responses. (ii) Design of a unit cell on the atomic/molecular level: When fabricating a novel metamaterial of micro/nanometre size, the size effects of these metamaterials must be considered. Additionally, the failure modes of the material as a unit cell also play a significant role in the structural design of various metamaterials. (iii) Coupling with natural materials: After nearly one decade, the topological design of metamaterials needs to be retraced to optimise the structure using inspiration from nature materials. This seems but definitely not a biomimetic approach. We intend to find what properties natural materials do not have, and then to create these properties, such as tunable piezoelectric sensitivity [52]. Thus, a main challenge will be to couple natural materials in order to realise desired mechanical properties. (iv) Tuning of metamaterials: This research direction is suitable the existing smart metamaterials, to make a bridge between their fundamental exploration and their industrial application. (v) New product development in metamaterials sensing: The goal of this research direction is to develop new products via existing optical or acoustic metamaterials for industrial application. The focus is on manufacturing and the control of information in modern product technology. Two techniques in smart metamaterials can be modelled or numerically simulated using gene engineering and related fabrication techniques.

All types of smart metamaterials presented here are associated with optical, acoustic, mechanical, and thermal metamaterials. Each of them is a relatively broad field of research. Hence, the main purpose of this section is to provide common and general background, and present the terminology that will allow further development of the analytical tools. We provide the general directions of research for various potential smart metamaterials and the immediate challenges. Most of these can also be extended to the development of mechanical metamaterials. At this time mechanical metamaterials is a new, emerging field.

3. Fundamentals of stiffness, rigidity and compressibility

This section is devoted to the fundamental issues of anisotropic elasticity that should be defined and summarised before specific problems are confronted. Some simple constitutive laws are also considered corresponding to material behaviour in the range of relatively low strains under approximately isothermal conditions. Definitions are established to relate to the elastic constants that theoretically underpin the design principles of various mechanical metamaterial structures. The notation introduced here is well-established in engineering [53], i.e., the third case in Fig. 1a [54], whereas the notation for the other can be found in many well-known textbooks [55–57]. The operational definitions of E, B, G, and υ for isotropic media also apply to single crystals, which is the second case in Fig. 1a. If these measurements are applied to a single crystal, the results depend on the test axis of the crystal (hkl). The elastic constants so obtained are designated E_{hkl}, G_{hkl}, and υ_{hkl}, and are related to the c_{ij} and s_{ij} by formulae found elsewhere [54]. Readers with sound knowledge in continuum mechanics [58,59] might want to skip these basics.

Typical mechanical metamaterials are closely correlated to four elastic constants: Young's modulus (E), shear modulus (G), bulk modulus (K) and Poisson's ratio (υ). The first three in the list measure the stiffness, the rigidity, and the compressibility of a structural material. The elastic constant for isotropic materials, Poisson's ratio, offers a fundamental metric by which to compare the structural performance of any real material, whether homogeneous or not, when strained elastically. The Poisson's ratio can be defined as the relative amount a given material contracts transversally when stretched axially. Some authors prefer to use the terms "technical", "practical", or "bulk" instead of "engineering", and "constants" instead of "coefficients" [54].

The elastic modulus and Poisson's ratio come from the Hooke's law. Consider an elemental elastic body with sides parallel to the coordinate axes (Fig. 1b [44]). For each pair of parallel sides of a cubic element, one symbol is needed to denote the normal component of stress, σ, and two other symbols to denote the two components of shearing stress, τ. In the case of normal stress, σ_{y}, the subscript y indicates that the stress is acting on a plane normal to the y-axis. Two subscript letters are used for shearing stress, for instance τ_{yx}. The first letter, y, indicates the direction normal to the plane under consideration. The second letter, x, indicates the direction of the component of stress. When discussing deformation of an elastic body, the components of strain are used, i.e., the increase in the length of the element, the units of elongation ε_{x}, ε_{y}, ε_{z}, and the distortion of the angle between the two elements, the unit shearing strain γ_{xy}, γ_{xz} and γ_{yz}. In general, Hooke's law refers to the linear relationship between the components of stress and the components of strain under a small deformation,

$$\varepsilon_x = \frac{\sigma_x}{E} \tag{1}$$

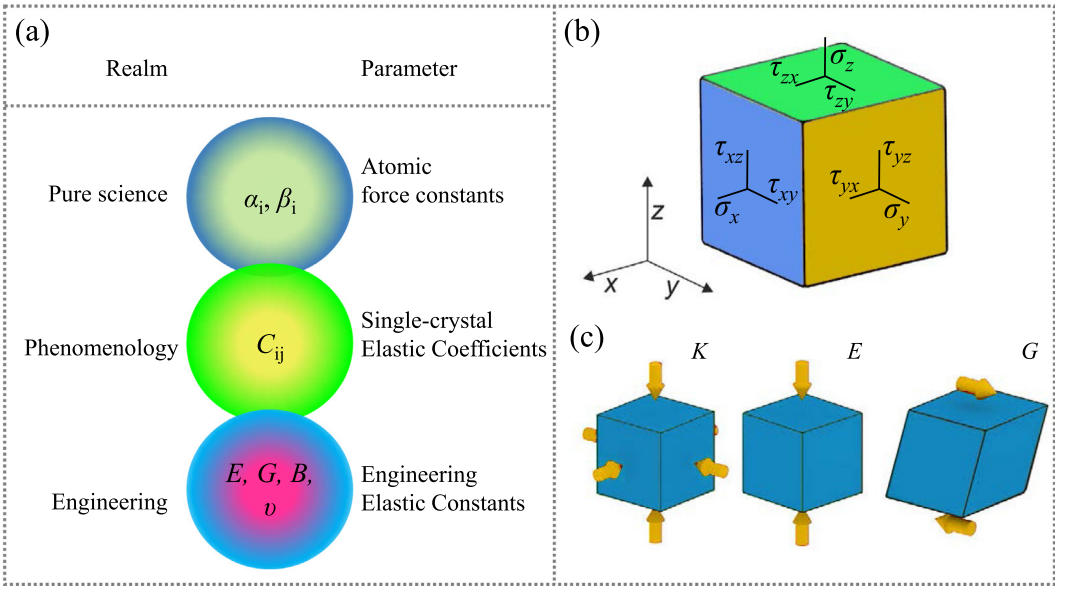

Fig. 1. (a) Schematic interconnectivity of elastic parameters of solids [54]. The α and β can be taken to represent extensions (or contractions) and bending of valence bonds between atoms in solids; subscript i denotes the various sets of atomic neighbours. The C_{ij} represent elastic stiffness coefficients that relate stresses to strains; both stress and strain are specified with respect to a set of axes denoted by indices i and j and usually chosen to coincide with crystallographic axes. E, G, B, and υ denote the Young's modulus, shear modulus, bulk modulus, and Poisson ratio, parameters arising naturally in characterising, respectively, uniaxial loading, shear loading, hydrostatic loading, and transverse strain under uniaxial loading. (b) Scheme of an elemental elastic body with sides parallel to the coordinate axes. The components of normal and shearing stress are indicated. (c) Schemes of experiments measuring the bulk modulus K (left), the Young's modulus E (middle) and the shear modulus G (right) [44].

where E is the modulus of elasticity, or Young's modulus (Fig. 1c). In other words, Young's modulus is defined as the ratio of uniaxial stress (tensile or compressive) to strain, measured along the same axis [54].

In most of the known elastic systems, the general stiffness refers to the ratio of the generalised force to the generalised displacement, such as the spring constant, k. The modulus is a continuum property independent of the geometry and size of the material. A three-dimensional solid viewed as a continuum in the context of elasticity theory, as in Eq. (1), experience stress as force per area and strain as displacement per length. An elastic object resists a given deformation by exerting a restoring force when pressed. A positive stiffness will occur when the deformation is in the same direction as the applied force, corresponding to a restoring force that returns the deformable body to its neutral position [60]. Any time we see the world as we are conditioned to see it, we see positive stiffness, but in metamaterials a negative stiffness is involved. Negative stiffness is possible in mechanical metamaterials, which assists the imposed deformation.

Huge variations in volume occur when different materials resist distortion under a mechanical load. Poisson's ratio can be introduced to compare the performance of materials strained elastically by locating the performance between narrow numerical bounds. In doing so, this extension of the element in the x-direction is normally accompanied by lateral strain components (contractions),

$$\varepsilon_y = -\upsilon\frac{\sigma_x}{E}, \quad \varepsilon_z = -\upsilon\frac{\sigma_x}{E} \tag{2}$$

where υ is a constant called the Poisson's ratio. Poisson's ratio is defined as the negative of the ratio of transverse strain to longitudinal strain in the case of uniaxial stress. Most solids contract laterally when stretched axially, i.e., $\varepsilon_y < 0$, $\varepsilon_z < 0$, compared to the positive σ_x. The Poisson's ratio is traditionally positive and generally ranges from 0.25 to 0.33 in conventional materials [61,62]. We will see that the numerical limits are changing rapidly as new experiments, computational methods and routes to materials synthesis emerge. We must thus change our understanding of the mechanical characteristics of modern materials.

When superposing the strain components produced by the three stresses, the relationship between elongation and stress is defined by two physical constants E and υ,

$$\begin{aligned}
\varepsilon_x &= \frac{1}{E}\left(\sigma_x - \upsilon(\sigma_y + \sigma_z)\right),\\
\varepsilon_y &= \frac{1}{E}\left(\sigma_y - \upsilon(\sigma_x + \sigma_z)\right),\\
\varepsilon_z &= \frac{1}{E}\left(\sigma_z - \upsilon(\sigma_x + \sigma_y)\right),
\end{aligned} \tag{3}$$

Similarly, the relationship between shearing strain, γ, and shearing stress, τ, can also be defined by the constants E and υ [53]. In the particular case of the pure shear condition, where $\sigma_z = \sigma,\ \sigma_y = -\sigma,\ \sigma_x = 0$, $\tau = \frac{1}{2}(\sigma_z - \sigma_y) = \sigma$, the relation is given by,

$$\gamma = \frac{2(1+v)\sigma}{E} = \frac{2(1+v)\tau}{E} \tag{4}$$

Often the notation,

$$G = \frac{E}{2(1+v)} \tag{5}$$

is used. Then Eq. (4) becomes $\gamma = \tau/G$. The constant G, defined by Eq. (5), is called the modulus of elasticity in shear, or the modulus of rigidity (Fig. 1c). The shear modulus and Young's modulus are therefore used for axial and torsional properties, respectively. In mechanical metamaterials, the shear modulus can approach zero compared to the bulk modulus, which is not the case for normal solid materials. This is similar to the behaviour of liquids which are difficult to compress but flow easily [34,63].

By adding Eqs. (3) together and using the following notation, we obtain the relationship between volume expansion $e = \varepsilon_x + \varepsilon_y + \varepsilon_z$ and the sum of normal stresses $\theta = \sigma_x + \sigma_y + \sigma_z$,

$$e = \frac{1-2v}{E}\theta \tag{6}$$

In the case of a uniform hydrostatic pressure of amount p, where $\sigma_z = \sigma_y = \sigma_x = -p$, then,

$$e = -\frac{3(1-2v)p}{E} \tag{7}$$

The quantity $E/3(1-2v)$ is called the modulus of volume expansion, i.e., the bulk modulus, K. As such, the compressibility of a solid, being the inverse of the bulk modulus [64], can be given by the derivatives [56], $K = -\frac{1}{V}\frac{dV}{dp}$, where V is volume. These elasticity constants are positive and definite. However, if we have just two materials, one sufficiently soft and the other sufficiently rigid, i.e., one with an extremely large elastic modulus and the other with an extremely small elastic modulus, it is possible to manufacture a family of sufficiently diverse microstructures to obtain the elastic properties that we desire [63].

To summarise, the important material properties, stiffness, rigidity, and compressibility, can be derived from four elastic constants, the Young's modulus, shear modulus, bulk modulus, and Poisson's ratio. The shear modulus, G, generally refers to a change in shape under constant volume. In ideal gases or liquids, $G = 0$. The bulk modulus, K, refers to the volume change of a cube, while maintaining shape. Extensive previous studies, described in the book referenced in [55], have proved that the Young's modulus, E, of a metal plate with holes is independent of the Poisson's ratio of the metal, particularly for hierarchically porous composite [29]. Two basic charts plot combinations of properties [65]: the modulus-density (E-ρ) chart, called the Ashby chart [44,66], and the bulk-shear modulus (K-G) map, the first quadrant of which is called the Milton map [29,44].

4. Basic classification of mechanical metamaterials

Mechanical metamaterials refer to a group of artificial structures with certain unusual mechanical properties, arising from the geometry of their subunits rather than the composition of the material. They belong within the family of metamaterials. The concept of a metamaterial has been extended from electromagnetics and acoustics to mechanics. Although composite structures are not entirely new to the field of mechanics, methods for the three-dimensional design of these engineered microstructures are just emerging, in particular with respect to anomalous macroscopic properties. Typically, these mechanical metamaterials carry a variety of significantly enhanced mechanical properties, such as zero or negative Poisson's ratios [26,28], vanishing shear modulus [20,33,34], negative stiffness [36], negative compressibility [37], singularly nonlinear behaviour [38,39], and customised topological microstructures [40–42], all of which distinguishes them from conventional natural materials. These qualities are expected to provide mechanical support and diverse protective functions in a variety of potential industrial, biomedical and bioengineering applications, such as tissue engineering scaffolds. Nevertheless, understanding and identifying the key features of these various mechanical metamaterials is a prerequisite to their realisation via the design principles and structural engineering. The following structural classification can describe the types mechanical metamaterial.

Fig. 2 provides a schematic diagram of the detailed classification of mechanical metamaterials. The order is established by following the basic elastic constants, because the various structures of mechanical metamaterials are often discussed in terms of their effective modulus and Poisson's ratio. Therefore, this section serves to survey micromechanical structures that seek to predict and explain various mechanical properties. Almost all mechanical metamaterials described here are related to the three elastic constants, i.e., the Young's modulus, shear modulus, bulk modulus, and a dimensionless parameter, Poisson's ratio. From an engineering point of view, the former three respectively correspond to three elastic material properties,

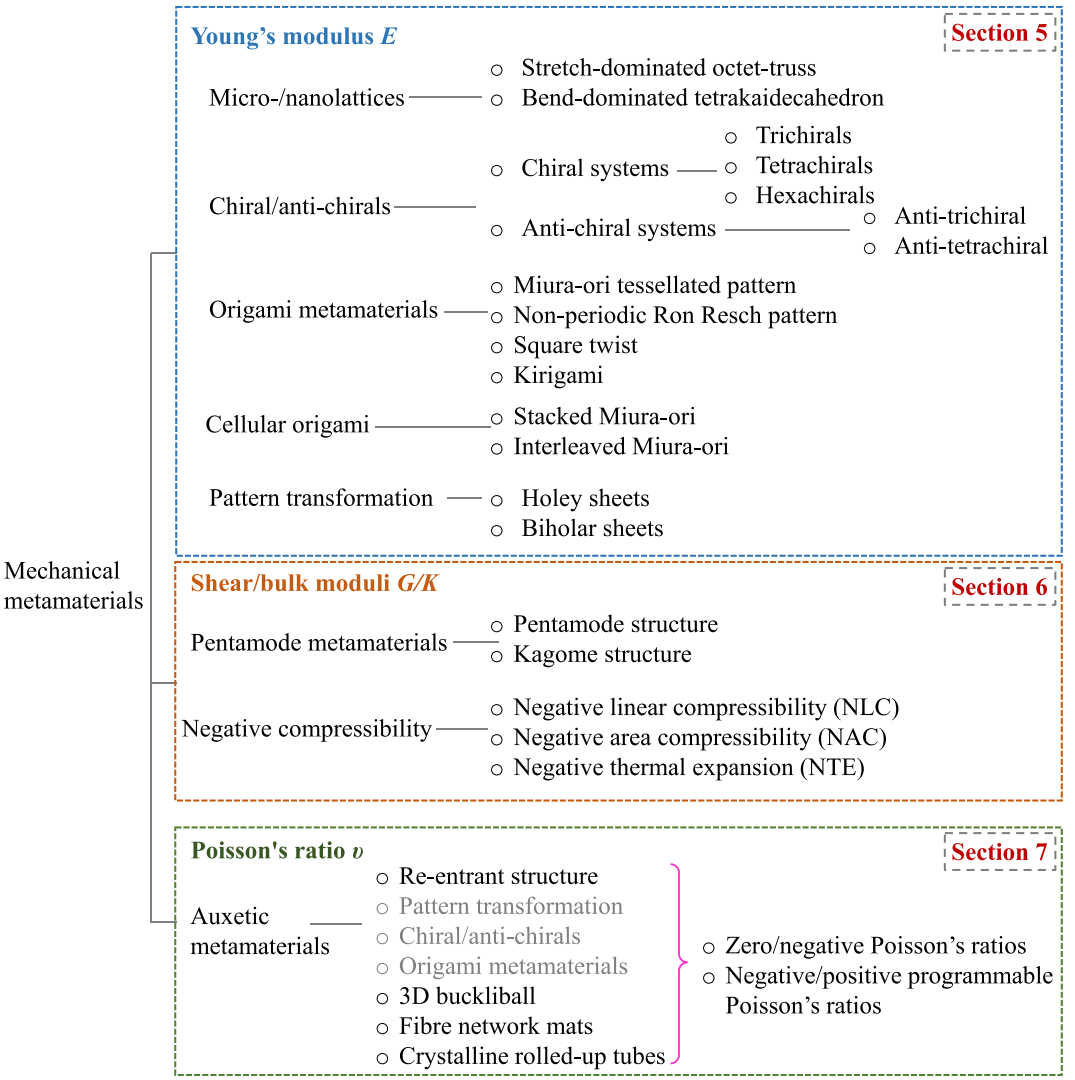

Fig. 2. Basic classification of mechanical metamaterials.

the stiffness, rigidity, and compressibility of a material. We hope to give a clear classification according to the fundamental mechanics of material structural design. Mechanical metamaterials can be divided into three general groups based on their elastic constants, rather than based on a composition of either metal alloys, ceramics, or polymers.

As shown in the study groups in Fig. 2, the types are all associated with a stiffness parameter, Young's modulus, E. One is strong and lightweight, such as micro-/nanocellular or the newly developed origami-inspired structures, represented by a scaling relationship between the Young's modulus and density ρ, E/ρ. Another is pattern transformation showing tunable stiffness E, for instance conventional holey sheets. Two accessible metamaterials, the Pentamode and kagome structures, are obtained when the elastic modulus appears as plotted on the K-axis of Fig. 3 [67,68], when the shear modulus G approaches zero compared to the bulk modulus K, $G \ll K$. Another condition from the middle group of Fig. 2 both is closely correlated to shear modulus G and bulk modulus K. The characteristic relationship regarding these elastic parameters can be presented in the K-G map, i.e., the Milton map shown in Fig. 3. The range of elastic moduli for materials with negative compressibility corresponds to the middle region of the lower right quadrant of the K-G map (Fig. 3), in which $G > 0$ and $-4G/3 < K < 0$. This region obeys the partially constrained boundary conditions of two subclasses of negative linear compressibility (NLC) and negative area compressibility (NAC). Only a few studies [37,69,70] focus on this sort of mechanical metamaterial by finding natural negative compressibility candidates [71–73]. Negative thermal expansion (NTE) is another approach that is expected to make the transition from theoretical fundamentals to potential engineering structures. The last type consists of auxetic metamaterials with zero or negative Poisson's ratios or with switchable negative/positive Poisson's ratios. These properties arise due to the structural design of mechanical metamaterials

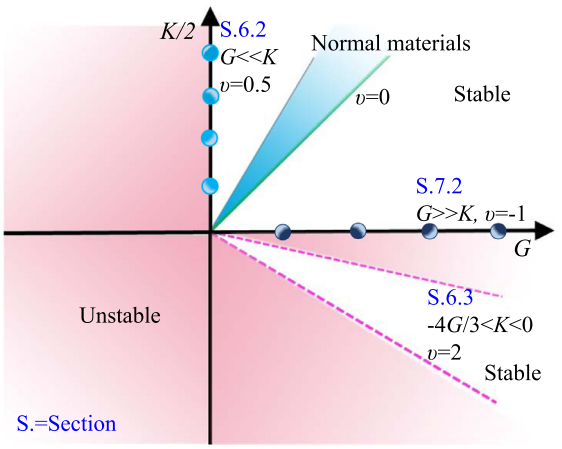

Fig. 3. The K-G map. Correlation of the bulk modulus K and shear modulus G with the Poisson's ratio and stability [67,68]. The three conditions, $G \ll K$, $-4G/3 < K < 0$, $G \gg K$, correspond to Sections 6.2,6.3 and 7.2 in this review, respectively.

5. Structural design and properties of mechanical metamaterials associated with stiffness

This section discusses mechanical metamaterials with exceptional combinations of mechanical properties (stiffness, strength, toughness, etc.) and low weight. From the structure-principle-property perspective, this section covers the development of various mechanical metamaterials, design principles behind these structures, and the corresponding enhancement of mechanical properties. First, various mechanical metamaterials are associated with strength and lightweight (E/ρ). We will introduce four main categories and one special case for the mechanical properties of tunable stiffness. These include micro-/nanolattices, chiral/anti-chiral hierarchical metamaterials, origami-inspired metamaterials, and cellular origami metamaterials. The special case is for pattern transformation. Second, the purpose of the second subsection aims to bring us some essential design principles behind various metamaterials. These involve Maxwell's criterion and material mechanics, topological optimisation, folding theory, geometrical frustration and elastic instability. Finally, part of the enhanced mechanical properties will be described, ultra-stiffness and lightweight, tunable stiffness, and the failure mode in corresponding mechanical metamaterials.

5.1. Mechanical metamaterials associated with strength and lightweight (E/ρ)

Here the subclass of these strong, lightweight mechanical metamaterials can be placed into four general categories based on their structure: micro-/nanolattices, chiral, anti-chiral, and hierarchical metamaterials, origami-inspired metamaterials, and cellular origami metamaterials. The last type in this subsection is pattern transformation, which demonstrates the mechanical property of tunable stiffness. A unit cell, or a primitive cell in classical physics, is the smallest structural unit where upon assembly in a tessellated solid, undeformed geometrical and loading patterns are recreated [74].

The reason for assembly is mainly two fold. First, these structures develop lightweight structures which are adequately stiff and strong, calculating the strength in the strength-to-density ratio, and the stiffness in Young's modulus-to-density. Secondly, we have to resort to crystallographic theory in natural materials for a good understanding of what we fabricated, particularly for various metallic or polymeric structures. An example of the first part of this subsection is the octet-truss lattice structure reported in Refs. [75,76], which have the characteristic stacking arrangements of a face-centred cubic (FCC) unit cell in cubic symmetry. Different lattice orientations can be represented by the Miller indices, where the lattice plane that forms a flat face is that to which the loading is applied. Furthermore, tunable directivity in metamaterials occurs within reconfigurable cell symmetry [77], which sounds like crystallographic orientation. Unlike classical hierarchical cellular structures, the newly developed origami-inspired mechanical metamaterials offer enhanced flexibility, deformability and compactness [78,79]. Their corresponding strengthening mechanism largely depends on crystallographic defects, such as vacancies, dislocations, and grain boundaries.

Another subclass in the third subsection here is pattern transformation associated with controllable stiffness. A holy sheet, which is a typical pattern transformation, can belong to a sort of periodic elastomeric cellular solid, but the difference is that the design concepts behind this structure are based on elastic material instabilities. Meanwhile, pattern transformation is also quite distinct from the conventional metamaterials with negative Poisson's ratio. This is mainly due to the stiffness that is constantly changing in the axial and normal direction under an external mechanical load, normally compression. The corresponding Poisson's ratios are thereby a variation of the duration of loading, whether negative, positive or both. This pattern switch has similarity to a phase transition from one microstructure to another. That is why we call this phenomenon a *pattern transformation* [26,80–82]. The pattern transformation event is nonlinear in nature, and thus relatively small changes in macroscopic strains can trigger a dramatic transformation in certain classes of simple periodic structures.

There is a relationship between origami and pattern transformation. They both share instability mechanics [25], particularly on the micro-/nanostructure level. Events causing buckling of a stiff film bound to a compliant substrate [83] happen on the micro-/nano scale. That is the basic concept in the design of origami folded structure and pattern transformation in a holy sheet. Thus the mechanics of origami design is also a form of instability. Another reason for this subsection is to gather all of these large structures together.

5.1.1. Micro-/nanolattices metamaterials

Generally, we define a general lattice material as a cellular, reticulated, truss or lattice structure made up of a large number of uniform lattice elements (e.g. slender beams or rods). Such a lattice material is generated by tessellating a unit cell through space [84]. The corresponding unit cell consists of just a few lattice elements. Hence, both the geometry of the unit cell and its tessellation are significant in the design of these lattice materials. Normally, stochastic methods can determine lattice architecture in conventional cellular materials, such as foams (>50% porosity [85]) and aerogels. Manmade micro-/nanolattice metamaterials are inspired by natural cellular solids, such as honeycomb and foam-like structures. Mechanical metamaterials are associated with relatively ordered hollow lattices which allow a high degree of control over the cellular architecture. As research on natural cellular materials is relatively mature, the reader is referred to previously published books [55,86]. This subsection is thus limited to engineered lattice metamaterials in the micro/nanosize.

Two factors, the unit cell and its tessellation, need to be considered in the design of micro-/nanolattice metamaterials. That is because most of manmade ultra-light (<10 mg per cubic centimetre) metamaterials are fabricated from a wide array of solid constituents. In such metamaterials with structural hierarchy, the stiffness depends on the relative density and the cellular architecture, i.e. the spatial configuration of voids in the solid [86,87]. Firstly, from a topological standpoint, the spatial configuration of cellular materials can be categorised as either open or closed cells [86,88], with either a stochastic or an ordered structure [89]. Porous microstructures in cellular solids may be either heterogeneous, as a result of the foaming process, or may be very regular due to specifically engineered structures such as honeycombs. Secondly, two-dimensional unit cells, i.e., periodic planar lattices, can be classified as regular lattices. By tessellating a regular polygon such as a triangle, square or hexagon to fill the entire plane, a semi-regular lattice results with two or more kinds of regular polygons [90–92]. For instance, the triangular-hexagonal lattice, also known as the kagome lattice [93], and in particular, the twisted kagome lattice (i.e., an isotropic structure with a vanishing bulk modulus) will be introduced in Section 6.2.2. Spatial or three-dimensional lattices can be tessellated with regular polyhedra with a small number of faces, to fill all of the space [86]. Alternatively, using combinations of different polyhedra, typically tetrahedral and octahedral cells [94–96] may be packed to form the octet-truss lattice [97].

5.1.1.1. Assessment of strength and density. To characterise the mechanical properties of metamaterials, the relationship between strength and density needs to be assessed for the micro-/nanolattices associated with strong, lightweight materials (E/ρ). A decrease in density can bring forth a drastic degradation in the mechanical properties of materials. This is because structural elements have a bending deformation at the ligament level under a macroscopically applied load [89]. Open-cell materials with stochastic porosity, particularly those with a relative density of less than 0.1%, carry a stronger scaling relationship between Young's modulus (stiffness) and density [$E/E_s \propto (\rho/\rho_s)^n$] thereby between strength and density [$\sigma_y/\sigma_{ys} \propto (\rho/\rho_s)^n$] [75,87]. The Young's modulus E of a mechanical metamaterial that is considered to be a continuum is given in terms of the Young's modulus E_s of the solid constituent material from which the materials is made, the density ρ, the yield strength σ_y of the solid constituent material, the density ρ_s and the yield strength σ_{ys} of the metamaterial. The power n of the scaling relationship between relative material density and the relative mechanical property depends greatly on the microstructure of the metamaterial. Generally, $n = 2$ is for an open cell [86] and $n = 3$ represents a closed cell [48,98] in macroscopic hierarchical frameworks. For instance, the Eiffel Tower can be represented by third-order and possesses a relative density only 1.2×10^{-3} times that of iron [87], which is similar to that of the low density aerogels [66] that are clearly structurally robust.

Furthermore, the approximate stiffness equations [$E/E_s \propto (\rho/\rho_s)^n$] in previous conventional cellular materials is independent of either the length-scale or the specific symmetry of the structure. Some initial studies reveal that the density-dependent modulus shows structural anisotropy for the $\langle 1\,0\,0\rangle$ and $\langle 1\,1\,1\rangle$ directions of the simple cubic [99], body-centred cubic [100] and face-centred cubic structures [101]. Structural anisotropy is responsible for this discrepancy. We can tailor and tune the degree of anisotropy through the beam/strut diameter ratio in a given cellular structure at a given density [102]. One influential idea is to design non-conventional cellular materials, particularly by making them isotropic structures. Mechanical metamaterials, defined by their geometry rather than their composition, can maintain a nearly linear scaling between stiffness and density spanning three orders of magnitude in density, over a variety of constituent materials [48,75,103]. This is because a smaller scaling exponent demonstrates less loss in the elastic modulus as the relative density decreases.

In recent years there have been many attempts to reduce the coupling between mechanical properties and mass density in micro/nanohierarchical networks [104]. The corresponding topological design of periodically ordered architectures enables precise control over the load transfer from the macroscale to the unit cell scale, thereby enhancing by an order of magnitude in the specific stiffness and strength. Some extensive reviews [48,84,86,105] discuss the range of such material properties, including high stiffness, strength and fracture toughness, exhibited by low-density in micro-/nanostructured metamaterials.

5.1.1.2. Typical structural designs for mechanical metamaterials. Through two examples of unit cells, we will discuss a stretch-dominated octet-truss geometry and a bend-dominated tetrakaidecahedron geometry (Fig. 4 [75,106]), in terms of their mechanical response to compressive loading. The former is generally made of metals (nickel-based) or ceramics (alumina), whereas the latter is normally packed into a cubic Kelvin foam.

One typical stretch-dominated microlattice with an octet-truss geometry [97] has been developed to achieve ultra-light and ultra-stiff metamaterials [75]. The load-bearing capacity of this octet-truss structure may be attributed to Alexander Graham Bell's interest in tetrahedral cells for building man-carrying kites [107], although the geometric configuration was proposed by Deshpande et al. [97] later on. Since a fully-triangulated truss-type architecture deforms primarily by axial stretching of the truss elements, this structure enables the modulus and strength to scale linearly with the relatively density [97,104]. A unit cell of the octet truss has a regular octahedron as its core, surrounded by eight tetrahedral distributed on its faces, which is identical in crystal structure to the face-centred cubic unit cell (Fig. 4). All of the strut elements have identical aspect ratios, with a nodal connectivity, or coordination number, of 12 solid rods or hollow tubes connected to each node, thereby packing into a stretching-dominated structure. As such, the unit cell structure consists of b struts and j frictionless joints, satisfying Maxwell's criterion, $M = b - 3j + 6 > 0$ [86,84]. The relative density of such octet truss unit cells can be approximated by $\rho = 26.64\ (d/L)^2$ [97], where L and d are the length and diameter of each beam element. On the macroscale, under uniaxial compressive loading, the relative compressive stiffness and yield strength of these structures will theoretically show a linear scaling relationship: $E/E_s \propto (\rho/\rho_s)$ and $\sigma_y/\sigma_{ys} \propto (\rho/\rho_s)$ [97]. Correspondingly, in a Ni-P stretch-dominated metallic microlattice, the specific stiffness stays nearly constant as the density is reduced from 40 mg/cm^3 to 14 mg/cm^3, measured as 1.8×10^6 m^2/s^2 and 2.1×10^6 m^2/s^2 at densities of 14 mg/cm^3 and 40 mg/cm^3, respectively [75,89,108]. In such an ultra-stiff microlattice structure, the fully triangulated truss-type architecture deforms primarily by axially stretching the truss elements, allowing the modulus and strength to scale linearly with the relative density [104,97]. As seen in the Ashby-chart in Fig. 5 [75,66,109,110], this nearly linear E-ρ scaling relationship outperforms traditional lightweight and ultra-light bending-dominated structural materials, whose properties scale as $E \sim \rho^2$ or $E \sim \rho^3$ [66]. Just recently, much more resilient two- or three-dimensional hierarchical metamaterials [111] have been designed using polymers, hollow ceramics, and ceramic-polymer composites [112], in order to obtain ultra-lightweight, recoverability, and a near-linear scaling of stiffness and strength with density.

These studies have successfully introduced an electron back scatter diffraction (EBSD) technique to examine the film microtexture while excluding the microlattice symmetry, in place of the obtained macrotexture analysis via X-ray diffraction (XRD). The orientation maps of the 15° cross-section indicate that all crystals are oriented along the ⟨1 0 0⟩ direction, and the pole figure shows clear texture along the family planes. The presence of this texture can be responsible for the decrease of the modulus and strength.

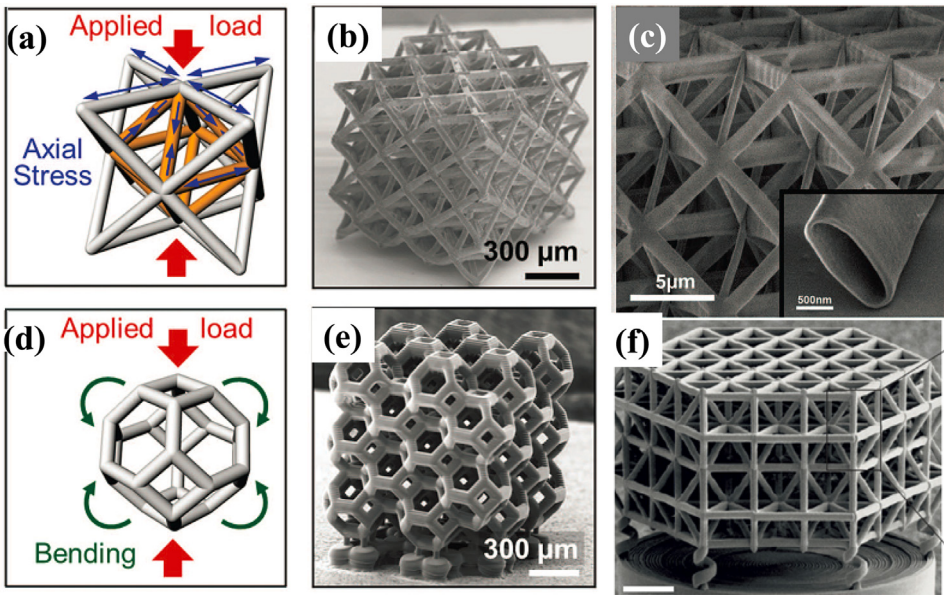

Fig. 4. Architecture of stretch-dominated and bend-dominated unit cells and lattices. (a) Mechanical response to compressive loading of a stretch-dominated octet-truss unit cell. (b) Octet-truss unit cells packed into a cubic micro-lattice [75]. (c) Zoomed-in section of the alumina octet-truss nanolattice. The inset shows an isolated hollow tube [106]. (d) Mechanical response to compressive loading of a bend-dominated tetrakaidecahedron unit cell. (e) Tetrakaidecahedron unit cell packed into a cubic bend-dominated lattice (Kelvin foam) [75]. (f) Pyrolysis of polymeric micro-lattices creates glassy carbon nanolattices [43].

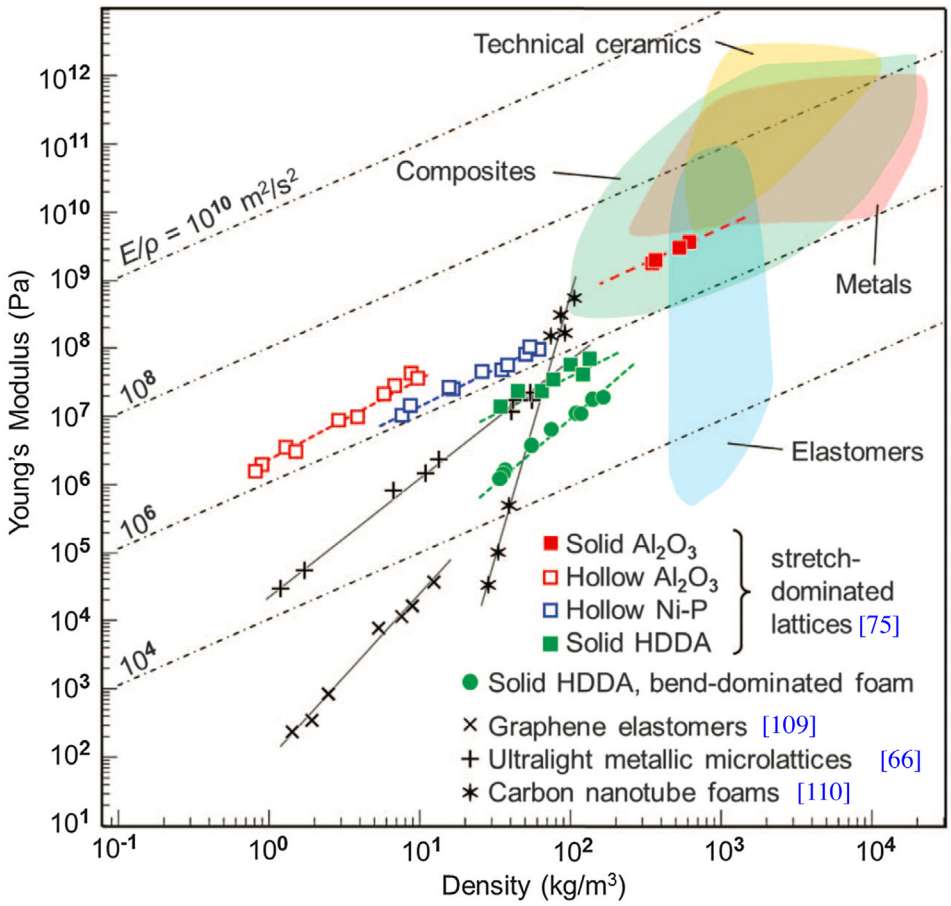

Fig. 5. An Ashby-chart plotting experimental stiffness versus density for currently reported mechanical metamaterials [66,75,109,110]. Dotted lines indicate contours of constant stiffness-density ratio $c = E/\rho$ (m^2/s^2).

Another typical lattice is the bend-dominated tetrakaidecahedron geometry. As we have seen above, the stretch-dominated microlattice are designed such that the trusses are in tension or compression with no bending as the absence of bending allows the stiffness and strength to vary linearly with relative density [104]. In contrast, here the bend-dominated tetrakaidecahedral structure with a network of elastic beams is also derived from a large pin-jointed framework connecting Z and j joints: the total number of bars b is approximately $jZ/2$ [113]. The hexagonal lattice is bending dominated, with $b = 3$, i.e. sharing a low nodal connectivity of 3 adjoining bars per joint [114,115]. The stiffness and strength of these three-dimensional structures relies upon the bending stiffness of the bars, which are consequently referred to as bending-dominated structures [84]. At the other end of the stiffness spectrum for elastic lattice structures are pentamode materials (PMs) with five easy modes of deformation, which will be introduced in detail in Section 6.2.1. In a previous study, the bend-dominated structure packed into a cubic Kelvin foam is softened as $E \sim \rho^2$ or worse [75].

Because of these two types of structural designs, it is reasonable to believe that the response of low-density lattice structures depends on whether the deformation occurs under a load dominated by stretching or bending. Nevertheless, this mechanical response in turn depends upon the coordination number, Z, the number of the nearest neighbouring joints in the unit cell. Recently, a general theoretical approach provided an algebraic formula for the effective elasticity of such frameworks [114,115]. The method yields the effective cubic elastic constants for three-dimensional space filling lattices with Z = 4, 6, 8, 12 and 14, the last being the 'stiffest' lattice proposed by Gurtner and Durand [114]. These results reveal that the displacement field under uniform loading conditions is refined on the microscopic scale [114,115], using a convenient set of criteria to identify the networks.

Such strong and lightweight mechanical metamaterials have shown exceptional potential for a broad range of applications, in particular for thermal insulation, battery electrodes, catalytic supports, and acoustic, vibration, or shock energy damping [66]. For example, an aerographite consisting of a nitrogen doped graphene aerogel with an ultra-light, three-dimensional graphene framework consisted main of a network of only a few graphene layers. Its ultra-low density was 2.1 ± 0.3 mg/cm^3. Its adsorption capacity for common pollution and organic solvents was as 200–600 times higher than its own weight, much higher than that of the best carbonaceous sorbents [116,117]. Nevertheless, these glass-like carbons

(often called 'vitreous carbons' [118]), have superior mechanical properties and chemical resistance, while being electrically conductive, as is required for electrode materials. Highly compressible 3D periodic graphene aerogel microlattices have been reported with a compressive modulus (E) of 1.1 GPa and a failure strength (σ_f) of 10.2 MPa for a structure with a relative density of 12.8% [118]. It is widely expected that these stiff elastic networks will compete or improve the well-known Hashin-Shtrikman bounds.

5.1.1.3. Recent theoretical and experimental advances. Recent advances in additive manufacturing and topological optimisation techniques make it possible to design periodic lattice structures with controlled anisotropy (Fig. 6 [119]), thereby it will be possible to explore the mechanical properties of lightweight metamaterials. These investigations suggest that the spatial distribution of Young's modulus over surfaces, i.e., elastic anisotropy of lattice structures, is only dependent on the spatial arrangement and dimension of the rods, and independent of the base material. In an example of the simple crossing-rod unit in Fig. 6a, the stiffness in diagonal directions is much higher than that in the axial directions. Something similar thing can be found in the other cases, such as the combination of face-centred and body-centred (FCC-BCC) unit cells [120]. One type of cellular material, called aerographite (density < 200 $\mu g\ cm^{-3}$) [117], is more than 4 times lighter than the Ni microlattices, which were up to now the most lightweight materials. Kang's group [121–123] has introduced a new type of ultralow density material named 'shellular' (Fig. 7), a combination of the words 'shell' and 'cellular', which consists of a continuous thin shell instead of hollow trusses. Note that in triply periodic minimal surfaces, P denotes primitive, and D denotes diamond [124]. In addition to P- and D-surfaces, the G-(gyroid) surface has also been investigated [125–127].

Through recent progress in graphene-based two-dimensional and granular materials [128], we realise that myriad bulk 3D assemblies of graphene, such as complex graphene aerogel architectures [116], can possibly offer a unique combination of low density, exceptional mechanical properties, large surface area and excellent electrical conductivity. Bauer et al. [43] have reported that pyrolysis of polymeric micro-/nanolattices can overcome these limitations and create ultra-strong glassy carbon nanolattices with single struts shorter than 1 μm and diameters as small as 200 nm. With a honeycomb topology, these carbon nanolattices can achieve effective strengths of 1.2 GPa at 0.6 $g\ cm^{-3}$ [43]. Discussion of the electrical performance is beyond the scope of the present paper.

Hollow nickel microlattices with arbitrary topologies have the potential to perform as structural damping materials for energy dissipation [129], and thereby are applied to specific engineering systems (e.g., bone implants [130]). Particularly, reports from Schaedler et al. [66,89,108,129,131] focus on nickel microlattice. Meanwhile, this energy absorption can also be significantly enhanced by inertial stabilisation, by the shock wave effect and by the strain rate hardening effect [131]. These observations suggest that inertial stabilisation originates by the suppressing sudden crushing of the microlattice and by contributing to the rate of crushing speed [131]. Because of the higher yield stress at the wrinkles, the initial buckling stress and post buckling stress can be improved to some extent [131]. This means that the strain rate effect increases the effective yield strength upon dynamic deformation and increases the energy absorption density.

As we have seen, it is true that some nanomaterials [132] such as ceramics and metallic alloys [133], for example nickel, can be lightweight, but we are still eager to find other microlattice, where performance may be the key. Nothing is perfect. Even though some black dots exist on the surface of the sun, we try to restrain the black dots, and improve the sun shining at just right level. That is analogous to what researchers will do in metamaterials [121–123].

5.1.1.4. Short summary of micro-/nanolattice metamaterials. In summary, mechanical metamaterials that combine ultra-stiffness with ultra-lightweight (generally less than 10 mg per cubic centimetre), are extending beyond the frontiers of existing natural materials. At the same time, most of the elegant ideas underpinning the structural design of mechanical metamaterials were inspired by natural hierarchical cellular solids, such as honeycombs, aerogels and foams structures. In a larger sense, hierarchical solids generally consist of structural elements which themselves are structured. Nice examples of macroscopic hierarchical frameworks are the design of the Eiffel tower, bridges such as the Garabit viaduct [87], and the Sydney Harbour Bridge. The idea of hierarchical structure serves as the basis for synthesising new structures on the micro/nanoscale which give rise to useful or even enhanced physical properties, including improved strength and toughness, and unusual mechanical properties combining ultra-strength with low density. The stiffness of such metamaterials with structural hierarchy, depends on the relative density and their cellular architecture, in other words, the spatial configuration of voids and solid matter [86,87].

In comparing the mechanical properties of a structured hierarchical cellular system, we can investigate the scaling relationship between Young's modulus and the relative material density, and between relative strength and density. That is because, as mentioned above, in such metamaterials with structural hierarchy, the stiffness depends mainly on the density and structure, in other words, the spatial configuration of voids and solid matter [86,87]. Here we attempt to introduce some of the basics of the stiffness/strength-density relationship associated with mechanical metamaterials. We also present some complicated mechanics, like iterations of the stiffness equation, which consider with difficulty the hierarchical order. Some elegant books and literature [86,87,113] are available which delve into the details of this case. In addition, the design principles behind this type of mechanical metamaterials, such as Maxwell's criterion, will be addressed in detail in Section 5.2.1.

The main challenge for strong-lightweight metamaterials is to reduce the coupling between mechanical properties and mass density in various hierarchical micro-/nanostructures. Simultaneously, the way in which we fabricate materials is changing rapidly. Much more advanced processing techniques [48] enable us to achieve topological designs with periodically ordered architectures. It is therefore possible to enhance specific stiffness and strength by an order of magnitude via the pre-

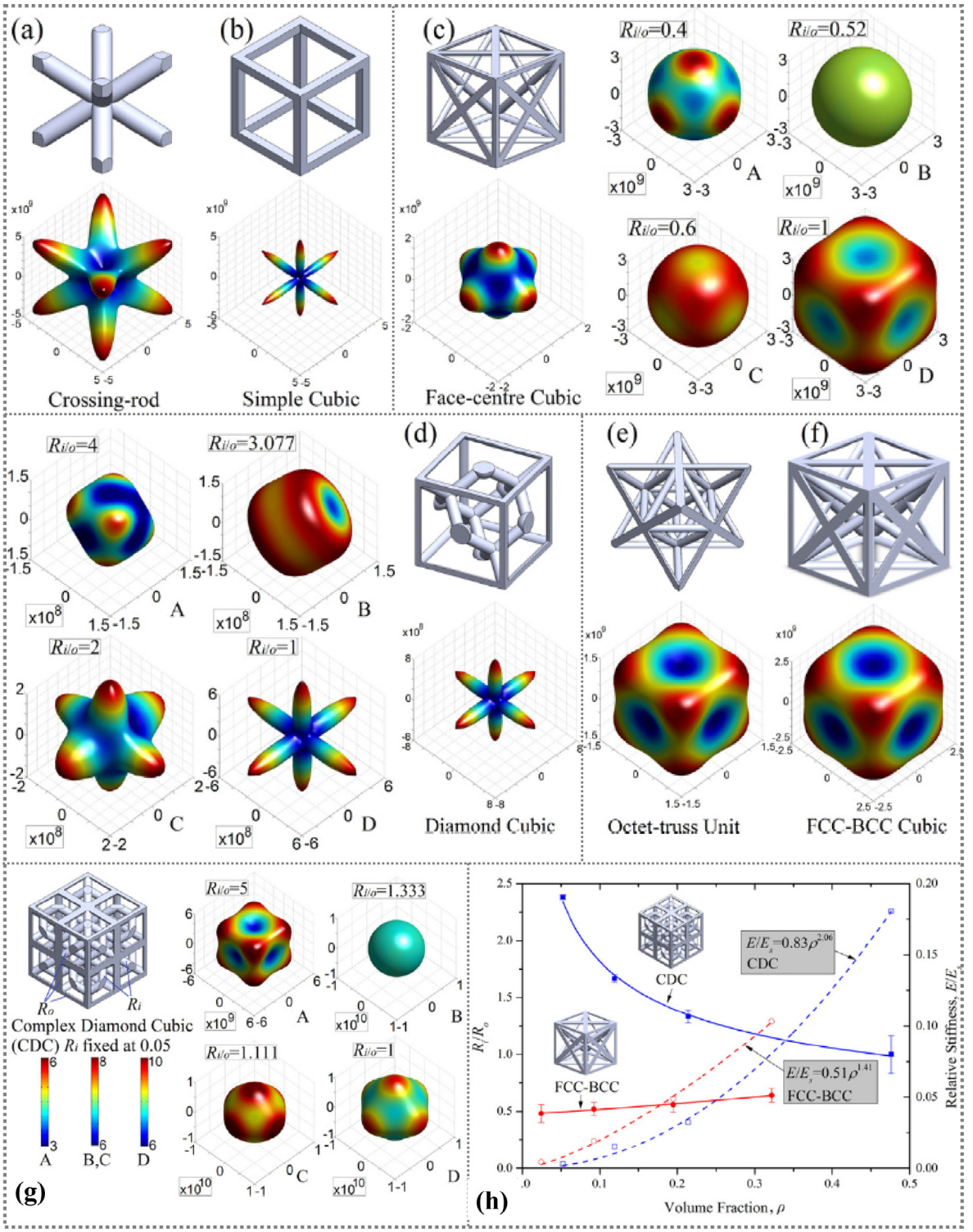

Fig. 6. Lattice structures with controlled anisotropy: architectures of typical representative units and the corresponding 3D spatial representations of effective Young's modulus surfaces: (a) crossing-rod unit, (b) simple cubic unit, (c) face-centre cubic unit, (d) diamond cubic unit, under the ratio of R_i/R_o, here taking the rod diameter of the crossing rod as R_i and FCC unit as R_o, (e) octet-truss unit, and (f) a combined unit of face-centred and body-centred units (FCC–BCC), (g) mirror operation on a diamond cubic unit to obtain a complex diamond cubic (CDC), (h) the variation in R_i/R_o ratio with the increasing volume fraction of two types of representative units, CDC and FCC-BCC, by fixing the diameter of one type of rod and adjusting another type (left vertical axis, solid lines). The relative stiffness (E/E_s) of the two structures in relation to the volume fraction (right vertical axis, dashed lines) [119].

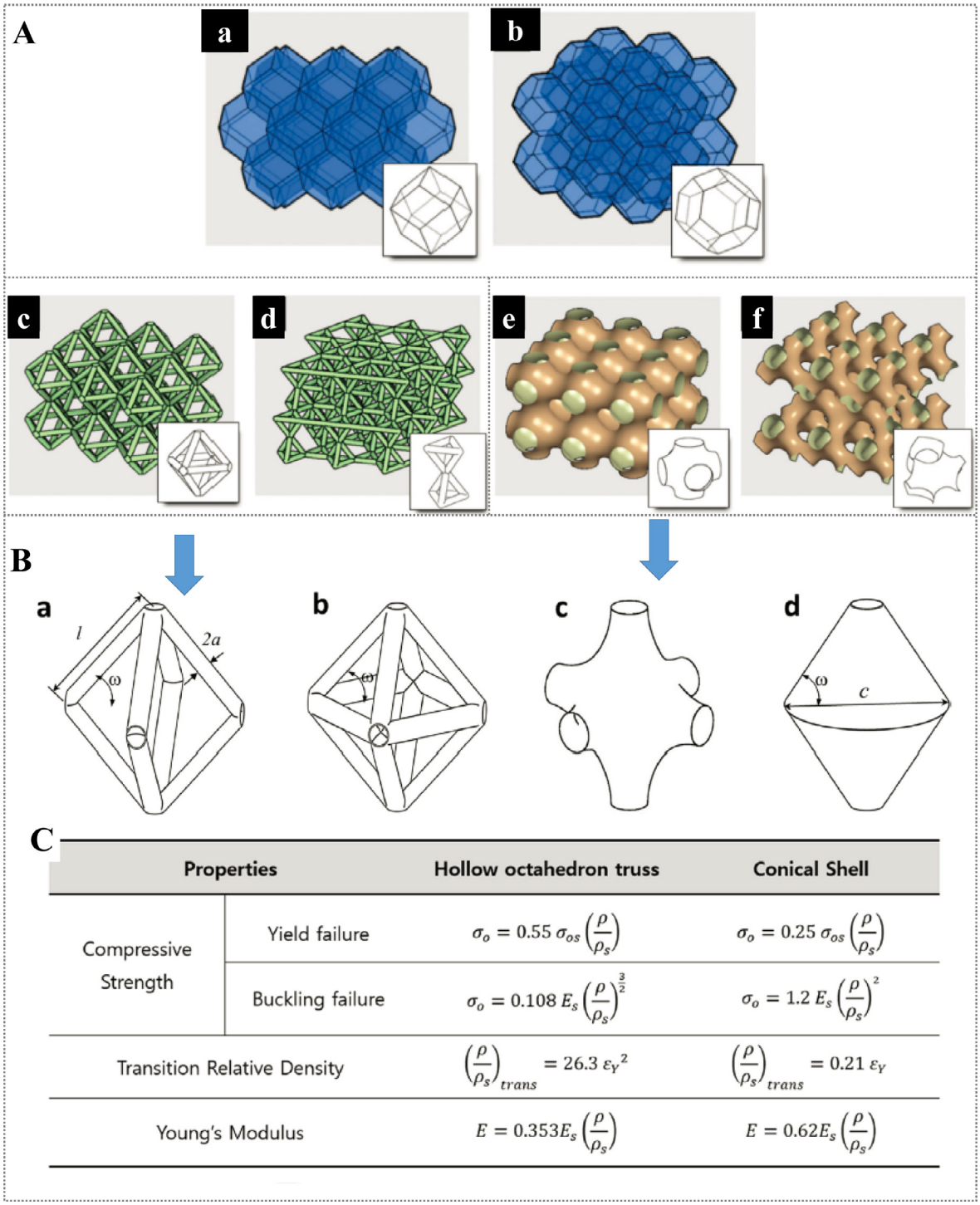

C

Properties		Hollow octahedron truss	Conical Shell
Compressive Strength	Yield failure	$\sigma_o = 0.55\,\sigma_{os}\left(\frac{\rho}{\rho_s}\right)$	$\sigma_o = 0.25\,\sigma_{os}\left(\frac{\rho}{\rho_s}\right)$
	Buckling failure	$\sigma_o = 0.108\,E_s\left(\frac{\rho}{\rho_s}\right)^{\frac{3}{2}}$	$\sigma_o = 1.2\,E_s\left(\frac{\rho}{\rho_s}\right)^{2}$
Transition Relative Density		$\left(\frac{\rho}{\rho_s}\right)_{trans} = 26.3\,\varepsilon_Y{}^2$	$\left(\frac{\rho}{\rho_s}\right)_{trans} = 0.21\,\varepsilon_Y$
Young's Modulus		$E = 0.353E_s\left(\frac{\rho}{\rho_s}\right)$	$E = 0.62E_s\left(\frac{\rho}{\rho_s}\right)$

Fig. 7. (A) Three options for artificial cellular structures with their unit cells to support loads at low density: polyhedron cells (a) rhombic dodecahedron, (b) tetrakaidecahedron; struts and truss (c) cells with octahedron trusses, (d) cells with kagome trusses, triply periodic minimal surfaces (e) cells with P-surface, (f) cells with D-surface, where P denotes primitive and D denotes Diamond [123,124], respectively; (B) (a–d) configurations of unit cells of microlattice, a hollow octahedron truss, and a truncated conical shell, respectively. (C) Analytic solutions for the compressive strength and Young's modulus of the cellular material composed of hollow octahedron trusses and Shellular composed of conical shells [121–123].

cise control over load transfer from the macroscale to the unit cell scale. The upshot of this development is that we need to know how to extend the limitation of natural material properties, e.g., here high stiffness, strength and fracture toughness [84,134,105]. In a word, these manmade ultra-light mechanical metamaterials fabricated from a wide array of solid

constituents can provide exceptional potential for a broad range of applications in automobiles, aircraft, and other applications, where light weighting materials could help conserve fuel without losing strength.

It is worth noticing that some other mechanical metamaterials can be based on the design concept of micro-/nanolattice cellular materials. Tailoring the porosity of structures [135] in topological designs can yield complex ordered patterns, thereby achieving selective buckling via states of self-stress [41,136]. It is therefore possible for a hierarchically structured nanolattice to be under ultrahigh stress and strain within a single unit cell during deformation [137]. If we couple this to buckling stability, a negative bulk modulus can occur. These corresponding behaviours will be address in Section 6.3.

5.1.2. Chiral, anti-chiral, and hierarchical metamaterials

A structure defined as *chiral* may be constructed as *a left handed* or *right handed* material, where the two are non-superimposable mirror images [138]. This type of mechanical metamaterial was first proposed by Wojciechowski [139], and later implemented as a hexagonal chiral honeycomb structure by Prall and Lakes [30]. Specifically, the unit cell of this network consists of a central cylinder called a node, with six tangentially attached ligaments, exhibiting a rotational symmetry of order six (for a complete description, refer to Fig. 25a). This connective structure composes the basic chiral unit, where the specific example given was classified as *hexachiral* by Grima [138,140].

These chiral building blocks can be divided into chiral and anti-chiral systems (Fig. 8 [138,141]), where the two-dimensional basic units are connected together either with nodes on opposite sides of the ligaments (in the case of the chiral system [142,143]), or with nodes on the same side of the ligaments (in the case of the anti-chiral system [140,144]). The anti-chiral system is racemic with equal amounts of left handed and right handed basic units [145]. In these five groups of chiral/anti-chiral networks (Fig. 8), if the thin ligaments are welded to the nodes, then a uniaxial on-axis load will result in a rotation of the nodes, accompanied by a flexing of the ligaments. Such deformation can therefore result in 'folding' of the ligaments around the node when the honeycombs are subjected to compressive loading, and 'unfolding' when they are subjected to tensile loading, a behaviour that results in auxeticity [138].

In examples of chiral, anti-chiral and hierarchical structures (Fig. 9 [146]), an array of cylinders (nodes) are connected by tangential ligaments (ribs). When each cylinder is connected to 3 and 4 tangential ligaments, we call the structures tri-, and tetrachiral or anti-chiral structures (Fig. 8). Previous studies [146] found that both chirality and hierarchy crucially affect the in-plane mechanical properties of these structures. As we have seen, hierarchical structures demonstrate a higher stiffness, behaving as cellular metamaterials, whereas chirality, particular anti-chiral structures, remains the only route to auxeticity. The deformation mechanism for this observation can be extend to the design the auxetic metamaterials, discussed in Section 7. The tetra anti-chiral [140,147,148] can even be used to form the mechanical metamaterials with negative thermal expansion (NTE) behaviour, as discussed in Section 6.3.3, although most studies so far have focused on the hexachiral lattices

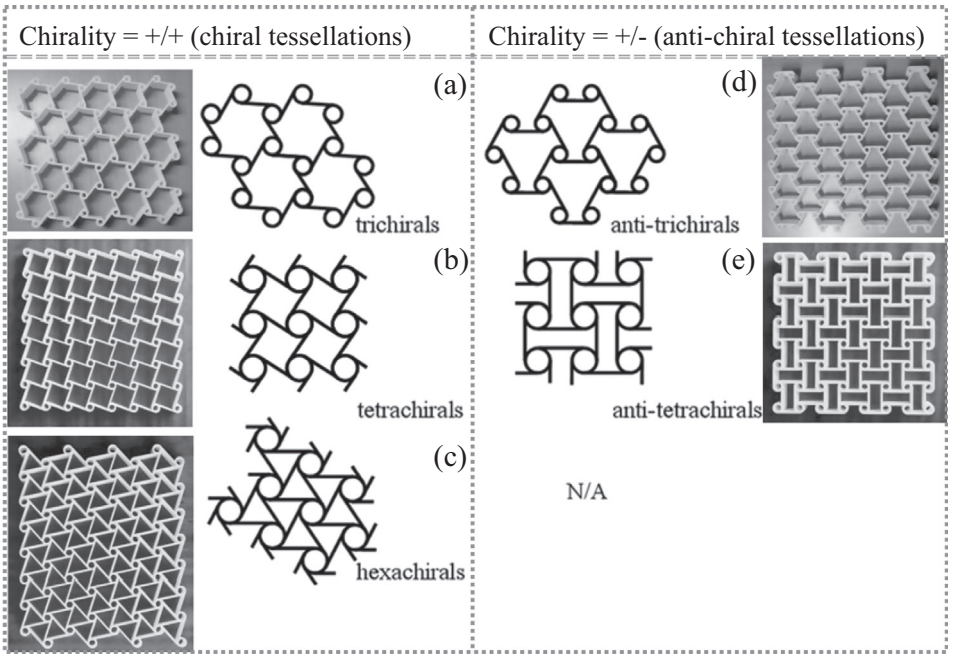

Fig. 8. Five tessellations and their rapid prototypes (figures in shade) that may be obtained from the 'chiral' basic units exhibiting rotational symmetry of order n [138,141]. The chiral systems with the nodes on opposite sides of the ligaments are termed as (a) trichirals, (b) tetrachirals, (c) hexachirals (for $n = 3$, 4 and 6 respectively), whereas the anti-chiral systems with the nodes on the same sides of the ligaments are referred to as (d) anti-trichiral and (e) anti-tetrachiral (for $n = 3$ and 4 respectively). Note that more systems can be obtained if the constraint that the basic units exhibits rotational symmetry of order n is relaxed.

A

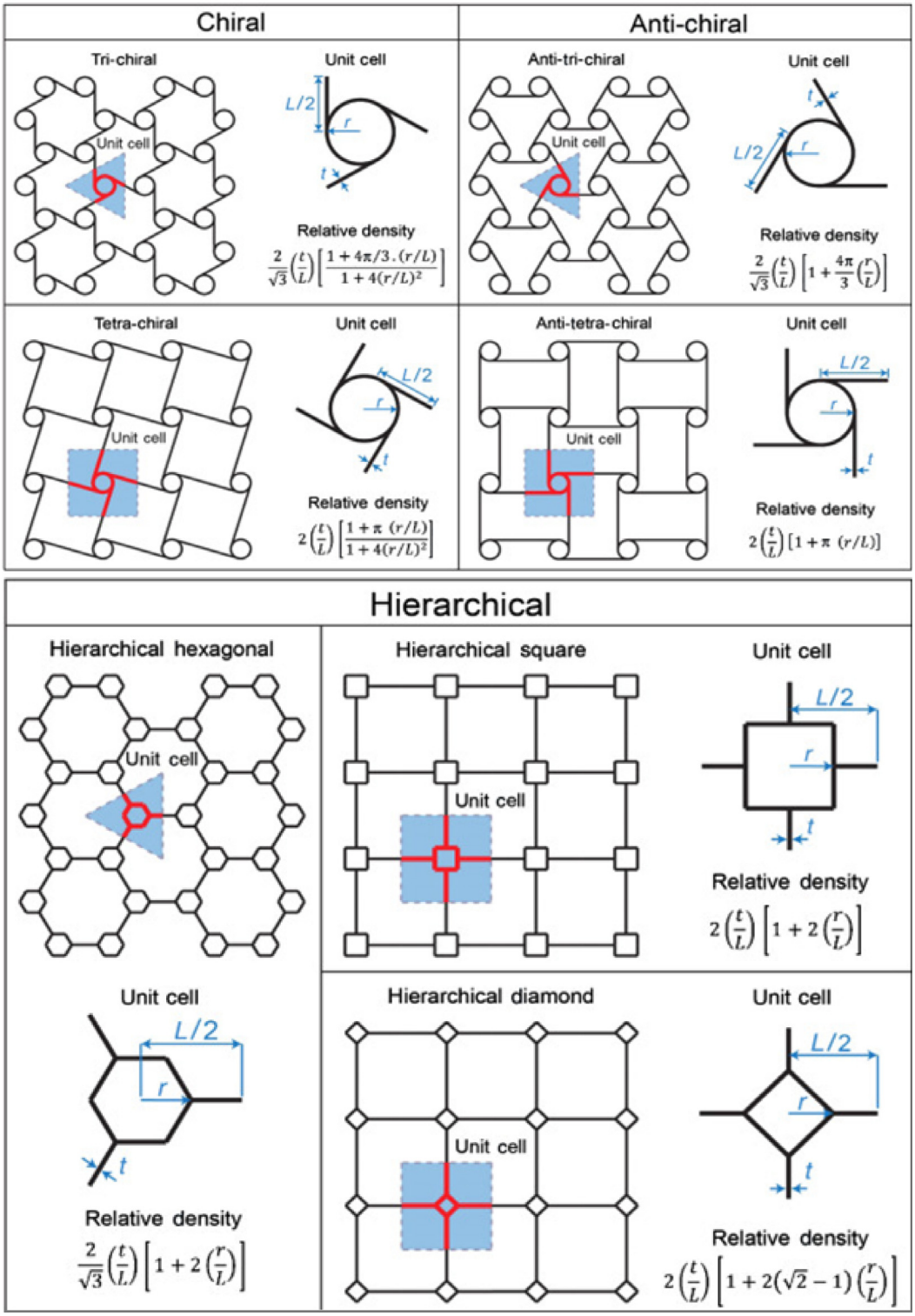

Fig. 9. (A) Schematic of the structure and the unit cell, and the expression of relative density for the chiral, anti-chiral and hierarchical honeycombs. Normalised Young's modulus as a function of geometrical parameter r/R for (B) three different hexagon based hierarchical and chiral lattices, (C) four different anisotropic square based hierarchical and chiral lattices, where r is the radius of the cylinders, and R is the centre to centre distance between any two adjacent cylinders [146].

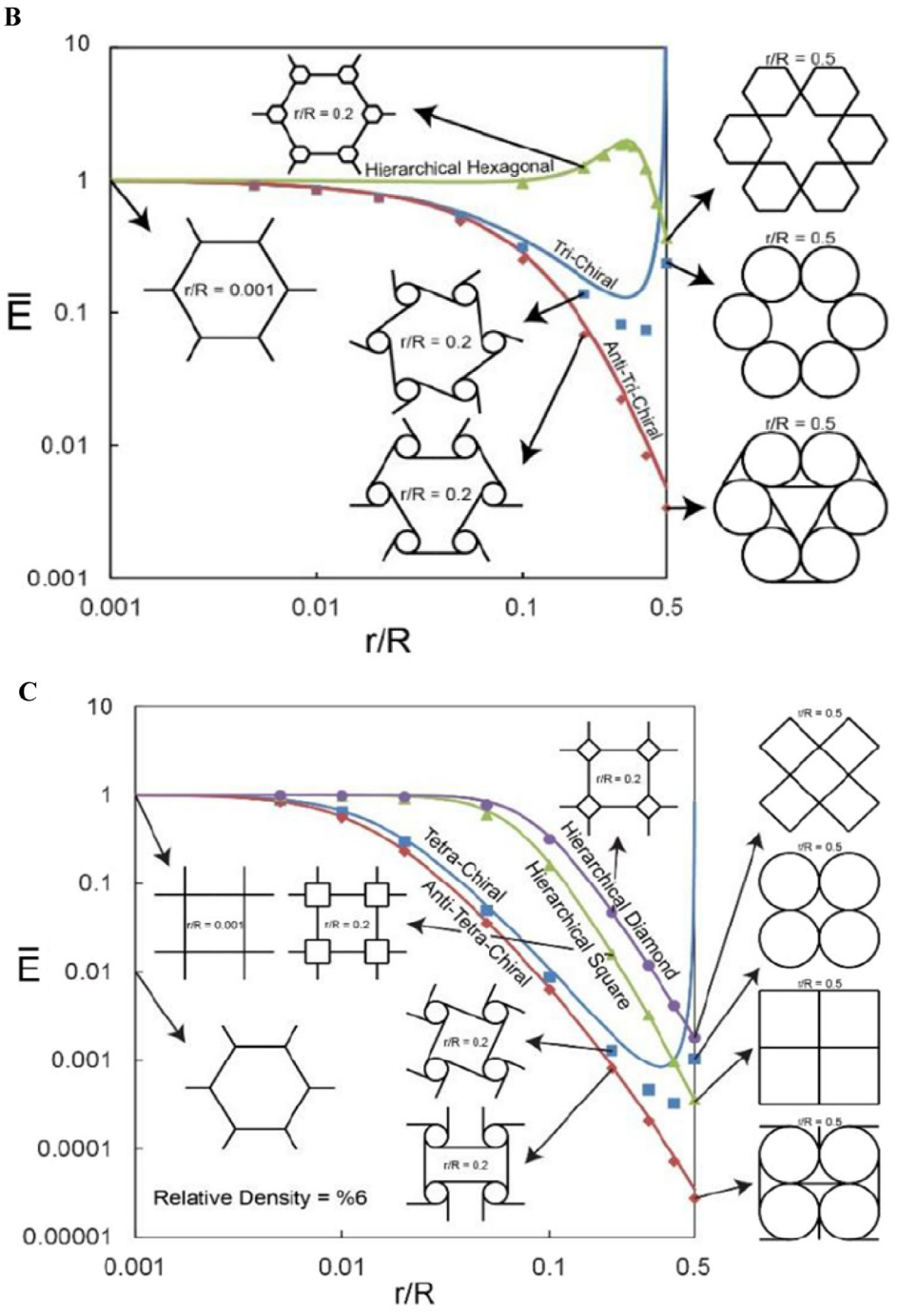

Fig. 9 (*continued*)

or tetrachiral lattices used in acoustic metamaterials [21,149,150]. This is mainly because the chiral lattice inserts exhibit unique characteristics such as frequency band gaps tuned by varying the parameters that define the lattice topology [151]. The hexachiral lattice [136] can be used to shape memory alloys or polymers [152], and also some chiral networks used in macrochiral components, e.g., air foil [153,154].

5.1.3. Origami-inspired metamaterials

The term *origami* is derived from the Japanese compound noun, 'ori' meaning 'folded', and 'kami' meaning 'paper' [155]. Currently, origami, the art of folding uncut sheets of paper into decorative and well-defined shapes, is now being used

beyond purely aesthetic pursuits to design ultra-light and customisable mechanical metamaterials [78,156–161]. This subsection will address some fundamental terms and the simple classification used by this research field. Subsequently, three classical origami patterns will be introduced, the Miura-ori pattern, a non-periodic Ron Resch pattern, and square twist. Finally, two other fields are included: one is the special case of paper cutting, kirigami, and another is the design mechanism behind origami-inspired frameworks. In doing so, an equivalent crystallographic classification will be summarised, targeting the origami building blocks for future development and design.

First of all, some fundamental definitions of origami terminology must be established before we start. In an analogy to haute couture design, origami also relies on folding and assembling planar material to create elegant three-dimensional shapes whose variety and complexity are governed by the number, order, and orientation of the folds. Correspondingly, in the computational origami field [162,163], certain basic geometrical parameters such as creases and vertices have been introduced (Fig. 10a). Formally, *creases* refer to the locations of localised folds on a planar sheet exclusively made through folding operations [162]. The endpoint at which several creases converge is termed as the *vertex*, whereas, sheet regions bounded by the creases are known as faces. Typically, a mountain-valley assignment is used to determine the fold direction of a crease. For mountain folds, faces on either side of the crease can be seen to be rotating into the page, whereas for valley folds, they can be considered to be rotating out of it [164]. Alternatively, positive folding angles as form valleys and negative ones as form mountains, when a folded state is described by the folding angles in a traditional spherical mechanism [159]. The creases, folding directions, folding magnitude, and folding sequence determine the ultimate shape of the origami structure.

To truly consider origami structures as a class of metamaterials, a simple and effective classification method needs to be introduced for action origami as the spherical mechanisms used in networks (Fig. 10b). From the perspective of vertices and tessellations, it is also necessary that these kinematic origami models can be classified further into a relatively small number of interconnected spherical mechanism combinations [165]. Kinematic origami networks include a single loop (e.g. a traditional square twist [166]), 1D periodic structures (e.g. Shafer's "Blinking eyes" [167]), 2D periodic structures (a particular case of the "Miura-ori pattern" [168,169]), and nonperiodic structures (e.g. Shafer's "Monster mouth") (Fig. 10b). Nevertheless, we can notice that many kinematic origami models are considered rigid, where the fold pattern can be modelled as a series of rigid polyhedra connected by rotating torsional frictionless hinges (i.e., creases). Consequently, each category of origami structure can be combined into a wide range of interesting motion with artistic variations in the composition of elements. From these we know that the origami design is based on a sort of plate-and-hinge compliant mechanism. Specifically, their creases act as mechanical links, i.e., joints or pins, to allow motion [165]. Such an origami structure is therefore capable of performing folding/deploying operations rather than being triggered by external forces or moments. In doing so, this suggests that the deformations of folding-based materials can be highly nonlinear owing to the complex constraint space imposed by the fold network. That is to say, their energetic landscapes arise from torsional spring interactions rather than central-force linear springs [159].

Current research interests are based on three representative origami patterns: a periodic Miura-ori pattern, a non-periodic Ron Resch pattern, and a square twist with a single loop (Fig. 11). Other combined systems such as cellular origami will be introduced in Section 5.1.4 for completeness. These origami-inspired mechanical metamaterials offer enhanced flexibility, deformability and compactness, which is primarily due to their properties coupled with a dynamically alterable folding pattern [164,170], specially, bio-origami hydrogel scaffolds and other buckled surfaces [171,172].

Firstly, the classic Miura-ori tessellated folding pattern [168,169] has recently been proposed as an origami mechanical metamaterial [157,158]. Mathematically, the geometry of a simple periodically folded Miura-ori structure is a herringbone

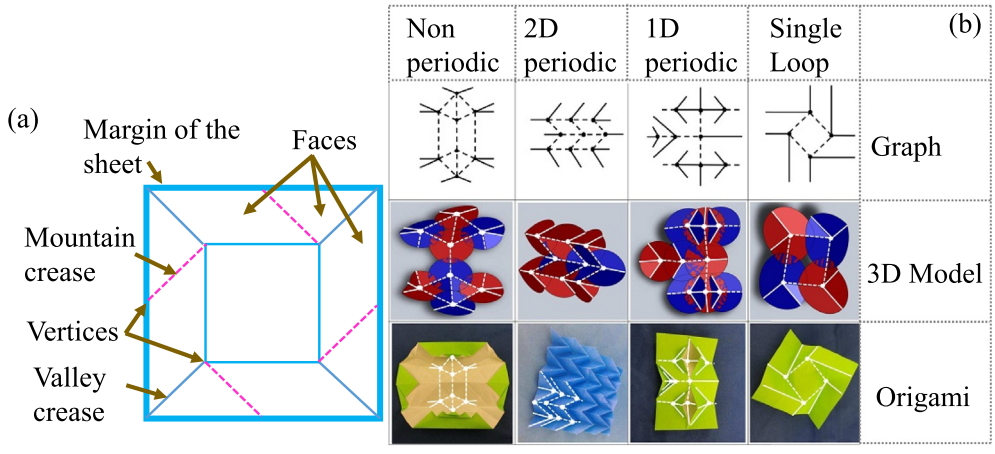

Fig. 10. Essentials of origami-inspired metamaterials. (a) Schematic of a pinwheel crease pattern illustrating various origami concepts [164]. (b) A classification of action origami as the spherical mechanisms used in networks [165].

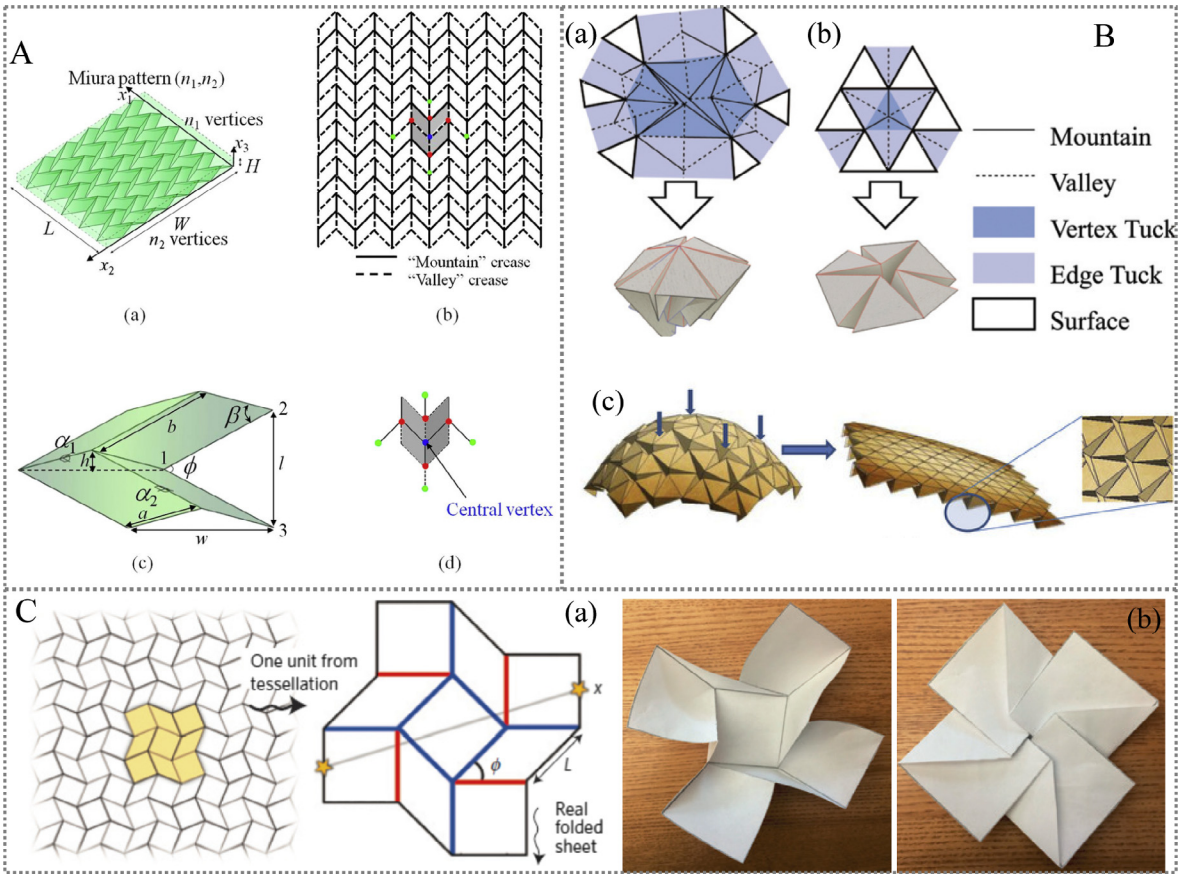

Fig. 11. Origami-inspired metamaterials. (A) Illustrations of Miura-ori [160]. (a) A Miura-ori (n_1, n_2) in its folded state with n_1 vertices in x_1 direction, n_2 vertices in x_2 direction. x_3 is the out-of-plane direction. Specifically here, $n_1 = 11$, $n_2 = 11$, $\beta = 45°$ and $a/b = 2.42$. (b) A Miura-ori in its planar state. (c) A unit cell of a Miura-ori. α_1, α_2 are two dihedral angles. In each parallelogram, the length of the short side is a and that of the long side is b, with the acute angle of β. The projected angle between the two ridges is ϕ. The size of the unit cell is l, w, and h, in x_1, x_2, and x_3 directions, respectively. (d) A non-local element for Miura-ori that focuses on the central vertex. (B) Ron Resch's tessellation. (a) Origamiser and (b) Ron Resch's tessellation. Both are comprised of surface polygons and tucks that are hidden. Resch's pattern can have the tuck folded halfway, whereas origamiser vertex keeps the tuck closed because of the crimp folds [181]. (c) Illustration of a Ron Resch dome deforms to a completely collapsed state upon compressive load from the top, where the three-fold supporting structure is shown in the inset [160]. (C) Square twist with a single loop. (a) Schematic of the square-twist folding pattern illustrating essential geometric properties, where the edges in black, mountain creases in red, and valley creases in blue. The geometry is defined by the length, L, and the plane angle, ϕ. The Euclidean distance, x, between the two yellow stars quantifies the macroscopic configuration between folded and unfolded states [166]. (b) Folding of the square-twist structure [182]. When compressed, the structure starts to fold by bending, except for its central facet, until it reaches an unbent folded configuration.

pattern (Fig. 11a [160]), consisting of identical unit cells of convex mountain creases and concave valley creases with four-coordinated ridges. Vertices are formed when four creases intersect, where the four adjacent vertices bind congruent parallelograms that are arranged with inversion symmetry. This morphology also naturally occurs in leaves [173], the embryonic intestine [174,175], and generally arises when thin sheets tethered to a surface undergo biaxial compression [83,173]. With respect to the mechanics behind this geometry, the two-dimensional deformation of a Miura plate can be characterised in terms of a one-dimensional beam theory because the effective bending stiffness of its unit cell is singular [158]. The folded metamaterial can be machined into any desired shape and still preserve its folding motion, thereby these morphologies are widely expected to open up new possibilities in materials engineering [78].

The main objective of the Miura-ori origami pattern in mechanical metamaterials was coming from the rigorously examined negative Poisson's ratio [47,176]. Several studies [157,158] in Miura-based mechanical metamaterials revealed that the folded shell structure provides a negative Poisson's ratio for in-plane deformations and a positive Poisson's ratio for out-of-plane bending [157], which is however equal in magnitude [158] and independent of the material properties. Until recently, Silverberg et al. [78] discovered that a Miura-based mechanical metamaterials with tunable stiffness is technically feasible via introducing a reversible pop-through defect. Analogous to crystallology, the introduction of pop-through defects can serve as models for emergent crystal structures [73], such as typical lattice vacancies (Fig. 12), dislocations, and grain boundaries [78,177]. The folded sheets with re-entrant geometries can contribute to the modulus at low densities. What we can see behind these observations is that these mechanically stable local defects are always based on the theory of instability to

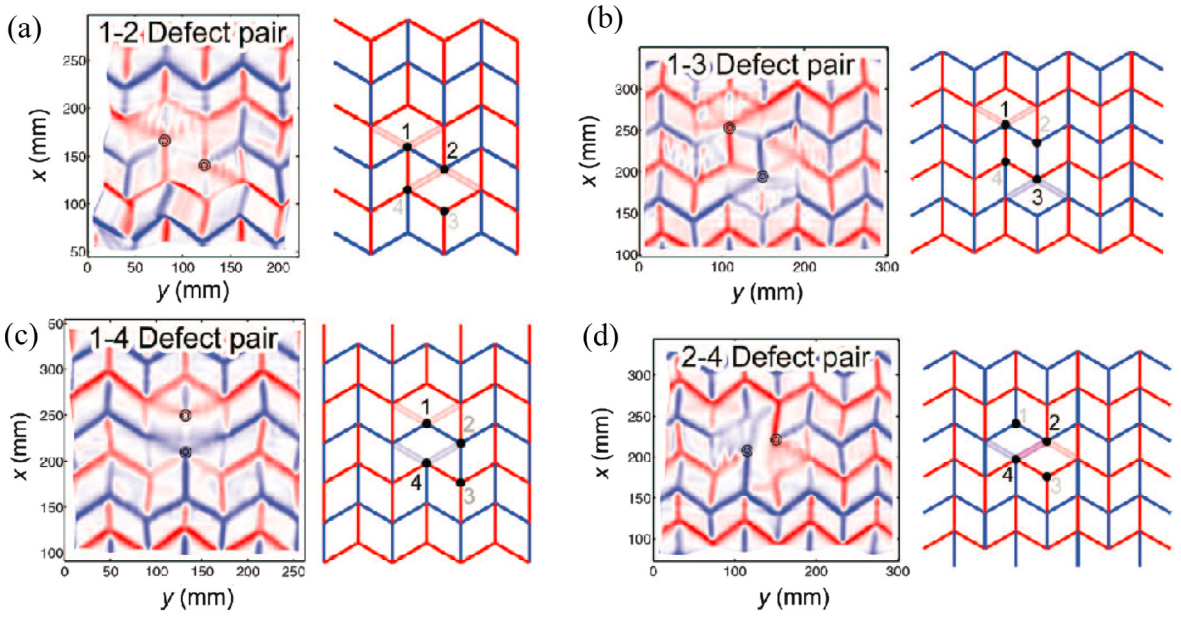

Fig. 12. Experimental data of two interacting pop-through defects. Mean curvature maps of (a) 1–2, (b) 1–3, (c) 1–4, and (d) a lattice vacancy 2–4 defect-pair configuration. The colour maps saturate at ±1 mm^{-1}. Schematic diagrams show defect placement (dots) and facet bending (double lines) [78].

permit plate bending, a specific example of bistability. Such elastic multistability in the folded planar structures may be desirable for the design of metamaterials. This is because elastic instability, including the symmetric water bomb vertex [161] and the hypersurface [178] (e.g., hypar [179]), allows a reconfiguration of the shape and the bulk properties [159]. We will further discuss the mechanisms related to geometrical frustration in Section 5.2.4.

Secondly, the non-periodic Ron Resch pattern [160,180,181] is gradually appearing as part of the discussion of mechanical metamaterials. In the 1960s and 1970s, Resch [180] proposed a series of origami tessellations via the insertion of a star-like folded tuck. Thus, this basic Resch-type pattern can also be called a star tuck (Fig. 11b). The design framework of Resch-like origami tessellations vary between polyhedral surfaces (Fig. 11b [160,181]). This non-periodic rigid origami folding pattern demonstrates a striking load bearing capability under axial compressive force [160]. Initial attempts reveal that higher order symmetry have even greater load bearing capability. Non-periodic Ron Resch tubes or domes need to be coupled with other origami patterns to achieve the desired load bearing.

Lastly, we introduce the rare square twist pattern (Fig. 11c). The reason for this scarcity in practice is due to computational modelling and simulation, rather than actual experimentation [182]. Specifically, in order to perform the folding of the square-twist pattern, we needed to consider two distinct modes of deformation, creasing and facet bending. In other words, the square twist cannot be folded by creasing alone. In the model proposed by Silverberg et al. [166], creasing is differentiated from bending in that creases represent a plastic mode of deformation, whereas bending is reversible. Mathematically, the traditional square twist folding pattern [179] has specific hidden degrees of freedom of bending separated by an energy gap from the degrees of freedom of creasing. This leads to a geometrically driven critical bifurcation between mono- and bistability, e.g., responsive micro-patterned hinges or creases [166,183]. Indeed, folding a piece of paper entails first the formation of a fold through bending, and then the creation of a crease. Square-twist-based mechanical metamaterials demonstrate a hysteresis in their folding dynamics when using temperature-responsive polymer gels, thereby they can be used to fabricate mechanical switches.

We need to add a final point here for the special case of kirigami (Fig. 13). Contrary to the paper folding of origami, kirigami is the art of paper cutting [184]. Paper cutting is emerging to create beautiful patterns and shapes in two-dimensional materials such as graphene and polymer films. Three promising routes have thus far been used to develop this type of kirigami metamaterials: One, kirigami itself has been used as two-dimensional materials [184–187]; another is lattice-based kirigami elements, combining the folding of origami with cutting and re-gluing techniques [188–190]; and a last technique combines the available cellular structure to create fabulous, complicated assemblies [191,192]. The various complex structures of two-dimensional materials related to kirigami, mentioned in the first case, is outside of the scope of this review. The idea of lattice-based kirigami in the second case can enable us to obtain various manmade crystallographic lattices, such as the honeycomb or kagome lattice [190]. Defect pairs are properly arranged and incorporated into an appropriate folding pattern to target a stepped surface, for instance by using arrays of disclination defect pairs on a dual or the honeycomb lattice (Fig. 13 [188,189]). A class of patterns combining origami folding techniques with kirigami is shown in Fig. 13b [191,192], which belongs to one-degree of freedom (DOF) cellular mechanical metamaterials [191,192], although the main purpose of this is to dislocate the zigzag strips of a Miura-ori pattern along the joining ridges.

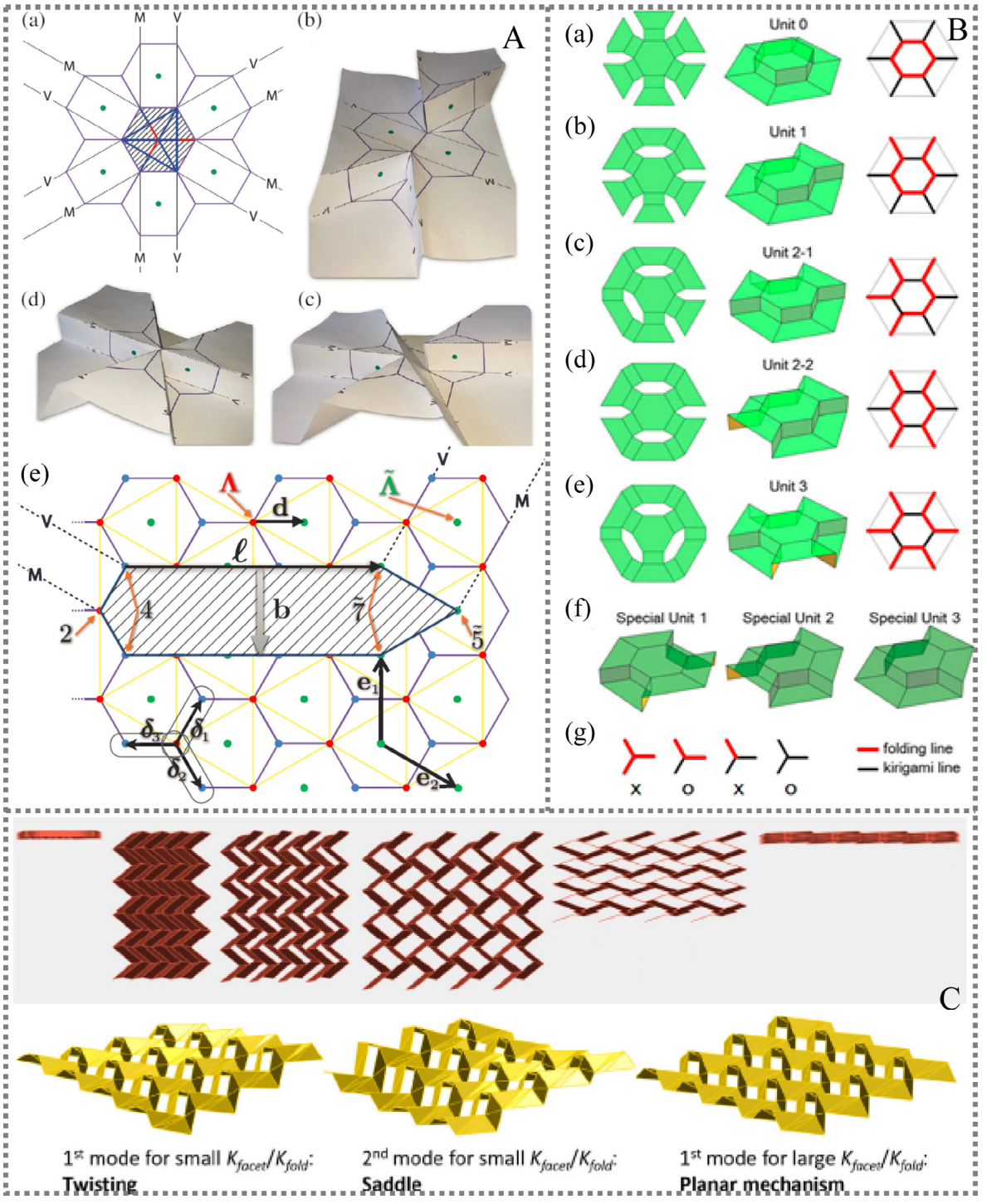

Fig. 13. Making the cut: kirigami metamaterials. (A) Lattice kirigami rules [188]. (a) The "sixon." basic template. (b) This structure is degenerate and can be split three different ways into matching 2–4 pairs with pop up and pop down configurations. (c) An intermediate state connecting (b) to the final state (d). (e) The two lattices Λ (red dots) and $\tilde{\Lambda}$ (green dots) offset by **d**. Yellow edges on Λ. We show the basis vectors of the lattices $\{e_i\}$ and the unit cells $\{\delta_i\}$. A 2–4 pair on the honeycomb is a standard 5–7 pair on Λ. The cut is absorbed by the $\bar{5}-\bar{7}$ pair on $\tilde{\Lambda}$ creating a partial climb. The plateaus of the 2–4 and $\bar{5}-\bar{7}$ pairs are different heights upon folding. (B) Algorithmic lattice kirigami [189]. (a–e) The basic building blocks of $\bar{5}-\bar{7}$ stepped surfaces. (Left) The unfolded configuration, where the excised hexagons sit on a larger-scale honeycomb lattice. (Middle) The folded configuration. (Right) A reduced representation suitable for easily designing target surfaces. (f) Folded configurations where the positive-climb paths of three dislocations converge. (g) Junction representation of the meeting of folding lines and cutting lines (i.e., places where excised regions had their edges identified) in the reduced representation. Only the junctions marked "O" represent allowed configurations. (C) Zigzag-base folded sheet [191]. Twisting, saddle-shaped and rigid origami behaviour (planar mechanism) of a 4×4 regular zigzag-unit-cell sheet with the holes oriented in various directions. Twisting and saddle-shaped modes are the first and the second predominant bending modes observed in materials with small values of $K_{\text{facet}}/K_{\text{fold}}$. Rigid origami behaviour is the predominant behaviour for large values of $K_{\text{facet}}/K_{\text{fold}}$.

Origami and kirigami, the arts of paper folding and paper cutting, create elegant patterns and shapes that have emerged as potential tools for the design of mechanical metamaterials, tuned by purely geometric criteria, particularly for two-dimensional materials (e.g., graphene, polymer films, etc.) [184,185]. The means for defining these cuts and for performing the folds are extending into the micro/nanoscale regime [186,187]. It is therefore possible that these emerging materials may be effectively applied to many types of advanced materials, such as brittle semiconductors.

One final remark about this area involves origami building blocks, the unit cell of origami-inspired frameworks, and particularly on their equivalent crystallographic classification (Fig. 14). Most of the origami metamaterials designed so far are based on the same single four-vertex geometry [193–195], i.e., four rigid panels connected by hinges that meet at a point form a four-vertex. This fundamental origami building block can fit into 16 special vertex types (Fig. 14A–E [196]) according to lattice theory. The concept of Gaussian curvature at a point on a unit radius sphere (the Gaussian sphere) [197], determi-

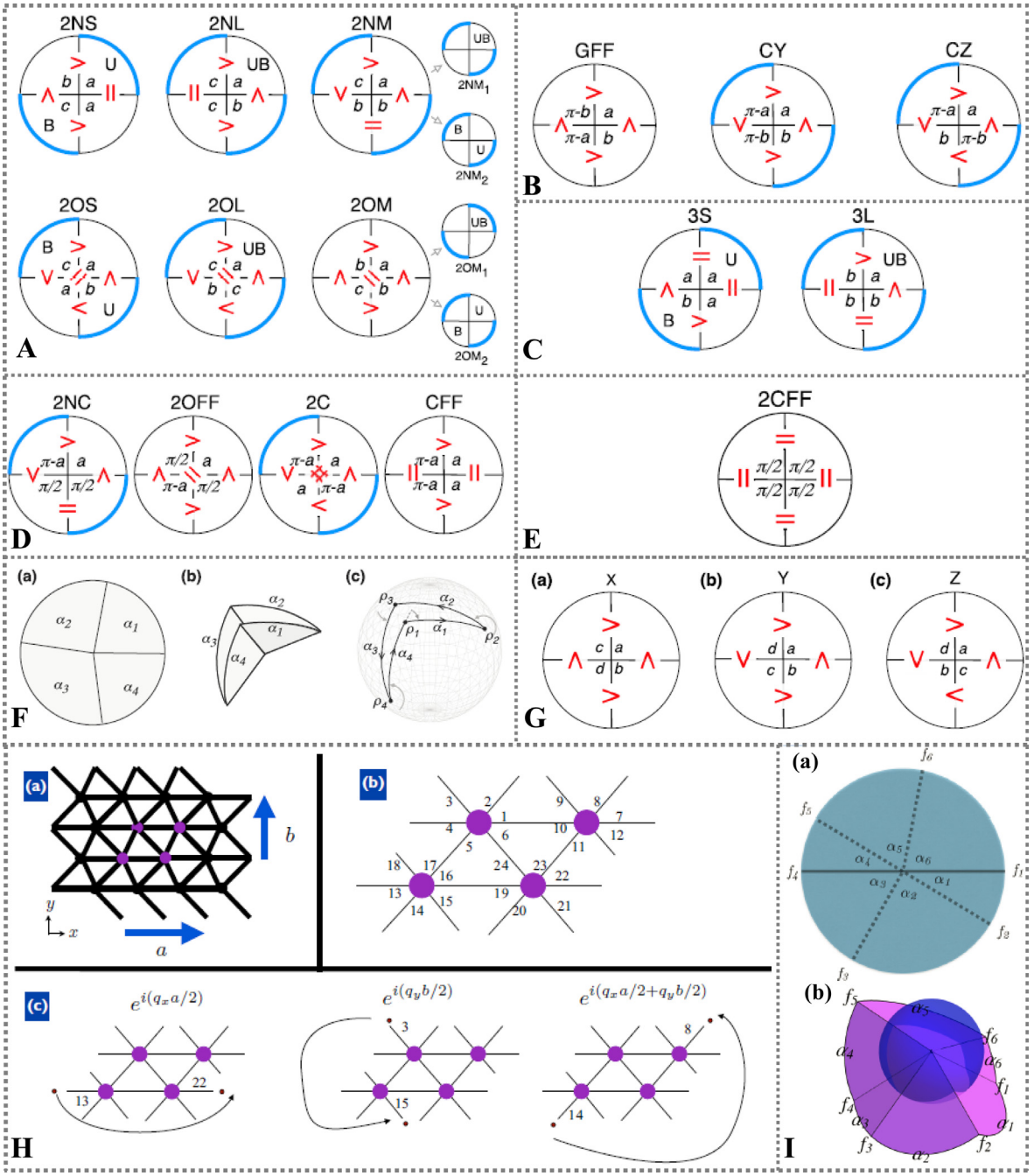

nes the possible mountain-valley arrangements and the resulting folding motions of Euclidean four-vertices [196]. Evans et al. [198] have also recast tessellated origami into the language of conventional lattice mechanics. While the crease pattern of a Miura-ori generally introduces only four folds per vertex, the bending of faces allows two extra folds per vertex. That is mean that the degree-6 vertex has its graph determined by the six sector angles α_i (Fig. 14I [198]). By doing so, we obtain a crease pattern that can be generalised to a triangulated lattice (Fig. 14H [198]), i.e., the kagome lattice (in Section 6.2.2), via crystallographic lattice theory. This formulation for examining the mechanics of origami tessellations can bridge origami and physics. To truly consider origami structures as a class of materials, methods are applied that are akin to solid mechanics. We can borrow from geometric crystallography knowledge of the Bravais crystal lattice, Miller indices, and even preferred crystallographic orientation, i.e., microtexture in Euler space represented by three Eulerian angles in Bunge notation [199], to provide a theoretical underpinning for the structural design of multistable mechanical metamaterials.

Almost all proposed origami-inspired mechanical metamaterial designs so far are based on the Miura-ori folding pattern [200], which has a single degree of freedom. There are many other origami-like structures with multiple degrees of freedom that can be used to design highly flexible and deformable three-dimensional structures [201]. Cellular origami coupled with the shapes of micro-/nanolattices and the theoretical instability of pattern transformation, will be addressed individually in Section 5.1.4. Various other shapes of origami structures (Fig. 11), such as kaleidocycles coming from continuously rotating n-jointed linkages [202], suggest that this type of structural design can offer potential to mechanical metamaterials. We will delve further into the details of folding mechanics in combination of other similar mechanical metamaterials in Section 5.2.3.

5.1.4. Cellular origami metamaterials

Extending origami design principles to three-dimensional cellular materials is now shaping foldable cellular metamaterials (Fig. 15). This type of mechanical metamaterials can be considered as a combination of structural design in micro-/nanolattices and newly developed origami patterns. The mechanics behind these are the same as the origami building blocks, i.e., instability mechanics, even in pattern transformation.

Two ways to combine them are stacked [79,157,193,203], or interleaved relations [204,205] (Fig. 15). Stacking origami was initially inspired by snapology, a type of modular unit-based origami where paper ribbons are used to create complex geometries, such as extruded polyhedra (Fig. 15c) [201]. We find that by stacking individual folded layers the symmetry of Miura-ori has been constructed [157]. The resulting rigid origami has been shown experimentally to be flat-foldable, according to deployment mechanisms. Additional freedom in the design of a metamaterial can be achieved by varying the fold pattern within each layer [157]. Nonetheless, one challenge for stacked cellular origami is to quantify a specific scaling value to assess effective density. This is primarily because a constructive relationship for relative density is not sufficient for the specific customer-responsive design of foldable cellular metamaterials. One important thing to consider is how to solve dynamic variation in the height of a stacking layer.

Another possibility for cellular origami is to interweave the origami tessellations into the given lattice pattern (Fig. 15). Interwoven cellular origami metamaterials may be derived from the assembly of rigidly folded origami tubes, tessellated to fill space through periodic and affine transformations [205,206]. For example, the anisotropic tube geometry consists of two orthogonal axes of interwoven tubes with high interfacial surface area, which is relatively stiff in the third orthogonal direction. These explorations suggest that the approximate closed-cell structures could yield the desired scaling factor with respect to low density and concurrently sufficient strength. For instance, the relative modulus can follow a power scaling law with a relative density of $E \sim \rho^{1.5}$ in its stiff (z-axis) orientation [204]. The power exponent increases to a value of 2

Fig. 14. Origami building blocks: 16 types of special four-vertices. Six codimension-1 special types arise if two sector angles are equal (A). Three more arise when sums of pairs are equal (B). Codimension-2 vertices include ones with three sector angles equal (C) and also those with two equal and sums of pairs equal (D). Note here this last type, CFF, is the base vertex for the classical Miura-ori pattern. The only codimension-3 vertex has all sector angles equal to $\pi/2$ (E). 2NS, 2NL, 2NM, 2OS, 2OL, and 2OM, where the "2, 3" stands for two or three angles being equal, "N" and "O" distinguish he whether the equal angles are arranged Next to or Opposite each other, and "S," "L," and "M" identify them as the Smallest, Largest or Middle, GFF denoting General Flat-Foldable ones, CY and CZ, with "C" denoting that they have Collinear folds and "Y" and "Z" signifying the parent generic type. The relative sizes of adjacent sector angles are indicated both by letters ($a < b < c < d$), and also by equal, less-than and greater-than signs. In addition, the dominant pair is indicated by the thick blue rim. (F) Geometry of a four-vertex that above-mentioned 16 special vertex types based on. (a) Illustration of flat four vertex geometry with sector angles α_i; (b) rendering in 3D of vertex in a partially folded state; (c) the vertex edges make a polygon on the unit sphere, where we use the vertex orientation (arrows) to define the folding angles ρ_i as the out-of-plane deviation angle from one plate to the next. (G) Generic four-vertices. The three types of generic vertices, X, Y, and Z, are determined by the arrangement of the ordered sector angles, $a < b < c < d$, around the vertex centre [196]. (H) A triangulated lattice theory for examining the mechanics of origami tessellations. (a) Miura-ori, without the assignment of mountain and valley folds, has a simple directed graph structure with a unit cell composed of four vertices. By tessellating these four vertices, the entire pattern emerges. Note that the tessellation is rectangular, with lattice vectors $\mathbf{a}_1 = a\hat{x}$ and $\mathbf{a}_2 = b\hat{y}$. (b) Each vertex has six folds, labelled in the fashion shown here. (c) In Fourier space, translations associated with connecting these folds together throughout the tessellation merely amounts to a phase factor associated with the appropriate wave number and lattice vector. Shown on the left is translating in the x direction. The middle shows translating in the y direction. The right shows that connecting the extra folds involves a diagonal translation across the unit cell. Note that the five internal folds have a phase factor identically equal to one. (I) Graph for a single vertex. This degree-6 vertex has its graph determined by the six sector angles α_i. Each crease has a dihedral angle f_i associated with it. In the flat case every $f_i = \pi$ or, equivalently, every fold angle is identically zero, since the fold angle is defined as the supplement of the dihedral angle. (b) By assigning fold angles to each crease, a three-dimensional embedding of the vertex (i.e., the folded form of the origami) is fully determined. Every face must rotate rigidly about the defined creases and the sector angles must remain constant. There is a limited set of fold angles that will solve these conditions [198].

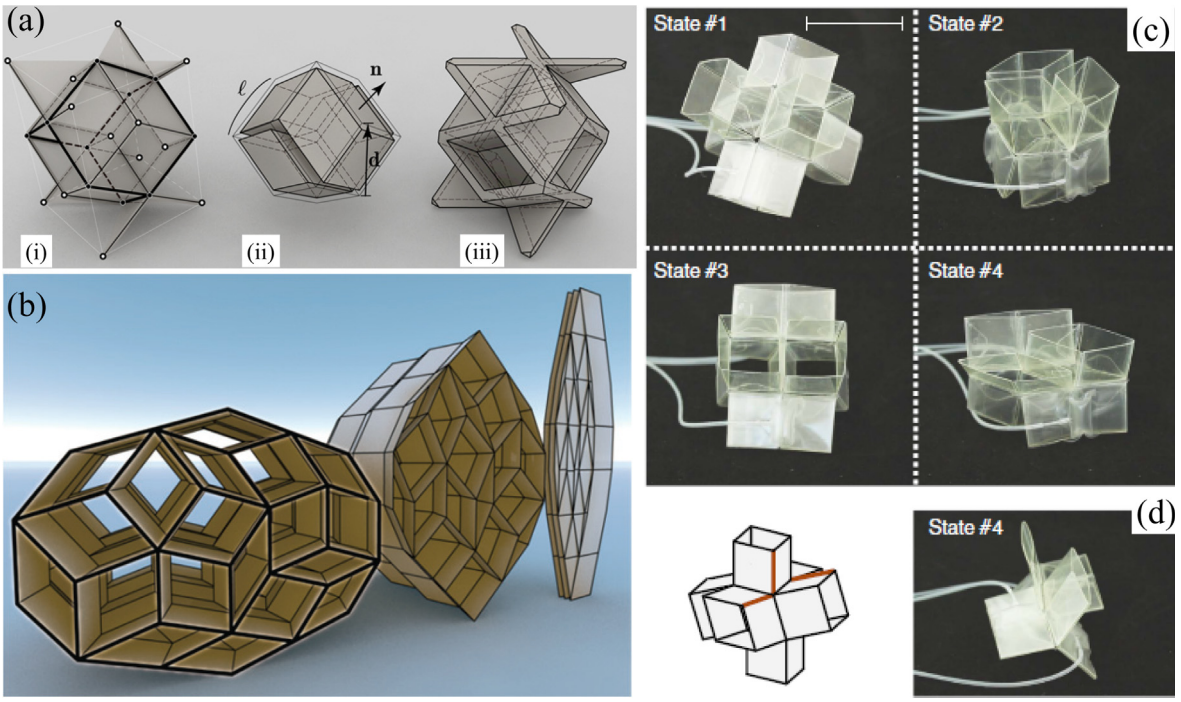

Fig. 15. Cellular origami metamaterials. (a) A unit cell of the interleaved tube cellular structure. Left: the white nodes have four incident edges while the black nodes have eight incident edges. The thick lines indicate edges with four incident facets while thin lines indicate edges with two incident facets. Middle: tubular deletions from the theoretical solid, to obtain the structure. Right: thickened cellular structure [204]. (b) Example of a rigid-foldable cellular structure constructed from a zonogon tiling (Penrose tiling) [205]. (c) Configurations obtained by actuating the unit cell (with 3 actuators). (e) Improved actuation strategy to reach state #4, where all six extruded rhombi are folded flat. As expected state #4 does not fold completely flat, but instead deforms into the state with lowest strain energy [201].

in the flexible orientations (*x*- and *y*-axes). These result are similar to the values in reversibly assembled cellular composite materials [207].

Extruded cube cellular origami structures have recast tessellated origami into the language of conventional lattice mechanics. Simultaneously, these attempts form a connection between more conventional materials and mechanical metamaterials constructed using an origami-based design. It is therefore possible to pattern creases, hinges, or folds into an otherwise flat sheet. If the mechanical properties of cells and patterns are not rigid, the coupled origami can exhibit temperature-dependent swelling. Thus these can produce other cellular origami mechanical metamaterials with temperature-dependent properties.

In brief, the geometry of origami provides a facile experimental platform to explore the various desired mechanical properties of a wide class of constraint-based metamaterials. These geometries and additional hidden degrees of freedom, such as facet stretching, facet shearing and crease torquing [166], offer great incentive to develop modern ultra-light and specific configurations with rich deformation modes (e.g., self-locking). The idea behind coupling geometry and physical properties for wrinkled membranes [208] and programmable metamaterials [78], is to tailor the bending and stretching energy barriers in thin shells [209,210], and thereby to obtain a broad range of multistable behaviours over a wide range of scale length [211]. For instance, in an analogy with the secondary structures of polymers that provide hidden lengths [183,212], the resistance to a predetermined force threshold can be achieved to make materials with extremely high toughness. The major challenge is now to delve further into the black box of how geometrical configurations and material properties are related, for instance how a folded sheet contributes to an overall mechanical response [162,213–215].

5.1.5. Pattern transformation: controllable stiffness

The definition of pattern transformation, a type of mechanical metamaterial, derives from a sort of tunable effective stiffness *E* in a given holy pattern under deformation. Specifically, this switchable metamaterial is similar to most examples of phase transition between microstructures. Here pattern transformation is from a form of matter with a defined periodic pattern to another on a larger scale. To be precise, it is a macroscopic phase change in the stress-strain properties when the metamaterial is compressed beyond a certain threshold. The underlying concept is a kind of cooperative buckling to make the metaproperties occur. These patterns are analogous to the equivalent crystal structures in different orientations, e.g. a tetragonal unit cell where the long axis points in different directions [67]. A macroscopic external stress can induce switching between patterns throughout the metamaterial.

Before starting, we need to make a clear distinction between pattern transformation and other mechanical metamaterials, particularly with emphasis on negative Poisson's ratio, i.e., the auxetic metamaterials in Section 7. In pattern transformation, the stiffness can change in the axial and normal directions under compression. This can lead to a variation in the corresponding Poisson's ratio in the duration of loading. That is to say, the incremental Poisson's ratio can be obtained, but the associated positive or negative sign may also change. Under some conditions, Poisson's ratio can be a large negative value, while under others it cannot be. This is different from the conventional fixed negative Poisson's ratio. This variable Poisson's ratio phenomenon also occurred in other mechanical metamaterials. Sometimes, this behaviour is called *programmable Poisson's ratio* or *tunable Poisson's ratio*, which is discussed further in Section 7.3. Another distinction is chiral metamaterials. These truly exist when the topology of the pattern is optimised in a chiral pattern [23]. Some overlapping between the sections occurs, see Section 5.1.2 for reference.

Two factors, with similar motif and tiling in the crystal structural construction, can determine one pattern transformation. In doing so, the pattern can be combined with pore shape (i.e. motif) and arrays of pores (i.e. tilings) in topology (Fig. 16). According to the geometric constraints of the tessellating Euclidean plane, various shapes of holes can be set in different tessellations. The shapes of holes can be regular circles, elliptical holes, or even irregular ones [216]. The tessellation of these hole settings can be one of four choices: square tiling, triangular tiling, trihexagonal tiling and rhombitrihexagonal tiling [23]. The geometry of the hole patterns plays an important role in mechanical metamaterials. Therefore, this subsection will discuss pattern transformation from these two perspectives: pore shape and pore arrays.

Firstly, the pore shape is relatively sensitive to both the onset of instability and the post-buckling behaviour. The effect can also be striking for square and triangular shapes, suddenly transforming into a periodic configuration of alternating,

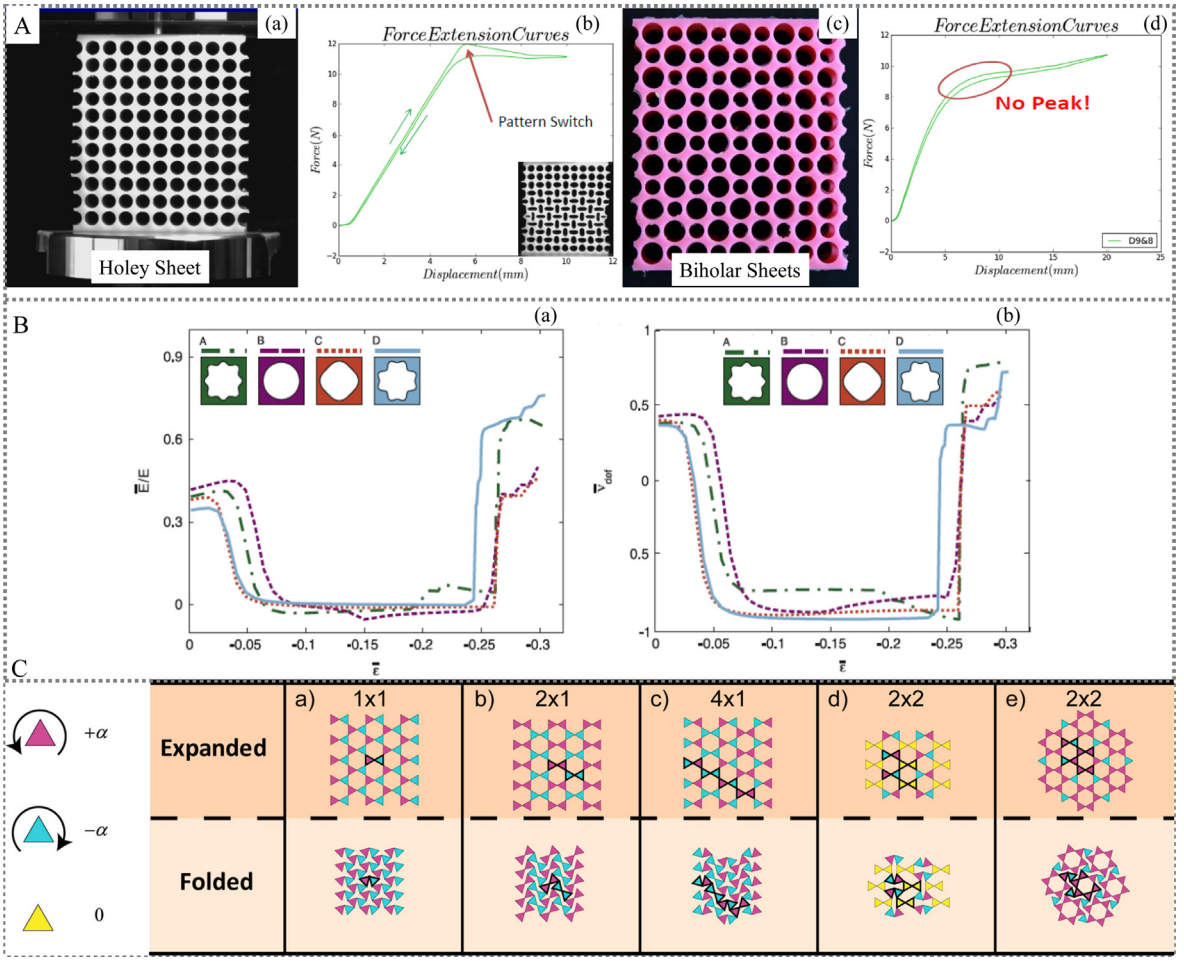

Fig. 16. Pattern transformation. (A) Patterns combined with the pore shape and the arrays of pores. Photo of an uncompressed (a) holy sheet [26], and (c) biholar sheet [221]. Force extension curves of (b) holy sheet, and (d) biholar sheet [81]. (B) Effect of pore shape [216]. Evolution of the macroscopic (a) incremental stiffness E_V/E and (b) Poisson's ratio with respect to the deformed configuration ν_{def} as a function of the macroscopic strain ε for four representative pore shapes in pattern transformation [220]. (C) A rigid kagome network. The basic unit cell for each folding mechanism is outlined in black. The colour of the triangles corresponds to their rotation. (a) Mode with a basic cell of size 1×1; (b) Mode with a basic cell of size 2×1; (c) Mode with a basic cell of size 4×1; (d) Mode with a basic cell of size 2×2; (e) Mode with a basic cell of size 2×2 [82].

mutually orthogonal ellipses with high-aspect ratios [24,81,216,217]. Computer analysis, known as shape and topological optimisation [218], has been routinely performed in an effort to identify the optimal shapes. This is expected to improve a certain performance under some constraints. Topological optimisation suggests that the response of mechanical metamaterials can be easily tuned by simply changing the shape of the holes with optimal compaction [219]. Overvelde et al. initially started to identify the effect of shape on material response by selecting three different hole shape [216]. After relating pore shape to a non-linear response, the initial response, elastic instability and post-buckling have been systematically explored to optimise the shape in periodic elastomeric structures [220].

To characterise the optimal pore shape, one generally can assess the effect of pore shape on the stress-strain response, on the incremental modulus of the structures, and on the evolution of the lateral strain (Fig. 16B) [216,220]. These observations demonstrate that there are three regimes in the stress-strain response that reflect the evolution of incremental stiffness and Poisson's ratio. Namely, the first region corresponds to the initial linear elastic stiffness. The second region plateaus when E is approximately equal to 0, after a sharp transition induced by instability. Finally, a sharp transition at $E > 0$ occurs when the pores collapse. These elegant findings provide compelling evidence that the pore shape can be used effectively to design material with desired properties. Therefore, it is also expected that attractive mechanical properties can be tailored, including Poisson's ratio, critical strain, but especially tunable stiffness.

Pore arrays combining different pore sizes can also be considered for topological optimisation of pattern transformation. For comparison, two patterns, holey sheets and biholar sheets (Fig. 16A [26,221]), are discussed in detail. In previous reports [26,80,81], *holey sheets* refer to quasi-2D slabs perforated with square arrays of holes having the same pore size. If the sheet have circular holes of two different sizes then they are known as *biholar sheets* [221].

The holey sheets can theoretically be approximated as a special lattice structure consisting of rigid regions connected by beams. The mechanics and structural properties of these cellular structures have rapidly been integrated into promising material designs for high energy absorption. When deformed beyond the initial linear elastic regime, significant energy absorption can be achieved in elastic metamaterials through large deformations and the collapse of cellular structures. Under compression a transition is made from linear elastic behaviour to either a yield or plateau stress or, in some instances, a yield with some subsequent strain hardening [80]. This nonlinear stress-strain behaviour usually comes from a member or a wall in the cell microstructure buckling. Then this can lead to localised deformation via collapsed bands, progressing through the structure at a relatively constant stress [222].

The biholar sheets have a negative Poisson ratio, while experimental results show that the strange peak in the force-compression curve is absent (Fig. 16A(d) [81]), instead of the completely regular pattern in the initial holey sheet [26,78,81]. A numerical simulation [223] reveals that an applied prestrain in uniaxial tension can delay the onset of the pattern transformation. Moreover, equilibrium dilation can interrupt the progress of the transitional states into elliptical patterns. Intrinsically, this effect originates from a broken rotational symmetry. By breaking the symmetry, highly nonlinear deformation coupling occurs along the two primary axes of biholar mechanical metamaterials [221]. Breaking the rotational symmetry can lead to buckling and snapping effects, as hysteresis corresponds to instability [224]. These findings suggest that the response of biholar sheets to uniaxial compression can be programmed by lateral confinement, allowing monotonic, nonmonotonic, and hysteretic behaviour [221]. This is similar to a sort of programmable mechanical metamaterial.

Finally, we need to talk a little about the mechanics of this type of mechanical metamaterials, mainly elastic material instabilities. Elastic instabilities originate from a softening in the material response (decay of tangent moduli) induced by a dilating mechanical deformation. Because of this, elastic instabilities traditionally can be viewed as a mode of failure. Pattern transformation here aims to achieve an appropriate failure mode, where one of its intrinsic characteristics is a sort of tunable stiffness (springiness). It is this reversible elastic instability that can trigger pattern changing. This pattern transformation can therefore be used to tailor material properties, such as tunable negative Poisson's ratio (switchable auxetics) [26,216,225,226], chiral patterns [74,152], phononic and photonic switches [224], and other reprogrammable colour displays [227,228]. It is worth mentioning that a reversible chiral symmetry-breaking mechanism, or rigid kagome folding lattice (Fig. 16C [82]), can be introduced to pattern transformation. Nonetheless, only a few systems have shown to be capable of reversibly switching between non-chiral and chiral configurations [23]. In any case, porous structures can possibly enable the reversible switching between the initial non-chiral and the buckled chiral pattern.

Finally we introduce the comprehensive studies from Bertoldi's group [18,23,26,80–82,135,216,217,220,226,228] in pattern transformation. Current results [229] demonstrate that a structure having holes of the same size cannot switch to another variant by using an external mechanical force. If an elastic structure is comprise of a slab of elastomers having a regular hole array of two sizes (Fig. 17b) [229], it is technically possible to realise pattern transformation, or even more evocatively, a shape memory effect. This is possibly by simply changing the external pressure, for instance, by using a pressure-controlled chamber. In other words, when exerting compressive stress isotropically to the structure, these holes can either stay open and form a square lattice, or collapse and twist the lattice into a rectangular shape, depending on the differential pressure between the exterior atmosphere and the pressure inside the sealed holes. This therefore allows us to achieve a *snap through* [52,230] of stress, similar to the switching behaviour in chiral and phononic properties [18], as the strain ε increased during compression (Fig. 17c) [229].

In a word, mechanical instabilities in periodic porous elastic structures can open avenues for a wide range of applications in smart materials. Their architectures can be dramatically changed in response to diverse external stimuli [216,231,232]. For instance, a purely mechanical metamaterial can stand alone, in contrast to conventional piezoelectric materials [233] that require an electric field. The major challenge of this type of mechanical metamaterials is to extend them to the other

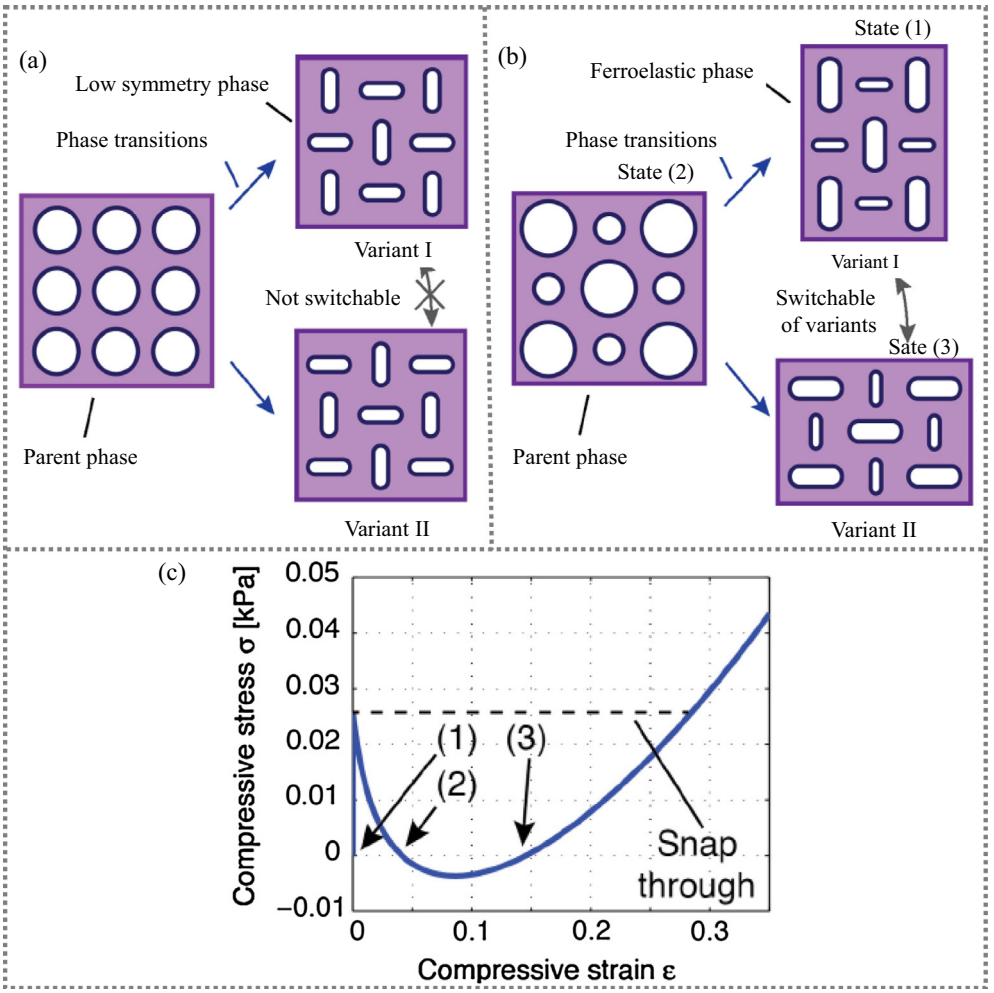

Fig. 17. Change of phases and switching between variants [229]. (a) For an elastomeric block containing holes of the same size, the parent phase transforms to a low-symmetry phase. In the low-symmetry phase, the structure has two variants of the same state of spontaneous strain, so that one variant cannot be switched to the other under external force. (b) For an elastomeric block containing holes of different sizes, the parent phase transforms to a ferroelectric phase. In the ferroelectric phase, the structure has two variants of different states of spontaneous strain, so that one variant can be switched to the other variant by an external mechanical force. (c) Simulated relation of the compressive stress σ and the compressive strain ε of a unit cell in (b) during domain switching.

parent materials (e.g. metals or alloys), not including soft materials. Current studies [185,226,234,235] indicate that totally different pattern transformations for sheets into a wide range of desired shapes and patterns can be introduced through a set of simple cuts, generating a multilevel hierarchy and different motifs. Each choice of hierarchical cut motif and cut level allows the material to expand into a unique structure with a unique set of properties. This can reveal an intriguing new insight into engineering the mechanical properties that define mechanical metamaterials.

5.2. Design principles behind structures

The purpose of this subsection is to describe the mechanism behind design principles. These include, (i) Maxwell's criterion and material mechanics for micro-/nanolattice metamaterials, (ii) topological optimisation of chiral/anti chiral metamaterials, and other pattern arrays, (iii) folding theory suitable for origami or kirigami, and cellular origami metamaterials, (iv) geometrical frustration involving nearly all mechanical metamaterials, pattern transformation, origami, and even cellular metamaterials. The reason this subsection is independent of Section 5.1 is that some mechanisms are independent of the various structural system. For example, the theory of elastic instability in geometrical frustration can be fundamental for the origami-inspired design. Also, it can be a pattern design for pattern transformation. It can be applied to the topographical optimisation of chiral/anti-chiral frameworks. Finally, it can be used for the analysis of failure mode in micro-/nanolattice metamaterials. That is why we organise this subsection to discuss some essential mechanisms behind the fabulous structural frameworks. Additionally, we believe that any complexities must be based on the simplest elements or attributes. Here we are as concerned as possible with the essentials.

5.2.1. Maxwell's criterion and material mechanics

Maxwell's criterion is essential for the design the micro-/nanolattice metamaterials. The basic structure that Maxwell analysed was a pin-jointed frame made of b struts and j frictionless joints. These frames can be hinged at their corners (Fig. 4). If a two-dimensional framework is barely rigid and cannot fold when loaded, at that time one of the properties of this structure is,

$$b - 2j + 3 = 0 \tag{8}$$

Extending to a three-dimensional framework, the equation will be,

$$b - 3j + 6 = 0 \tag{9}$$

Later on, Calladine et al. [236] generalised this to the widely accepted Maxwell rule in three-dimensional space,

$$b - 3j + 6 = s - m \tag{10}$$

where s and m count the states of self-stress and mechanisms, respectively. Each of these can be determined by finding the rank of the equilibrium matrix. The corresponding matrix formalism describes the frame in a full structural analysis [236]. Maxwell's criterion suggests that the number of self-stresses and mechanisms can determine the nature of the engineered metamaterial. Based on this criterion, a stretch-dominated structure will be defined in Section 5.1.1.2. For further detailed mechanics, refer to the referenced literature [84,86,236].

Material mechanics involves two main laws, the Hall and Petch hardening law for plastic flow in metals, and Griffith's law for the lack of plastic flow in ceramics [237]. Firstly, plastic flow in metals generally occurs by motion of dislocations along a preferential slip system. As dislocation motion is hindered by grain boundaries, the yield strength of a polycrystalline metal increases with reducing grain size. This hardening law was formalised by Hall and Petch as follows [238,239]:

$$\sigma_Y = \sigma_0 + \frac{k}{\sqrt{d}} \tag{11}$$

where σ_0 expresses the resistance to dislocation motion through the lattice, k is a material parameter, and d is the average grain size.

This equation predicts enormous strengthening as the grain size is reduced to the atomic scale (and the microstructure becomes amorphous). In practice, once the grain size drops below 10 nm, plasticity is controlled by other mechanisms (primarily grain boundary sliding [240] and shear banding [241]). For most metals, these mechanisms induce softening as the grain size reduce, with the implication that optimal yield strength is achieved at a grain size of ~10–20 nm. Nevertheless, the large surface energy associated with extensive grain boundaries makes the architecture much more challenging.

Secondly, the lack of plastic flow at the crack tip results in low toughness, and causes failure at applied stresses much lower than the yield strength of the material. According to Griffith's law [242], the fracture strength of a material, σ_f, can be expressed by the following relation:

$$\sigma_f = \frac{K_c}{Y\sqrt{a}} \tag{12}$$

where a denotes the size of the largest crack in the material (assuming that cracks are uniformly distributed in all directions), Y is a numerical constant, and K_c is the fracture toughness (a material property that expresses resistance to crack growth).

Finally, Ashby charts (Fig. 5) are typically used for material selection considering multiple requirements. This chart can be established by means of basic engineering analysis that reveals the material indices (a combination of properties) corresponding to each performance metric. Any two indices can be cross-plotted in a log-log chart that encompasses the realm of existing materials [237]. For example, in terms of an Ashby-chart, a universal scaling law is therefore characterised for effective stiffness and for strength as a function of the density (Fig. 5). By contrast, when ceramic octet-truss nanolattice structures were created with wall thicknesses of 5–60 nm and densities of 6.3–258 kg per cubic metre, their strength and Young's modulus follow a power law scaling with the relative density as $E \sim \rho^{1.76}$ and $E \sim \rho^{1.61}$ [106,243]. This implies that the size difference (micro- or nanoscale here) between the smallest and largest structural features will determine the degree of hierarchy that can be achieved. In any case, these micro-structured lattices enable the exploration of the potential nanoscale mechanical effects, such as size effects in plasticity and fracturing, thereby enhancing the desired mechanical properties of metamaterials.

5.2.2. Topological optimisation

The topological optimisation for structured metamaterials can be determined from theory and, reducing the design problem to scale [237]. Some types of pattern transformation can be simplified to a classical Euler-Bernoulli beam, which can further be modified to incorporate non-uniform elastic beams, similar to the classical structures of auxetic metamaterials addressed in Section 7. Various lattice structures can be reduce to a single beam subject and the action to a set of linear and torsional springs, thereby the problem can be solved through a transfer matrix method [244]. Thus, we are at present using previous and elegant theoretical studies, and thus can benefit from brainstorming before realising myriad fabrication techniques.

Mathematically, the optimisation goal is defined as minimising the error between the actual and the pre-defined values of parameters over a discrete range [245]. Generally, to ensure scalable fabrication of certain architectures, several geometric constraints are imposed on the topological optimisation design problem. A requirement of uniform structural features can be implemented as a combination of imposing a minimum and a maximum length scale. In micro-/nanolattice metamaterials, the topological optimisation step can lead to a beam-like layout. The lattice framework may be converted into a simplified design composed of a set of parameterised unit cells [245]. The solution to this problem is typically plotted on a log-log scale. In the case of pattern transformation, the kink in the optimal design curve delineates the transition between buckling-dominated and yield-dominated designs [113,246].

Computer analysis to optimise the shape and topology [218] has been performed routinely in an effort to identify the optimal shapes and to improve performance under some constraints. In pattern transformation, the response of mechanical metamaterials can be easily tuned by simply changing the shape of the holes under optimal compaction [219]. Therefore, it is possible topological optimisation will play an increasingly significant role in the design of mechanical metamaterials, particularly as computer techniques advance.

5.2.3. Folding features

The folding of origami structures involves bending deformations that are not explicit in the crease patterns [182]. Silverberg et al. [78,166,198] have elegantly explored the assembly. Simultaneously, recent studies from Overvelde et al. [201] extended snapology to cellular origami metamaterials.

To truly consider and understand the folding theory behind origami-inspired metamaterials, methods akin to solid mechanics must be developed. Particularly, the study of mechanically frustrated origami leading to multistable metamaterials should be conducted [194,196]. Generally, the origami-based design can be subdivided into two major branches, the origami-inspired design and origami-adapted design. The former is extracted from the concept of origami to obtain stiff and lightweight structures that are manufactured by folding flat sheets, such as self-folding membranes [247], sandwich panels with origami cores [168] (called chevron folded paper [248]), cellular metamaterials [157,204], and also molecular origami with precision lighting [21,164]. The latter draws directly from classical origami models to obtain flexible, deployable devices [249–251], particularly for engineering the aspects of origami [170], such as micro/mesoscale folded stents [252], and macroscale solar panels for space missions [169,253–255]. These prototype origami models created by various origami artists can be found in books by Lang [163] and Shafer [167], as well as an elegant review in origami-inspired active structures [164,212]. This brief summary primarily focuses on the former origami-inspired mechanical metamaterials associated with the deformation kinematics. If required, these models can be easily extended to include simple constitutive behaviour at the fold lines [213,256], for instance, for elastic or plastic behaviour [163].

The origami idea can be found ubiquitously in micro- and nanofabrication. An example of capillary origami is shown in Fig. 18a [257], the interaction between elasticity and capillarity can be used to produce three-dimensional structures through spontaneously wrapping a liquid droplet in a planar sheet. These experiments suggest that a wide variety of resulting encapsulated shapes, whether spherical, cubic, or triangular (Fig. 18a), can be achieved by tailoring the initial sheet

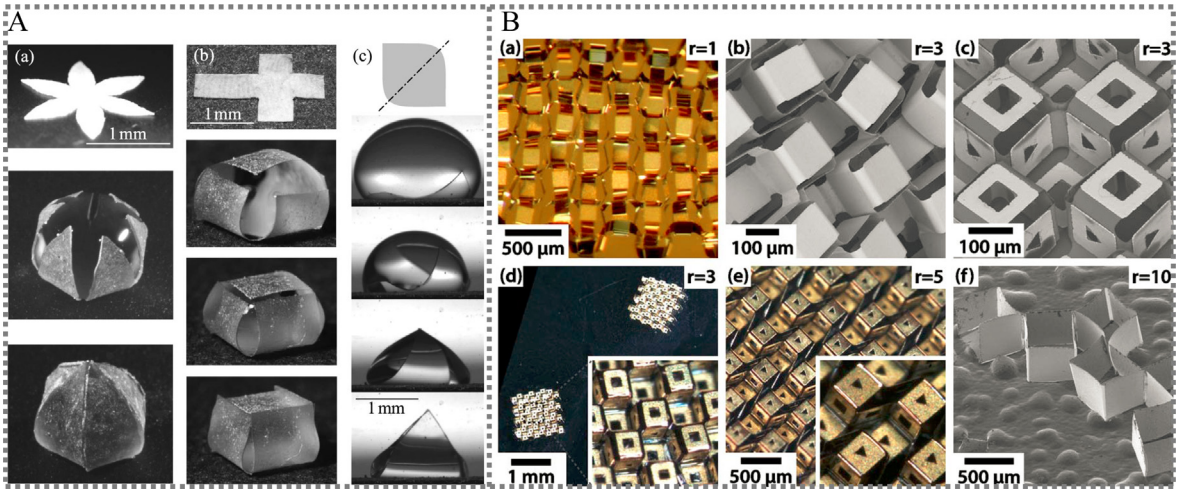

Fig. 18. Capillary origami: spontaneous wrapping of a droplet with an elastic sheet [257]. (A) Tuning of the initial flat shape to obtain (a) a spherical encapsulation, (b) a cubic encapsulation, or (c) a triangular mode-2 fold. (B) Microassembly based on hands free origami with bidirectional curvature [258]. Bidirectional origami used to spontaneously assemble complex microscale cubic cores with varying r ratios, where r refers to the ratio of rigid panel length and hinge length. (a) Optical image of a core with $r = 1$. (b) SEM micrograph of a core with $r = 3$. (c) SEM micrograph of a lithographically patterned core with $r = 3$ featuring square pores on horizontal faces and triangular pores on vertical faces. (d) Optical image of the entire structure shown in (c) with 224 hinges, magnified view inset. (e) Optical image of a core with $r = 5$ featuring triangular pores on horizontal faces and square pores on vertical faces, magnified view inset. (f) SEM micrograph of a torn portion of a core with $r = 10$.

geometry. In addition to liquid droplets, thin films of patterned metallic, semiconducting, and polymeric materials can also be used to create a variety of functional structures. A brilliant idea [258] to obtain spontaneous bidirectional folds of any desired angle consists of using a sacrificial layer. This layer can be dissolved causing the sheet to assemble while being lifted off the substrate (Fig. 18b [258]). The folding and unfolding of complex origami structures (Fig. 18) offers a promising insight to the fields of tissue culture, deployable medical devices, robotics, sensors, auxetic materials, and 3D circuitry.

The extension of origami design principles to three-dimensional cellular materials is now shaping foldable cellular metamaterials, as discussed in Section 5.1.4. Two such structures can be used in combination by assembling them into stacks [79,157] or interwoven structures [204], or other architectures currently residing in the imagination [204,205]. For example, a periodic structure can consist of extruded cubes [201]. A family of prismatic structures include all the possible prismatic deployable frameworks consisting of quadrilateral facets and four-crease vertices [193].

5.2.4. Geometrical frustration and elastic instability

Geometrical frustration refers to a theoretical system that cannot simultaneously minimise all interactions because of geometric constraints [135,259]. This phenomenon plays a major role in many systems leading to disordered state configurations. For instance, we can find geometrical frustration in the kagome lattice in pattern transformation, in the Miura-ori pattern in origami-inspired metamaterials, and in the chiral/anti-chiral arrangement of mechanical metamaterials. The origin of this phenomenon can be the arrangement of spins with antiferromagnetic interactions on a triangle. In contrast to the case of a square, each spin on a triangle cannot be anti-aligned with both of its neighbours (Fig. 19 [135]). As such, the system is frustrated and is characterised by degenerate ground states. This suggests that geometrical frustration typically gives rise to disordered configurations. In mechanical metamaterials, this mechanism becomes significant in generating order in frustrated systems, e.g., buckling-induced geometrically frustrated triangular cellular structures [135]. Therefore, a potential research route couples elasticity and geometrical frustration in continuum structures.

The interaction between structure and elastic instability is becoming an efficient method for the rational design of mechanical metamaterials. Elastic instability can be used as a route to uni-directional, planar, and auxetic behaviour [244]. In an example of holy sheets in pattern transformation, mechanical instability plays a significant role in complex ordered patterns [135]. Indeed, elastic material instabilities originate from a softening of the material response and a decay of tangent moduli induced by a dilating mechanical deformation. That is why tunable stiffness can be achieved by elastic instabilities that are traditionally viewed as a failure mode. Furthermore, the number of constraints, struts in the case of the Maxwell frames, can also lead to a special isostatic state. Additionally, temperature can also influence the mechanical instability of mechanical metamaterials [260]. In origami-inspired metamaterials, the geometry of the Miura-ori can be considered as a decoration of the folds with torsional springs, and thereby revealing nonlinear rigidity and bending responses [196]. It is also worth mentioning the work of Hecke et al. [39,159,196,221,261–265]. These studies range from an initial jamming system [39,261–264], to pattern transformation [221,265], to currently the origami structure [159,196]. As we can see from these previous studies, the only constant is the buckling instability of structures, which is theoretical fundamental to all of these findings.

In the case of one pattern transformation, the collapsed surfaces of periodically buckled patterns in perfect cellular materials are essential to the onset of failure in the corresponding real materials that contain inevitable imperfections in their underlying microstructures. Buckling stress can be quantified to obtain an upper boundary for the initial failure in some two-dimensional cellular structures, including square/triangular grids, chiral and hierarchical honeycombs (Fig. 20

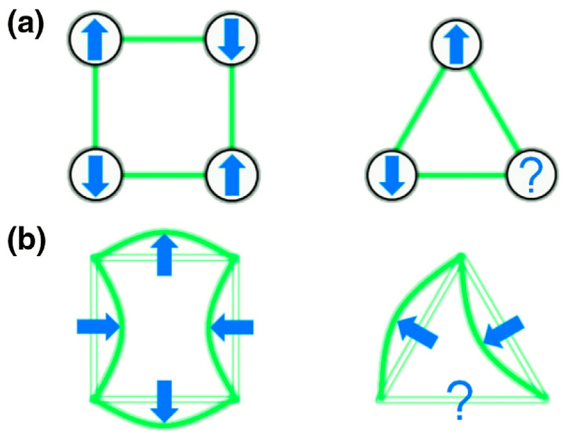

Fig. 19. Mechanical instability induced geometrically frustrated triangular structures [135]. Geometrical frustration. (a) In antiferromagnetic systems nearest neighbour spins want to align in opposite directions. This rule can be easily satisfied on a square. However, due to geometrical frustration it is not possible to satisfy it on a triangle. (b) Similarly, buckled beams on frames want to preserve angles at joints to minimize the deformation energy. Again this can be realized for square frames, but not for frustrated triangular frames.

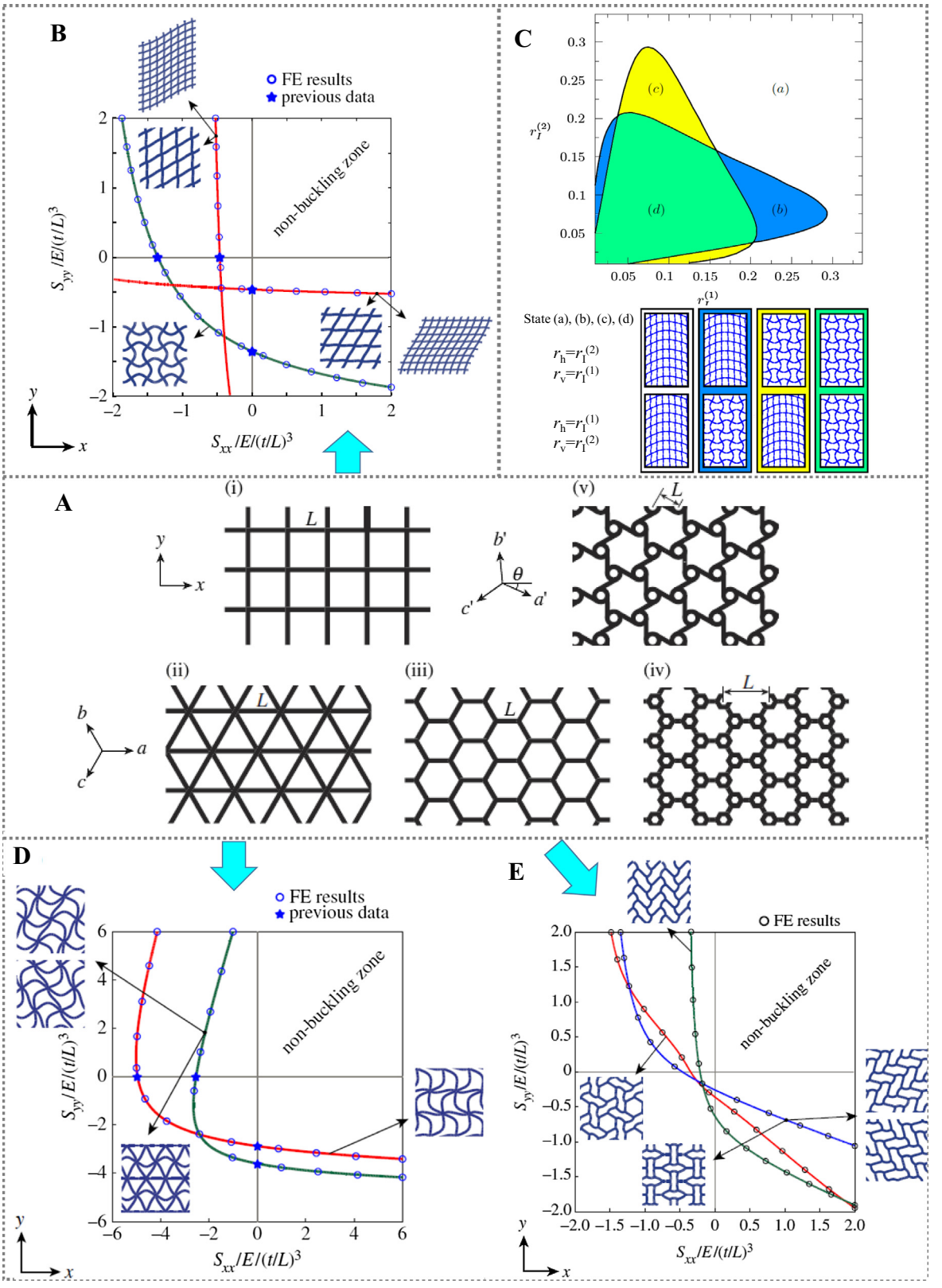
B
FE results
previous data
non-buckling zone
$S_{yy}/E/(t/L)^3$
$S_{xx}/E/(t/L)^3$
C
(a)
(b)
(c)
(d)
$r_I^{(2)}$
$r_I^{(1)}$
State (a), (b), (c), (d)
$r_h=r_1^{(2)}$
$r_v=r_1^{(1)}$
$r_h=r_1^{(1)}$
$r_v=r_1^{(2)}$
A
(i)
(ii)
(iii)
(iv)
(v)
L
θ
D
FE results
previous data
non-buckling zone
E
FE results
non-buckling zone

[74,244]). Specifically, we need to be careful of the effect of cell wall lateral loads (i.e. the non-axial components of the cell wall reaction force) suppressing the instability of periodic structures. For instance, the lateral reaction forces in cell walls are essentially zero in a triangular grid with a stretching dominated behaviour. As a result, the cell walls in the structure do not undergo a pre-buckling bending deformation. Bifurcation of the macroscopic load–displacement curve can be observed under all stress states. Thus, although we have followed the fundamental buckling rules, buckling of different period patterns carries various failure modes, such as secondary modes of buckling in hexagonal and triangular honeycombs. Additionally, the amount of theoretical work needs to be quantified in periodic patterns with distinct shapes, to combine plastic-collapse criteria [266]. It will then be possible to construct comprehensive multi-axial, multi-failure surfaces for cellular structures.

5.3. Enhanced mechanical properties

This subsection will deal with some enhanced mechanical properties that are shared by all mechanical metamaterials associated with stiffness. These intriguing properties include ultra-stiffness and lightweight, tunable stiffness, and some other failure modes. Specifically, the significant mechanical properties that these micro-/nanolattice mechanical metamaterials share is a high strength/stiffness at low density, while other properties can also be found, such as a high stiffness and a high damping coefficient in acoustics metamaterials, a negative Poisson's ratio in auxetics, as discussed in Section 7, a negative coefficient of thermal expansion, as discussed in Section 6.3.3, and other tunable functional properties. Some related properties can be found in Section 5.1.

5.3.1. Ultra-stiffness and low density

In micro-/nanolattice metamaterials, a decrease in density can bring about a drastic degradation in the corresponding mechanical properties. This is because the structural elements will experience a bending deformation at the ligament level under a macroscopically applied load [89]. In the cellular materials found in nature, the scaling factor is usually a power of two (quadratic) or three (cubic) or higher, leading to deleterious nonlinear effects that result in a dramatic loss of stiffness with decreasing density. Natural materials tend to have more random variation in pore size and distributions that lead to bending under stress. The strength-to-density ratio of the relative compressive stiffness and yield strength of these structures theoretically show a linear scaling relationship.

The stiffness and density scale linearly over this range of magnitudes.

$$\frac{E}{E_s} \propto \left(\frac{\rho}{\rho_s}\right)^n, \quad \frac{\sigma}{\sigma_s} \propto \left(\frac{\rho}{\rho_s}\right)^n \tag{13}$$

where the power n is the scaling relationship between relative material density and the relative mechanical property. The related metallic micro-/nanolattice can be found in work presented by Jacobsen et al. [66,89,108,118,134,267–269].

5.3.2. Tunable stiffness

Tunable stiffness can be achieved by pattern transformation and chiral/anti-chiral metamaterials. In pattern transformation, as some extensive studies [216,220] have reported, the pore shape has a strong effect on both the onset of instability and on the post-buckling behaviour. This is particularly true when square or triangular arrays of circular hole patterns are suddenly transformed into a periodic configuration of alternating, mutually orthogonal ellipses with a high-aspect ratio [24,81,216,217]. An elastic metamaterial with dynamically controllable stiffness emerged that can be employed using a remote magnetic force to adjust its vibration absorption properties in acoustic applications [270].

A sufficiently large amount of prestrain can prevent pattern transformation, leading to the monotonous pattern of ellipses [223]. These deformed configurations suggest that the appearance of transitional states in the presence of prestraining is a consequence of the particular combination of the selected polymer and solvent. In other words, there might exist competition between tensile stress due to prestraining and compressive stress due to solvent swelling [24]. This would allow us to create and design a richer variety of periodic patterns from one polymeric film with a square lattice of circular holes.

It is noted that here negative stiffness in acoustic metamaterials has a slightly different meaning than in mechanical metamaterials. Both are denoted as the general stiffness, referring to the ratio of the generalised force to the generalised displacement. In acoustic metamaterials [270,271], negative stiffness and negative density are limited to the stiffness of

Fig. 20. Buckling of some two-dimensional cellular structures including square/triangular grids, chiral and hierarchical honeycombs under a general macroscopic stress state [74]. (A). Types of lattice structures analysed by the beam-column matrix method: (i) square grid, (ii) triangular grid, (iii) hexagonal honeycomb, (iv) hierarchical hexagonal honeycomb, and (v) tri-chiral honeycomb. The angle θ gives the orientation of straight walls in the tri-chiral lattice. Buckling of (B) square honeycomb according to swaying, non-swaying and long-wave modes of buckling, (C) The response of a square system with the vertical and horizontal beams discontinuity in second moment of area described by parameters r_v and r_h respectively. All other parameters are equal in the two sets of beams. For each pair of values $(r_I^{(1)}, r_I^{(2)})$, two calculations are performed: $r_v = r_I^{(1)}$; $r_h = r_I^{(2)}$ and $r_v = r_I^{(2)}$; $r_h = r_I^{(1)}$. Region (a) depicts the area of parameter space where long wavelength instability is the active mode in both orientations, (d) shows where short wavelength mode will be active for both, while (b) and (c) show where the two orientations will give different modes [244]. (D) the triangular grid according to modes I and II of buckling, under x-y biaxial loading. (E) Biaxial buckling collapse of regular hexagonal honeycomb under biaxial loading along x (the so-called armchair or ribbon direction) and y (the so-called zigzag or transverse direction) according to uniaxial, biaxial and flower-like modes of buckling [74].

the matrix in the effective governing equations of design structure via the boundary conditions of wave propagation [272]. In mechanical metamaterials, stiffness is defined as the mechanical properties without acoustic boundary conditions. Mechanical metamaterials could perhaps be used to independently tune the bulk modulus (permittivity) and density (permeability in electromagnetic or acoustic metamaterials. Elastic metamaterials that independently realise negative density and stiffness are emerging constantly [273,274].

5.3.3. Failure mode

Here failure mode can be triggered by a state of stress in the micro-/nanolattice metamaterials, rather than the material mechanics themselves, as discussed in Section 5.2.1. Generally in hollow-tube lattice structures, the failure modes are associated with a combination of three competing mechanisms: fractures in the tube walls, Euler (beam) buckling of a truss member or local (shell) buckling [134]. In the nanolattice structures, however, two sets of failure modes dominate: yielding (or elastic buckling) versus shell buckling, and yielding versus Euler buckling [106].

In most cases, yielding in the tubes will occur under a state of tension, whereas, Euler and shell buckling will occur under a state of compression [41,97]. For instance, in an idealised pin-jointed stretch-dominated structure, the stretching of the horizontal members under tension (tube yielding) will govern the strength and stiffness of the lattice [97]. In this case, the beams in these lattices are assumed to only experience uniaxial tensile or compressive stresses. In the case of a hollow lattice, shell wall bending can occur at constrained nodes during the load transfer, thereby having a detrimental effect on the strength and stiffness. As such, a large concentration of stress in the vicinity of the nodes can cause large deflections and ovalisation at the nodes, and vice versa [106,108]. A study of a stainless steel microlattice structure under states of tensile and compressive stress indicates that the distribution of this localised stress in the strut members is responsible for a macroscopic cracking mode, such as tensile opening and shear cracking, and a ductile fracture for a transgranular form [275].

Here we can take the example of a failure mode in metallic microlattice structures via an emerging selective laser melting (SLM) technology. The investigation of the localised stress field near the joint [275] reveals the nature and evolution of stress: the tensile stress mainly concentrates on the top and bottom surfaces of a nodal joint, while the compressive stress largely on the lateral surface of the joint. Accordingly, this development of localised stress states (tension or compression) would lead to different crack separation modes (Fig. 21 [275]) inside the material components of the microlattice during the fracture process.

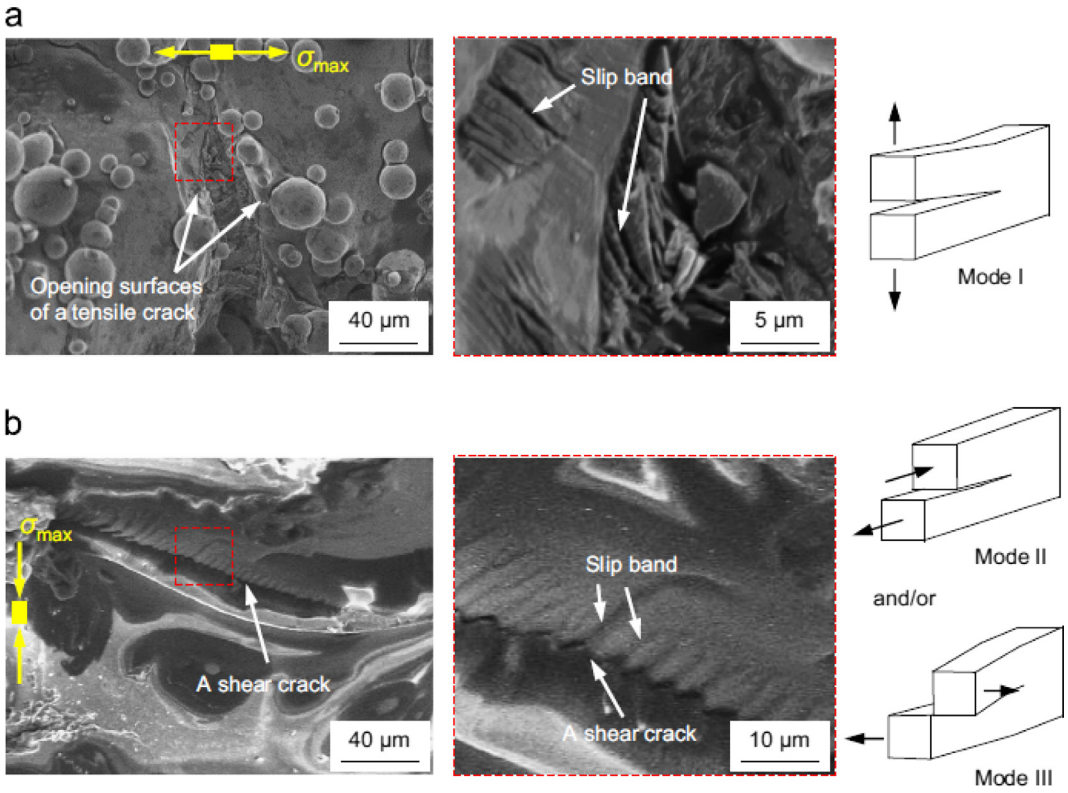

Fig. 21. Failure behaviour in selective laser melted stainless steel for micro-lattice structures [275]. SEM images (left and middle) of the fracture surfaces in two different zones near an nodal joint in an SLM316L micro-lattice structure and the corresponding schematics (right) showing the dominant fracture modes: (a) in the tension zone, and (b) in the compression zone. (Note: the middle figure is the high magnification SEM image in the boxed-in area of the left figure).

States of self-stress refer to tension and compression of the structural elements that result in zero net forces. Self-stress also plays an important role in determining the load-bearing ability of structures ranging from bridges to metamaterials with tunable mechanical properties [276]. This state is analogous to topological quantum states that sculpt localised buckling regions in the interior of periodic cellular metamaterials.

6. Structure and properties of mechanical metamaterials associated with shear/bulk moduli

6.1. Mathematical classification

Mathematically speaking, the mechanical metamaterials associated with shear/bulk moduli include three regions of the Milton map (Fig. 3): the first is the G (x) axis, i.e., the auxetic metamaterials of Section 7; the second is the K (y) axis, i.e., vanishing shear modulus; and the third is located in the lower right quadrant, $E > 0$ and $-4G/3 < K < 0$, i.e., negative compressibility. The first case, auxetic metamaterials, encompasses the original aspiration for mechanical metamaterials, and thus is a relatively mature research field for this subject. Thus auxetic metamaterials alone will be described in detail in Section 7. Therefore, this section is devoted to the emerging vanishing shear modulus and negative compressibility. With respect to this Milton map, the upper right quadrant was previously discussed by Milton [55] to elucidate the role of a negative Poisson's ratio in relation to the moduli. Later, Lakes et al. [67,68] located other metamaterials in the corresponding position on this map.

Two main groups can be found in the Milton map, i.e., K-G map (Fig. 3). The subsection here will just focus on the K (y) axis and the lower right quadrant. Firstly, on the K axis, the shear modulus G is equal zero, like it is for ideal fluids. If a three-dimensional structure is on this K axis, its shear modulus has vanished. In other words, we can obtain a sort of nondetectability in two dimensions, but seemingly not in three-dimensional structured materials. The first part of this section will introduce two types of mechanical metamaterials that are located on the K axis: the influential pentamode metamaterials and the varied kagome lattice. Secondly, we will treat the lower right quadrant of the Milton map representing the range of elastic moduli, G, $E > 0$ and $-4G/3 < K < 0$. Negative bulk modulus $K < 0$ is shown to be possible in selected unit cells. In isotropic solids, the bulk modulus $K < 0$ can be attained when a negative Poisson's ratio is sufficiently small, below the stability limit (for stress control). Such a material is unstable with respect to global deformation. It can be stabilised by constraining its boundaries. In analogy to crystalline metal-organic frameworks (MOFs) in materials chemistry, we can say that this type of mechanical metamaterial has negative compressibility. This involves contraction in one direction of a crystal under tension, which is termed negative linear compressibility (NLC), and the contraction in two directions, termed negative area compressibility (NAC). With regard to negative thermal expansion (NTE) behaviour, we can introduce its design concept. Micro/nanosize inclusions can be inserted into the interior of bulk materials, thereby obtaining NTE or NLC/NAC properties. The ideas in these domains are not new, but the challenge for the experimentalist to fabricate these structure still exists. With rapid development in micro-/nanofabrication techniques, it is expected that design concepts will take shape, and many more ideas will appear. We introduce negative compressibility as a current vision for future materials.

6.2. Vanishing shear modulus ($G \ll K$)

This type of three-dimensional metamaterial can be defined as an ideal fluid, where the shear modulus G approaches zero compared to the bulk modulus K, i.e., $G \ll K$ [20,277]. Two subclasses will be addressed, the influential pentamode metamaterials [63,278], and the mechanical metamaterials with a kagome lattice. The functional characteristic that both types of mechanical metamaterials share is their three-dimensional structural shape which displays two-dimensional properties, similar to the behaviour of liquids. In other word, these types of metamaterials are difficult to compress but flow easily [63,265]. We say vanishing shear modulus due to the shear modulus G approaching zero, but they can be called a meta*fluid* or an *anti-auxetic* meta*material* [20,277].

6.2.1. Pentamode structural design

The name *pentamode* meta*material* is derived from its material properties which easily support five modes of infinitesimal strain, and only one single stress. Such a structure was independently theoretically conceived and predicted by Milton [55,63,279] and Sigmund [278] in 1995, and further improved since then [114,115]. Pentamode extremal materials are considered to be a diamond-type structure in which four linkages meet at a point [63,115,278]. This is distinguished from the conventional two-dimensional honeycomb or inverted honeycomb where three linkages meet a point [30,141]. Hence, this structure supports a stress having Eigenvalues of the same sign. By moving the meeting point to the other side of the unit cell, another structure can be obtained to support a stress having Eigenvalues of mixed signs (Fig. 22A(a) [63]).

Mathematically, in the material 5 (*penta*) of the 6 diagonal elements in the 6×6 elasticity tensor approach zero, and one is a non-zero [33,55]. Suppose the forces F_1, F_2, F_3 and F_0 are directed along the linkages outwards from the meeting point p, and the corresponding elastic constants are k_1, k_2, k_3, and k_0, then,

$$F_1 = k_1(a_1 - p),\ F_2 = k_2(a_2 - p),\ F_3 = k_3(a_3 - p),\ F_0 = -k_0 p \tag{14}$$

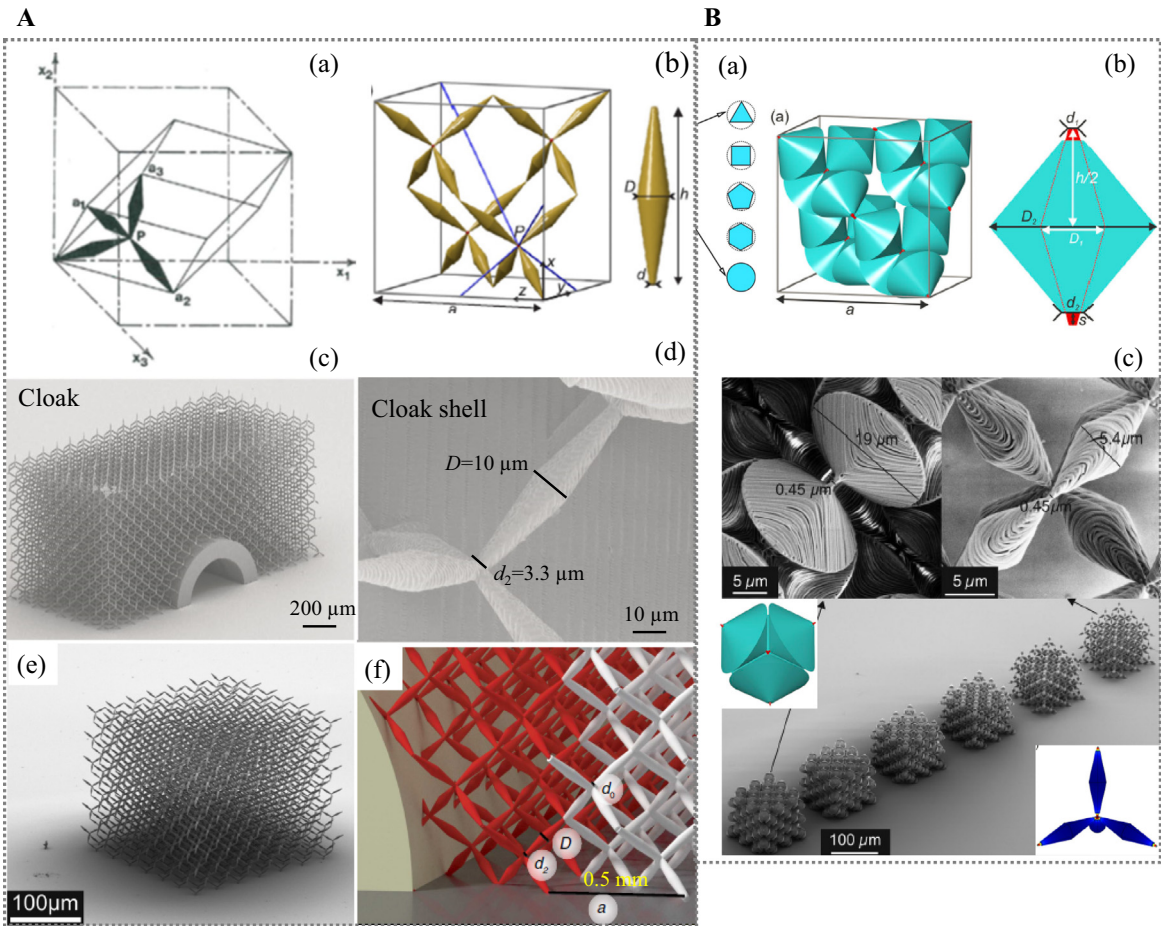

Fig. 22. (A) Pentamode metamaterials. (a) Ideal model suggested by Milton and Cherkaev in 1995 [63]. The artificial crystal with lattice constant a has diamond symmetry. (b) A pentamode structure proposed by Wegener et al. in 2012 [33,283], consisting of elements made by two connected truncated cones. In contrast to (a), the connection regions of touching cones have a finite diameter d. The diameter of the thick end of the cones, D, and the total double-cone length, h, are also indicated. (c) Fabricated elasto-mechanical structures for the unfeelability cloaking [20,280], rigid hollow cylinder and cloaking shell (the 'cloak'), and (d) magnified views of the cloak in (c) are depicted. (e) Oblique-view electron micrograph of another polymer pentamode mechanical metamaterial with 7 × 7 × 6 face-centred-cubic unit cells (hence total size 261 μm × 261 μm × 224 μm) and with h = 16:15 μm, D = 3 μm, and d = 1 μm fabricated by dip-in direct-laser-writing (DLW) optical lithography [33]. (f) The magnified view for unfeelability cloak reveals the details of the pentamode metamaterial the cloak is composed of. The local bulk modulus K is tuned via the diameter d of the double-cone connections with respect to the fixed lattice constant a. For the surrounding, d_0/a = 5.3% (white), for the cloaking shell, d_2/a = 2.4% (red) for the choice R_2/R_1 = 4/3. The fixed diameter D/a = 8% at the thick ends is also depicted [20]. (B) Another structural Pentamode metamaterials. (a) The cross-section shape of primary unit includes regular triangle, square, pentagon, hexagon and circle [284]. (b) Metamaterial structure [286], the diameters d_1 and D_2, the lattice constant a of the fcc lattice. The ratio d_1/a determines the effective bulk modulus K/K_0, and the ratio D_2/a determines the effective relative static mass density ρ/ρ_0, which is equal to the volume-filling fraction f. (c) Electron micrographs of selected fabricated metamaterial with fcc lattice constant a = 40 μm, s/h = 0.05, D_1/a = 0.12, and d_2/a = 0.04. These polymer structures have been made by three-dimensional dip-in galvo-scanner-based laser lithography and demonstrate the feasibility of the concept of pentamode metamaterials [286].

According to the balance of these forces,

$$kp = \sum_{i=1}^{3} k_i a_i, \quad k = \sum_{i=0}^{3} k_i \tag{15}$$

Following that the meeting point p lies within the unit cell if and only if,

$$0 < \frac{k_i}{k} < 1 \; for \; i = 1,2,3 \tag{16}$$

Then the integral of the stress within the unit cell is,

$$\sigma_l = \sum_{i=1}^{3} k_i a_i \otimes a_i - kp \otimes p \tag{17}$$

Hence, there are many possible strategies to obtain a specific stress σ_l proportional to a prescribed supporting stress σ, via selecting the elastic constants k_1, k_2, k_3, and k_0 to satisfy Eq. (16), and selecting vectors a_1, a_2, a_3 in the unit cell. This is the principal idea of the pentamode metamaterials: when the ratio of the integral stress and a prescribed stress is constant, there is only the normal stress without shear elements in the stress tensors. According to this theory, we can fabricate pentamode metamaterials using building blocks for materials with completely arbitrary elastic properties [63].

The pioneering fabrication of pentamode metamaterials did not occur until early 2012. The Wegener group [20,103,277,280–283] proposed a metamaterial structure, consisting of elements made by two connected truncated cones (Fig. 22A(b) [33,283]), and further fabricated by current state-of the-art lithography [33,283]. In doing so, the finite connection to replace the strictly theoretical point-like tips was achieved to obtain stability under certain conditions, for instance, the dependence of the bulk and shear modulus on the finite connection diameter [33]. The asymmetric double-cone element has been presented for a pentamode metamaterial consisting of two connected truncated cones with differing and thin diameters [265]. Of the different cross-sectional shapes, including regular triangles, squares, pentagons, hexagons and circles (Fig. 22B(a) [284]), it was found that the triangular case has particularly nice acoustic properties [284]. In general, the unit-cell of pentamode metamaterials is composed by 16 double-cone elements [20,33,44,277,283,285]. It is also possible to modify the diameters d_1 and D_2 (Fig. 22B(b–c) [286]), to thereby obtain various structural pentamode metamaterials.

Of the pentamodes implementing a three-dimensional transformation of elastodynamics, similar to the transformation optics, current studies mainly focus on the application of acoustic free-space cloaks [20], such as layered pentamode acoustic metamaterials. The team of Wegener has extensively and systematically investigated on this subject, from an initial attempt in 2012 [33], the verification and implement of the previous proposed theory [33,283], then the examination of the related geometric parameters [277,282], and finally the application of the acoustic cloaks (Fig. 22A(c–f) [20,280]).

Specifically, three-dimensional polymer microstructures were fabricated by dip-in direct laser writing optical lithography, and the resulting ratio of the bulk modulus to shear modulus was as large as about 1000 [33]. In the static-dynamic transition, Martin et al. [283] have calculated the phonon band structures of 3D pentamode metamaterials for phase velocities of the compression and shear waves. The mechanical properties of the 3D anisotropic pentamode metamaterials were studied and its large anisotropy ratio may be desirable for implementing 3D free-space cloaks [277]. Direct measurements of the static shear modulus and the Young's modulus reveal that their ratios is approximately 1000 when the smallest accessible values of $d/a \sim 1.5\%$ [282]. Subsequently, inspired by invisible core-shell nanoparticles in optics, an approximate elasto-mechanical core-shell non-detectability cloak has been designed and manufactured based on pentamode metamaterials [20,285]. Studies from other teams also concern pentamode acoustic cloaks, including two dimensional (2D) plain strain space [287], transformation methods and other theoretical research [285]. These investigations suggest that pentamode metamaterials have potential in some applications of nonlinear optical transformation, e.g., acoustic invisible cloaking.

In addition to applications for acoustic metamaterials, pentamode metamaterials with five easy modes of deformation can be developed for strong and ultra-light metamaterials, as mentioned in Section 5.1.1. In general, the lamination of a pentamode leads to metamaterials with effectively anisotropic uniaxial dynamic mass density tensors [286]. The effective mass density, in addition to the bulk and shear moduli, can be modified by introducing geometric perturbations to pentamode metamaterials. The effective properties of pentamode metamaterials, both isotropic and anisotropic, are obtained from the general formulation in the stretch-dominated limit of $Z = d + 1$, when considering a periodic lattice structure in $d = 2$ or 3 dimensions with a unit cell comprising Z thin elastic members emanating from a similarly situated central node [115]. The stiffest lattice proposed is based on these analytical simulations [114]. These anisotropic pentamode metamaterials can be translated to a zero Poisson's ratio and even auxetic behaviour. This type of mechanical metamaterial has potential for growth extending beyond mechanical metamaterials by tailoring the symmetry of the pentamode diamond lattice.

6.2.2. Kagome lattice

The second system possessing a vanishing shear modulus is associated with the kagome lattice (Fig. 23), i.e. rotating triangles in the geometry of auxetics metamaterials [288–291]. Torquato's group identified the kagome structure [292] as an ideal stiff and statically determinate lattice [93,293], initiating dozens of studies on its mechanical properties and its technological importance on the macroscale [294–296]. A revival of the kagome lattice has recently emerged due to both experimental measurements and computational simulations. The concept of a kagome lattice is in essence derived from a cellular lattice [93], where study of the various mechanical properties focus on the shear/bulk moduli. Some stacked kagome lattices, also called the cellular kagome lattice [276], have been addressed in Section 5.1.1.

The C3v twisted kagome lattice (Fig. 23A) is relatively simple, and can be formed from the kagome [293] and other periodic isostatic lattices [41,260,297]. This kagome lattice is isotropic with a vanishing bulk modulus. This unusual behaviour, i.e., the vanishingly small bulk modulus, can cause the speed of acoustic surface waves to vanish [298,299]. Distorting the kagome lattice, characterised by vanishing bulk moduli and negative Poisson ratios, depends with high sensitive on the boundary conditions and on the nature of the kagome distortions [298]. Alternatively, a kagome lattice in periodic elastomeric structures comprises a triangular array of circular holes having multiple folding mechanisms [82,292]. A geometrical analysis of two-dimensional rigid periodic networks yielded highly tunable phononic crystals.

Recently, Paulose et al. [41] fabricated the topological modes of prototypic kagome lattices from rigid triangular plates (Fig. 23). Square lattices with primitive vectors introduce a single point and thereby produce a deformed kagome lattice which contains only four-coordinated points, exhibiting a specific region of the triangle or pentagon. This implies the existence of a dislocation. Consequently, the topological soft modes can be positioned at desired locations in a metamaterial

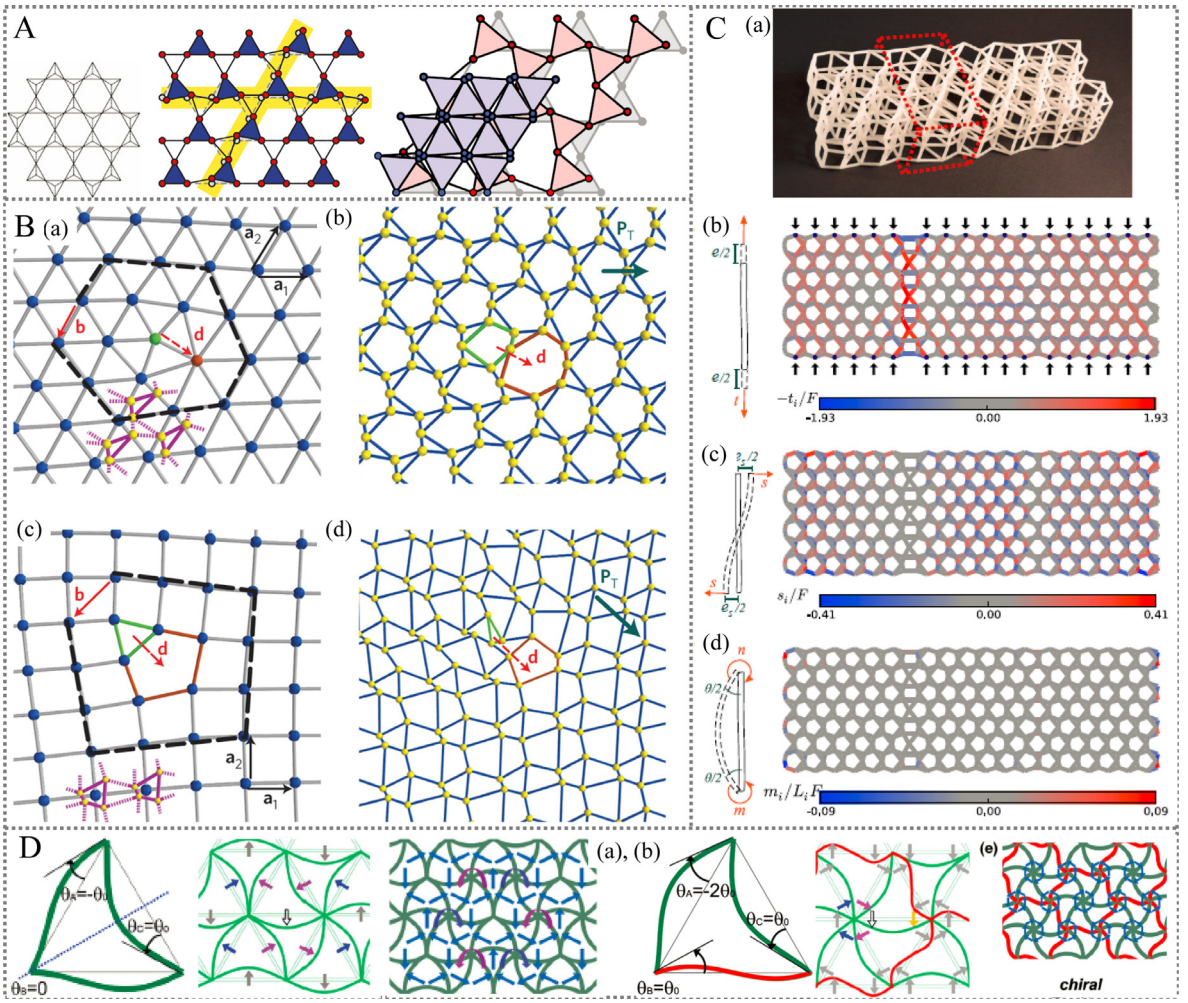

Fig. 23. Kagome mechanical metamaterials. (A) Isostatic kagome lattice. (a) (left) The macro kagome plane and tetrahedral core of the kagome plate structure [292,296]; (middle) The kagome lattice and its floppy modes, with the reference state in grey and deformed state in red. Two of its floppy modes are shown in this figure marked by the yellow ribbons [297]; (right) Superposed snapshots of the twisted lattice showing decreasing areas with increasing an angle [298]. (B) Dislocations in polarised isostatic lattices: (a) Hexagonal lattice with primitive vectors $\{\boldsymbol{a}_1, \boldsymbol{a}_2\}$. (b) Deformed kagome lattice obtained by decorating the triangular lattice in $\boldsymbol{a}$. (c) The topological polarisation. (d) Decorating each point in c with the four-point unit cell (yellow points and magenta bonds) gives a distorted square lattice which incorporates a dislocation of the same dipole moment, and has a non-zero topological polarisation [41]. (C) Stacked kagome lattices. (a) A 3Dprinted realisation of the design made of flexible plastic: a unit cell size of 25 mm and beams with circular cross-section of 2 mm diameter. The stacking creates a pile-up of states of self-stress in a quasi-2D region, highlighted by dotted lines [276]. (b–d) Stretching, shear, and bending contributions to the linear in-plane response of the cellular metamaterial, subject to a vertical compressive force F (solid arrows) at each point highlighted along the top and bottom edges. The structure is modelled as a network of flexible beams connected by rigid joints at the nodes, and with each beam providing torsional stiffness in addition to axial stiffness. The beams are coloured according to (b) axial compression; (c) shear load; and (d) bending moment [276]. (D) Mechanical instability induced geometrically frustrated triangular cellular structures [135]. (a) Representative critical eigenmodes for a single triangular frame in the symmetric pattern. The dotted line indicates the mirror plane, (middle) a schematic showing how spins define a buckled pattern when all of the beams buckle into a half sinusoid, and (right) ordered symmetric configurations predicted. (b) A single chiral triangular frame, the spinlike model under bulking, and the chiral ordered state emerges when two spins are assigned to each beam.

while being insensitive to a wide range of structural deformations or changes in material parameters [40,299,300]. These protected modes, localised at dislocations in the deformed kagome and square lattices, are therefore the mechanical analogue of the topological states bound to defects in electronic systems. Some advanced studies of atomically resolved nanostructures using three-dimensional characterisation techniques enable the placement of dislocations of crystal defects.

Vanishing shear modulus aims to make the effective shear modulus approach approximately zero in comparison to the bulk modulus. Pentamode metamaterials can be employed for acoustic metamaterials, and also extended to ultra-lightweight, ultra-stiff pentamode cellular lattices. Study of the fundamental mechanics of planar kagome lattices need to be continued because two-dimensional geometric frustration can springboard the exploration of three-dimensional materials. Concurrently, three-dimensional kagome lattices can be translated to stacked cellular metamaterials, and other twist triangle pattern transformations. Various applications are encouraging the development of mechanical metamaterials because

of their three-dimensional configuration and shape, and because their intrinsic properties resemble a sort of ideal fluid. This really does accord with the aspirations of mankind. We always want to envision beyond what our eyes see. Mechanical metamaterials associated with vanishing shear modulus are not confined to only these two types, the pentamode and kagome lattice. Fabulous structures for metamaterials are appearing unexpectedly from the seemly silent sea of possibilities.

6.3. Negative compressibility ($-4G/3<K<0$)

Compressibility is the inverse of the bulk modulus K, and is a measure of the relative volume change of a solid or fluid as a response to a pressure change [64]. Hence, normally the compressibility is positive sign, only in the regime of strong ellipticity [67] it may be negative in few natural materials. The negative compressibility, i.e., the negative bulk modulus K here, is refer to a material undergoes expansion when pressured, or contraction when tensioned [37,301]. Representing in the K-G map, the range of elastic moduli, K, G, corresponds to the lower right quadrant (Fig. 3) hence to $E>0$ and $-4G/3<K<0$.

This type of mechanical metamaterials are those where the effective elastic moduli of these manmade structures requires that $-4G/3<K<0$ when $E>0$. This special effect can only occur if the system under force moves from one stable state to another metastable state, termed the *negative/inverted compressibility transition* [37,70]. In mechanics, this condition is similar to bistability [302], where energy is stored in [303] or supplied to [304] a deformed object, including post-buckled elements [52,67,69]. In most case, buckled tubes also exhibit negative incremental stiffness, similar to perturbations of a deformed configuration. Similarly, the snap through phenomenon occurs in sufficiently small particles, serving as constrained inclusions. This snap through phenomenon is mainly due to surface energy effects in a composite that achieve large mechanical damping and anomalies in the modulus [36,305].

This subsection will introduce three types of negative compressibility and one implication from recent chemistry research in the field. Negative linear compressibility (NLC) is the one-directional contraction in a crystal under tension [73]. Negative area compressibility (NAC) is contraction in two directions [306] (Fig. 24). Both categories of negative compressibility can be identified by uniaxial or biaxial negative thermal expansion (NTE), i.e., contraction upon warming in natural candidates [307,308]. This accessible approach to investigate anisotropic NTE behaviour is the last this section will address.

6.3.1. Negative linear compressibility

NLC involves expansion in one direction upon uniform compression, and is closely related to auxetic behaviour (Fig. 24d). The latter entails lateral contraction under axial compression, as occurs in materials with a negative Poisson's ratio (NPR in Section 7). Compressibility normally denotes the relative volume change of a material as a response to a pressure change. As such, NLC metamaterials are distinct from NPR, i.e. auxetic metamaterials [28,62,309,310], in that they respond differently to different external stimuli. For instance, plastically deformed foams and honeycombs are known [28,29,311] to provide either negative Poisson's ratios or a Poisson's ratios whose sum exceeds unity along a stretch direction. However, NLC behaviour is only displayed by honeycomb structures [301].

Currently, four types of NLC materials have been proposed on the basis of the microscopic mechanisms responsible for NLC behaviour [35,301] in natural materials. These four NLC materials include: (a) compounds with NLC derived from certain quasi-ferroelastic phase transitions; (b) the network solids with NLC driven by correlated polyhedral tilts; (c) helical systems; and (d) a framework material with either wine-rack [301,312], honeycomb [312,313], or a related topology [308,314,315], where the NLC behaviour arises from the framework hinging [71]. A variety of new families of natural materials has therefore been distinguished in an extensive current review [71] and a benchmark review of NLC [301]. Since the former three types are natural materials rather than manmade materials, the last type of NLC metamaterials serves as the underpinning of negative compressibility in artificial materials in this review.

Natural NLC materials are generally much weaker than the ordinary materials that typically display positive compressibility. This is because a linear magnitude of compressibility usually reflects bond strengths in conventional engineered crystalline materials. The typical value of positive linear compressibility normally lies between 5 TPa^{-1}, in the stiffer and compact materials such as metals, alloys and ceramics, and 100 TPa^{-1} in softer materials such as polymers and foams [56]. In the case of steel and concrete, contraction in the length is only approximately 0.5% when applied pressure increases by 1 GPa, corresponding to a linear compressibility of $K\sim 5$ TPa^{-1} [54]. Only a dozen or so NLC compounds had been identified [301]. The most negative values observed have been just -2, -1.2 and -12 TPa^{-1} for R-cristobalite structured $BAsO_4$ [316], trigonal Se [317], and $KMn[Ag(CN)_2]_3$ [318], respectively. In most of these, the NLC effect is relatively weak.

How can NLC metamaterials be designed to reach a much higher value of NLC than observed in natural materials? NLC behaviour is just emerging, and the field of materials chemistry is currently limited to crystalline metal-organic frameworks (MOFs). The reason for this is that on the macroscopic scale the phenomenon of NLC is not counterintuitive, both trellis fencing and wine racks can be packed away by pulling in one direction [318]. The challenge for material design is to engineer this same functionality on the atomic scale such that it becomes an intrinsic material property to be exploited. On a fundamental level, there are strong implications associated with understanding the mechanism of negative compressibility from the molecular framework. We will retrace these innovations and explorations in Section 9.1 for future fabrication methods of micro/nanolattice mechanical metamaterials.

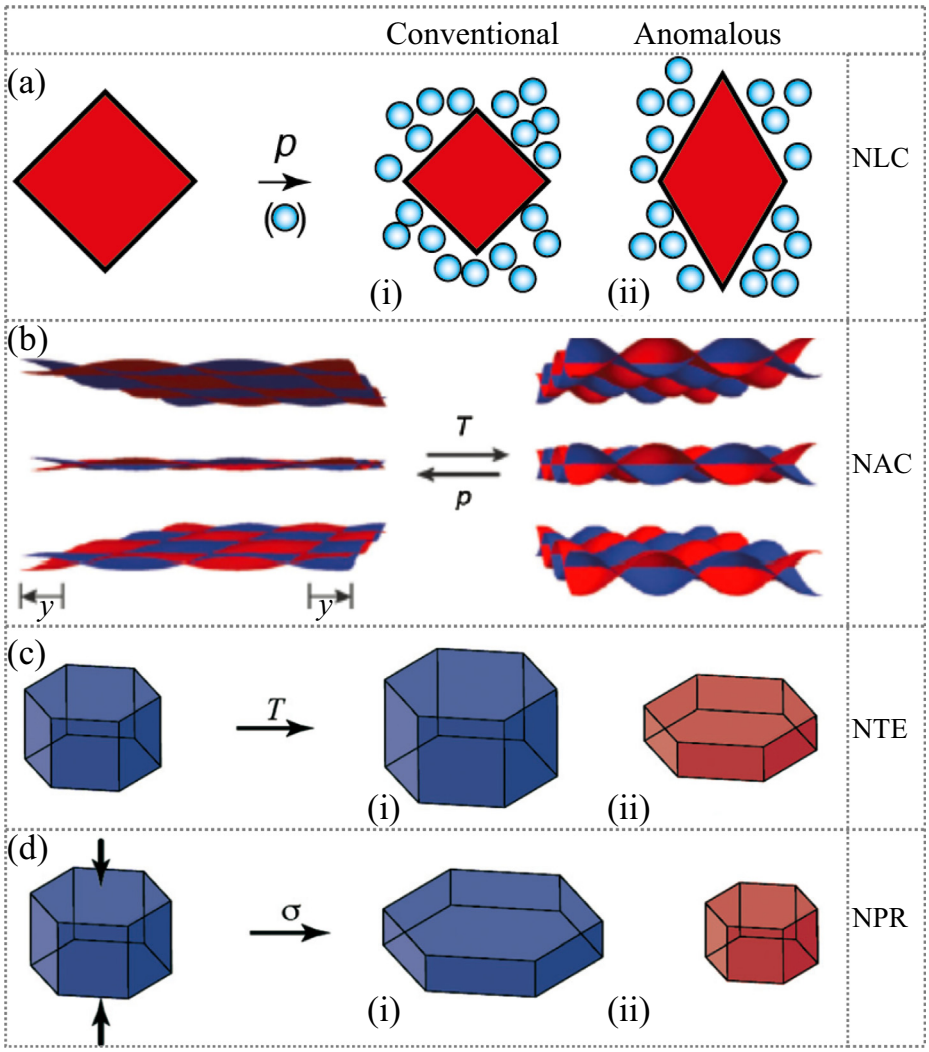

Fig. 24. Diagrammatic representation of anomalous mechanics for materials exhibiting negative linear compressibility (NLC), negative area compressibility (NAC), negative thermal expansion (NTE) and negative Poisson's ratio (NPR). (a) Mechanical responses to hydrostatic pressure, (i) positive compressibility showing the contraction in all directions, (ii) NLC: linear expansion in one direction under the pressure-transmitting media (blue circles) [71]. The system volume (represented here by the solid red area) is reduced in all cases. (b) A typical layer-rippling mechanism for NAC: densification of layered structures lead to collapse in the stacking direction, while the variation of the parameter *y* in the two perpendicular directions within the layer with increasing pressure [313]. (c) Uniaxial NTE: contraction in one direction upon heating [315]. (d) Auxetic response upon axial compression (indicated by the arrows), whereby a NPR is observed for comparison [315].

6.3.2. Negative area compressibility

Negative area compressibility, an extremely rare property, refers to the two-directional contraction when under one directional structural tension [306]. In analogy to a typical mechanism (Fig. 24b), the densification of layered materials usually proceeds via collapse in the stacking direction, which in turn results in an expansion in the two perpendicular directions within the layer. From a structural viewpoint, the phenomenon can be understood in terms of pressure-driven damping through layer rippling, which acts to increase the cross-sectional area of the layer at larger hydrostatic pressures [313].

Compared to the rigorously and extensively studied NLC, modest effects of NAC have been observed or predicted to occur in a handful of layered materials such as silver (I) tricyanomethanide [313], and sodium vanadate [319]. The reason for this effect occurring in layered structures is that a layered material is usually more compressible along the stacking axis than it is along a perpendicular direction [307]. By choosing a plane with a negative area compressibility as the predominant crystal face, a crystal can be obtained with NAC effects where the total surface area increases under hydrostatic (uniform) pressure [301]. Thus, NAC materials rather than NLC can be used as substrates to provide an order of magnitude increase in the amplitude of piezoelectric response in ferroelectric sensors [301], artificial muscles and actuators.

The four types of mechanisms are responsible for NLC, which are discussed in this last subsection. Densification under area expansion will be identified [320], in conjunction with the specific geometries of the various wine-rack and

honeycomb-like topologies [312,315]. It is unlikely that NAC will ever be as strong an effect as NLC. This is mainly due to the mechanical stability criterion of positive volume compressibility. This stability criterion implies that positive linear compressibility (PLC) along the axis perpendicular to the plane of negative compressibility must be at least twice as large as K_{NAC}. That means that NAC can only ever be half as strong as PLC [71]. NAC materials are much less common and their magnitudes are even weaker than NLC [306].

This NAC behaviour is identified upon flattening honeycomb-like layers during a rapid pressure-driven collapse of separated interlayers [313]. Specifically, a soft porous material $[Zn(L)_2(OH)_2]_n$·Guest (where L is 4-(1*H*-naphtho [*2,3-d*] imidazol-1-yl) benzoate, and Guest is water or methanol), exhibits the strongest observable NAC behaviour [306]. Similar to NLC exploration, the same thing happens here in the research field of NAC. Only a handful of materials displaying NAC properties has been identified, and engineered metal–organic frameworks (MOFs) [321] are also limited. We need to start from the fundamental level to find how to characterise NLC/NAC properties.

6.3.3. Negative thermal expansion metamaterials

To identify negative compressibility, an accessible approach is to investigate anisotropic negative thermal expansion (NTE) behaviour [322], i.e., contraction upon warming [307,308]. Dynamic instabilities result from NTE [73], which is frequently indicative of NLC behaviour in natural candidates [72,306,312,323]. NTE is often associated with a structure that contracts in one or more direction upon heating [313,308] (Fig. 24c).

First of all, we need to clarify the subtle meanings of related terms. The property of negative specific heat is rare, but it does exist in nature. This counterintuitive effect indicates that the temperature, energy or entropy of a system decreases when heat is supplied [69], such as by rapidly cooling amorphous materials near the glass transition temperature [324]. NTE is clearly different from negative specific heat. NTE does follow the law of conservation of energy, but the whole effective structure when heated will contract in one or more directions, rather than expanding as is normally the case. Another is negative Poisson's ratio, where several newly developed NTE structures have initially come from the frameworks designed for NPR. Current topological optimisation has revealed that there is no mechanistic relationship between NTE and NPR [325,326]. Contrary to NPR, there is empirical evidence of a specific link between anisotropic NTE and NLC/NAC in framework materials [318]. Indeed, it is the similarity in compression mechanisms under cooling and compression [307] that originally indicated the existence of the relationship between NTE and NLC/NAC properties.

From a material chemist perspective, some specific molecular framework materials [73,314,318,327] can fit this similarity. In a topical example using elemental Se, the mechanism responsible for NTE along the Se spiral axis probably accounts for NLC along the same direction [317]. Furthermore, in most other anisotropic materials, the mechanisms of buckling and bond compression are almost always more effective at reducing crystal volume than is uniaxial or biaxial lattice expansion [313]. Thus, it is possible to realise a dynamic transition from discontinuous negative compressibility to continuous negative volume compressibility behaviour in a chemical system. A feasible approach might employ inhomogeneous chemical doping to remove the transition pressure. This concept has been used elsewhere to convert discontinuous thermal volume collapse to NTE [328], and NLC in molecular co-crystals [320,327]. But these are beyond the scope of this review.

Alternatively, from the perspective of thermodynamic formalisms, when omitting shear terms, the thermal expansion to compressibility in anisotropic materials is [307],

$$\alpha_i = \frac{C_T}{V}\sum_j S_{ij}\gamma_j \tag{18}$$

where C_T is the isothermal specific heat, V is the unit cell volume, S_{ij} is the elastic compliances, and γ_j is the components of the anisotropic Gruneisen function (weighted sums over the anisotropic mode of Gruneisen parameters [73]). If substituting $K_i = \sum_j S_{ij}$ when S_{ij} is negative for the anisotropic materials and γ_i is positive for uniaxial NTE [307],

$$\alpha_i = \frac{C_T}{V}\left(K_i\gamma_i + \sum_{j\neq i} S_{ij}\gamma_{ji}\right) \tag{19}$$

where $\gamma_{ji} = \gamma_j - \gamma_i$. For flexible framework materials, the Gruneisen function is relatively isotropic i.e., $\gamma_{ij} \ll \gamma_i$, hence the cross-linking term of Eq. (18) becomes a second-order correction. This means negative values for the coefficient of thermal expansion, α_i are likely to correspond to negative K_i values whenever the material as a whole exhibits positive thermal expansion.

In any case, the link between NTE and NAC is deduced from the variation in the framework geometry during heating. For instance, the established model of NTE in layered materials predicts coupling between NTE and the extent of layer rippling, as quantified by the inter-network torsion angle [313]. Similarly, the NAC is driven by the same layer-rippling mechanism as NTE, which is evident by varying the parameter y (Fig. 24) with increasing pressure. Therefore, these investigations suggest that NTE behaviour, whereby a material contracts upon heating, can be used to produce mechanical metamaterials with tunable thermal expansion based on existing topologically optimised architectures.

If extending planar honeycomb chiral lattices from auxetics [30] to NTE metamaterials, a controllable thermal expansion of large magnitude can be achieved in chiral negative Poisson's ratio lattices (Fig. 25). Specifically, the effective thermal

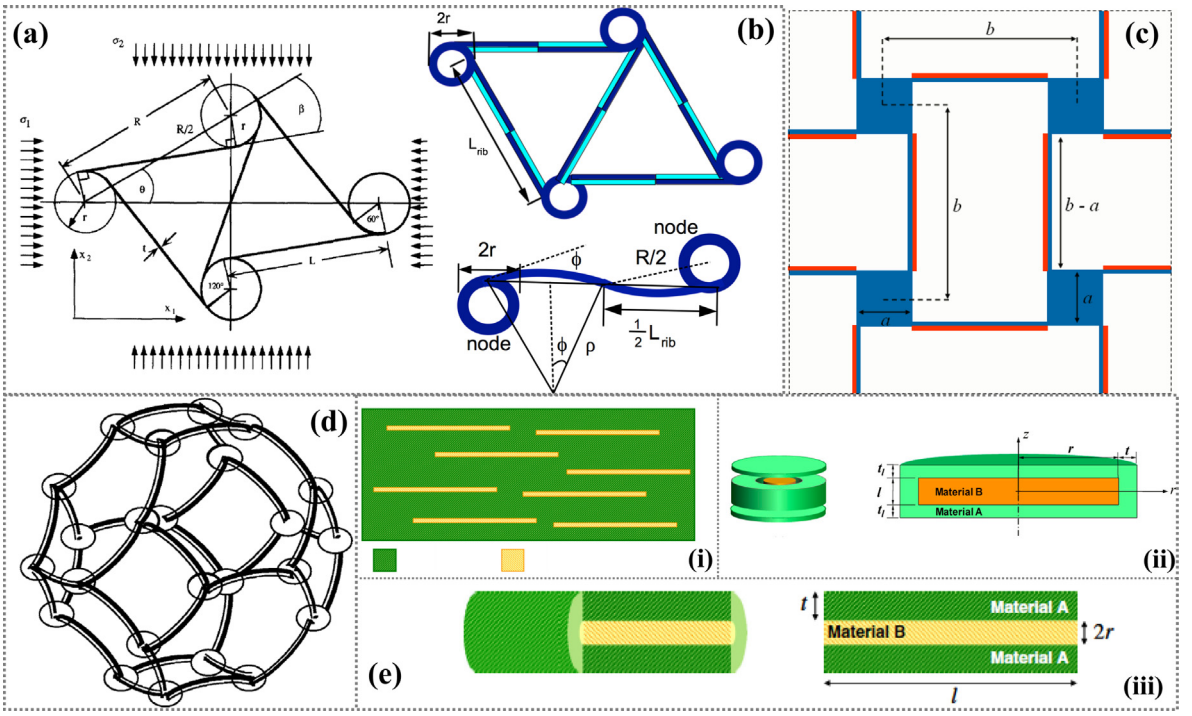

Fig. 25. (a) Geometry of planar chiral honeycomb lattice structure with Poisson's ratio approaching −1 [30], (b) NTE (negative thermal expansion) modified chiral lattice structure with bi-material ribs with alternating orientation. Two materials indicated as light and dark, differ in their thermal expansion [329], and (lower) kinematics of the deformation (bending) in a ligament (rib) in a chiral honeycomb lattice structure. In the chiral lattice, strain is geometrically linked to rotation ϕ (θ or β in Fig. 25a), node outer radius r and the spacing R of nodes between centres, the rib length L_{rib} (or L). A temperature change causes bending of the bi-material rib segments which produces curvature with radius ρ [30,329]. (c) Geometry of the modified chiral structure made up of bi-material ligaments of thickness $t_1 + t_2$ connected to a square node. Note that the squares and part of the ligament thickness (thickness t_1) are made from Material 1 (in orange colour) which has a Young's modulus E_{S1}, while the other part of the ligament is made from Material 2 (in blue colour) which has thickness t_2 and Young's modulus E_{S2} [35]. (d) Tetrakaidecahedral foam cellular metamaterials (two dimensional hexagonal lattice) with curved bi-material ribs inverted hexagonal cell for large NTE [326]. (e) Negative thermal expansion from disc, cylindrical, and needle shaped inclusions. (i) A cross-section of a possible composite where the highly expanding and hard needle shaped inclusions are moulded inside the matrix in a random but aligned manner [331]. (ii) The modified and (iii) initial cylindrical structure (orange) consisting of an inclusion of material B embedded in a matrix (green) of material A, and a cross-section showing its dimensions [331,332].

expansion coefficient α of the lattice is about $-3.5 \times 10^{-4}\,\text{K}^{-1}$ [329]. The thermal expansion α is expressed in terms of specific curvature ρ_s,

$$\alpha = \frac{r}{4\rho_s}\frac{1}{\sqrt{1+(2r/L_{rib})^2}} \tag{20}$$

In the chiral lattice (Fig. 25), of nodal outer radius r, and rib length L_{rib}, a temperature change causes the bi-material rib segments to bend, producing curvature of a radius ρ [30,329].

From this case, we see that the investigation of NTE metamaterials is in its early stages of development. The basic concepts for their structural fabrication can be traced largely to other common mechanical metamaterials, specifically auxetic metamaterials. A variety of NTE metamaterials (Fig. 25) have been fabricated where their topologies ranging from chiral metamaterials [329,35], to cellular metamaterials [326], to rotating triangles or squares [322,330], and to needle shaped inclusions [331,332]. The principles behind these critical framework geometries is that NTE can be easily achieved in the lattices by placing a material of higher expansion on the outer portion of the curve [326]. In other words, when two materials have different coefficients of thermal expansion and are glued together, they will curve when subjected to a change in temperature, as is the case of a bi-metallic strip in a thermostat mechanism [35]. These analyses suggest that the framework geometry plays a crucial role in determining the mechanical response of framework materials which show anisotropic responses via hinging. It is therefore expected that bi-material ligaments may be used as structural components in the construction of mechanical metamaterials which may exhibit negative compressibility and particularly negative thermal expansion.

6.3.4. Recently proposed mechanisms behind negative compressibility

Various mechanisms have been proposed to explain the occurrence of negative compressibility. These range from the use of bi-material strips, whose components have different properties [35], to systems that exhibit this property due to their

particular geometry [333] or due to constraints [69]. A currently proposed metamaterial with a negative-compressibility transition is derived from a force potential mechanism [37]. The potential principle is similar to the MOFs mechanisms that attribute electronic and magnetic transitions to transverse atomic and molecular vibrations [334]. These conjectures indicate that bistability is both a necessary condition and an indication of negative compressibility [302] in terms of a strong ellipticity condition [69].

Compared to finding natural negative compressibility [70], few previous studies focus on artificial NLC/NAC though mechanical metamaterials. The major challenge is that negative compressibility may disappear in realistic dynamical systems, unless strongly coupled to an external loading, which stabilises a metastable state in an open thermodynamical system [302]. Currently, an influential concept [37] for negative compressibility transitions offers a possible design for metamaterials effective negative volume compressibility by judiciously selecting pairwise force potentials. These destabilisations give rise to a stress-induced solid-solid phase transition associated with a twisted hysteresis curve for the stress-strain relationship. Thus strain-driven metamaterials having negative compressibility transitions have promising application in actuators, force amplifiers, micromechanical controls, and protective devices [37]. Moreover, structures made up from bi-material elements can also exhibit negative properties, in particular negative compressibility [35].

A bi-directional evolutionary structural optimisation method [64] in topology is used to design materials, covering various properties such as stiffness. A statistical physics theory for negative compressibility transitions exists. In an experimental attempt, geometric transformation of the two-dimensional materials into extended three-dimensional layouts by compressive buckling has been presented by more than 40 representative frameworks, from single and multiple helices, to toroids and even to flowers [186,187].

When taken together these various pioneering studies clearly reveal a number of design laws for maximising NLC/NAC: (a) the compressibility in an orthogonal direction remains positive if the volume compressibility is positive; (b) the desired bonds, ribs or fibres can be used to extend the stability range; (c) the network topology is likely related to a wine-rack or honeycomb motif; (d) if volume compressibility is also negative, the stiffness gradient of the elements in bi-material or high level structural hierarchy is supposed to be sufficiently large to result in negative compressibility within the entire system. Finally, mechanical metamaterials with negative compressibility behaviour are of strong practical interest for the development of highly sensitive pressure detectors and other various smart materials in bioengineering and biomedical engineering, particularly over a large possible pressure range.

7. Recent advances in mechanical metamaterials associated with Poisson's ratio

By definition, Poisson's ratio is the negative ratio of transverse to axial strain [53]. In view of most solids, when a natural object is stretched axially, it will contract laterally. Poisson's ratio is normally a positive value ranging between 0.25 and 0.33 [61,62]. In nature, just a few types of materials have negative Poisson's ratio $\upsilon < 0$ or the relatively infinite $K/G \ll 1$ and $\upsilon \sim -1$, thereby they can exhibit a counterintuitive dilatational behaviour, expanding laterally when stretched and contracting laterally when compressed [62,309,335]. That is why more materials in this class have been made, and named.

The currently accepted term *auxetics* introduced by Evans [336], refers to an exceptional mechanical property, negative Poisson's ratio (NPR). This term is derived from the Greek word *auxetikos*, meaning "that which tends to increase." Auxetic geometries with hierarchical laminar structure were introduced by Milton [29], and thereafter Grima et al. [138,234,288,289,291,337–346] have done an amount of elegant work varying structure to achieve a negative or zero Poisson's ratio. There are two approaches pursued in the design of auxetic metamaterials. One is to chemically synthesise a highly modular network, and another is to mechanically manufacture a hierarchical lattice structure on the meso- or macroscale. The latter approach is mainly applied to the mechanical metamaterials addressed in this review.

7.1. Classification of cubic auxetic metamaterials

Currently an amount of micromechanical models exist that seek to predict and explain auxetic behaviour. Four subclasses of auxetic metamaterials have been defined, based on the structural design leading to the various mechanical properties: (i) the original re-entrant structure (Fig. 26), similar to the folded-in cells fabricated from polyurethane foam, including various re-entrant open-cell microstructures [76,339,347], rotating squares [138,337,341,348] or triangles [288,289,291,344]; (ii) NPR induced by an elastic instability, particularly the missing rib models [339,349] to pattern transformation [26,226,308] (Section 5.1.5); (iii) NPR using chiral building blocks, chiral [30,142,150,153] or anti-chiral lattices [141,329,350] (Section 5.1.2); (iv) a portion of origami metamaterials (Section 5.1.3), inspired by the egg rack structure [351]. Much interest has centred on the first type of auxetics discovered, i.e., the re-entrant structure for NPR [62,225,289,337,340,352]. The other three types are also a hot topic that we have addressed in previous sections. These studies may lead into much more exotic auxetic metamaterials. Consequently, a number of comprehensive reviews [32,62,309,335,353–355] and books have been written concerning auxetic metamaterials. This section intends to describe auxetic metamaterials from the perspective of their mechanical properties, zero or negative Poisson's ratio, and negative/-positive programmable Poisson's ratio, rather than their various structures.

In analogy to negative Poisson's ratio for cubic crystals and micro/nanotubes [356], it is entirely feasible to divide auxetics metamaterials into two types: complete auxetics and partial (semi-) auxetics. In complete auxetics, the Poisson's ratio is

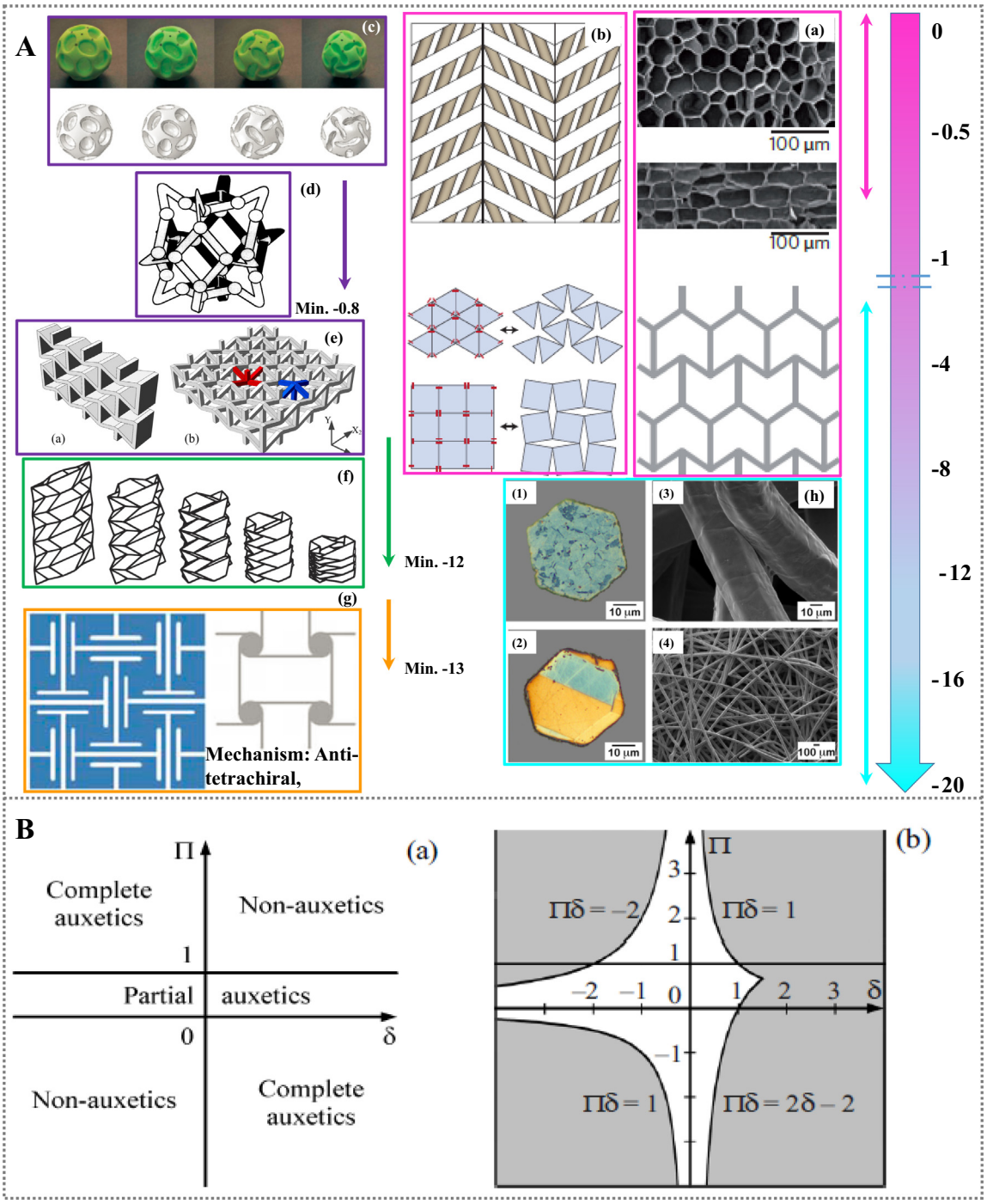

Fig. 26. Schematic showing the range of negative Poisson's ratio in auxetic metamaterials. (A) Structural classification, (i) Two-dimensional structures with Poisson's ratio close to −1, (a) cellular structures: honeycomb structure found in cork [352] normal to the direction of growth (upper) where $\upsilon \leq 0$ and parallel to this (middle) where $\upsilon > 0$ [62]. Semi-re-entrant honeycomb structure proposed to model zero Poisson's ratio materials (lower) [62,289]. (b) Auxetic geometries: hierarchical laminate (upper) [29]. Rotating hinged triangle and square structures (lower) [337,338,340]. (iii) Three-dimensional structures with Poisson's ratio close to −1, (c) Buckliball is made of silicone-based rubber under pressurised by a motorised syringe pump-[360]. (d) Idealised re-entrant unit cell in three-dimensional [76]. (e) Interlocking assembled auxetic cellular structures [376]. (iiii) Negative Poisson's ratio lower than −12, (f) re-entrant origami-based metamaterials [176]. (g) Slit perforation patterns based on anti-tetrachiral mechanism [346]. (h) Out-of-plane auxeticity in stainless steel sintered fibre network mats [85,359]. (B) Mathematical classification for (a) cubic auxetic metamaterials, (b) with boundaries for cubic crystals [356].

always negative, or zero. Partial auxetics share both positive and negative Poisson's ratio depending on the orientation of the meta-atoms subjected to a deformation, e.g., uniaxial tension. If this orientation is represented by three Eulerian angles φ, θ, ψ, as is the case in crystallographic theory, then the Poisson's ratio depends on these three Eulerian angles and on two dimensionless complexes, Π, δ (Fig. 26B, some theoretical details can be found in Ref. [356]). That is why this section here will address the auxetics metamaterials from these two perspective: complete auxetics with Poisson's ratio being zero or negative irrespective of orientation, and particle auxetics where the Poisson's ratio changes sign as a function of the orientation and the applied conditions.

7.2. Zero or negative Poisson's ratio ($G \gg K$)

Natural cork serves as a well-known example of a material displaying a zero Poisson's ratio (Fig. 26). With regard to some advances on auxetic metamaterials, Fig. 26 schematically shows the wide range of negative Poisson's ratios measured experimentally for various materials. These auxetic metamaterials include re-entrant or hinged honeycombs and foams [28,30,76,339,347], similar to another directional semi-auxetic solid based on combining or rotating units. Similar levels of auxeticity consist of microporous polymers [357], pattern transformation [26,226,235], nanotube metamaterials [225], and chirality [142,329]. Auxetic effects have also been observed in fibre composites involving the use of auxetic constituents or a selection of suitable stacking sequences of unidirectional laminae [358]. Nevertheless, high levels of auxeticity in fibre composites have only been achieved by incorporating metallic fibre networks [85,359], which exhibit a high negative Poisson's ratio ranging from -20 to -4. Such fibre assemblies are highly oriented (fibres oriented mostly in-plane) and are produced by sintering fibres together at crossover points. These investigations suggest that nanostructures having metallic, ceramic, and polymeric constituents have potential for the development of auxetic metamaterials. In addition to the metamaterials presented above from pattern transformation, chirality and origami, here we provide a simple description of the concept and advances in the classical re-entrant structure, and some specific metamaterials such as 3D Buckliballs [310,360,361], fibre networks [85,359] and other crystalline rolled tubes.

The geometry of the 3D Buckliball (Fig. 26A(c) [310,360]), derived from a geometry reminiscent of a Buckyball, comprises a spherical shell patterned with a regular array of circular voids. Below a critical internal pressure, the narrow ligaments between the voids buckle, leading to a cooperative buckling cascade of the skeleton of the ball. This ligament buckling leads to closure of the voids and a reduction of the total volume of the shell by up to 54%. The auxetic metamaterials using Buckliballs as a building cell can extend the strain range further to 0.3.

Alternatively, mats of metallic fibre networks (Fig. 26A(h) [85,359]) are expected to develop relatively high, negative Poisson's ratios. A measured value of an out-of-plane Poisson's ratio was as negative as -18 [359]. The auxetic effect is attributed to fibre straightening (i.e. outward bending) in response to in-plane tensile testing, particularly fibre kinking induced by an applied pressure during processing. Such large out-of-plane auxeticity in fibre networks can be enhanced by weak interlayer bonding, high fibre content and low network thickness.

Finally, many crystalline rolled tubes, inspired by the carbon micro- and nanotubes are also auxetic materials [362]. Depending on the orientation of the crystalline structure relative to the axis of the tubes, these metamaterials can be obtained by rolling plates of cubic, hexagonal, and rhombohedral crystals, using the elasticity theory to classify and group these structures together [356]. As such, when independent elastic constants are achieved for anisotropic materials, strong auxetic effects are theoretically permissible [359]. These observations suggest that the Poisson's ratio can be designed to reach much higher negative values for anisotropic auxetic metamaterials [363].

7.3. Negative/positive programmable Poisson's ratio

This subsection covers mechanical metamaterials having both positive and negative Poisson's ratios, i.e., the so-called partial or semi-auxetics, depending on the structural orientation under tension [356]. Some natural materials behave as directional semi-auxetic solids [32], such as certain cubic metals when stretched in the [110] direction [364,365]. It is noted here that this classification is based on materials having cubic symmetry. The cubic structure is essential to other types of symmetry, for instance hexagonal symmetry [363]. With regard to most preferred crystallographic orientation, the cubic symmetry frequently appears as the mesostructured of self-assembled materials. Similar to the crystallography of natural materials, it is probable that various mechanical metamaterials, particularly in auxetics, can also conveniently be represented by three Eulerian angles in Bunge notation [199]. In an example of auxetic metamaterials with randomly oriented cuts, the highly ordered pattern of slits in traditional auxetic perforated systems can be replaced by an arrangement where each slit is oriented in a quasi-random manner [226,234,235].

The purpose is to design mechanical metamaterials with negative/positive programmable Poisson's ratio to: (i) obtain a desired response over a broad range of strains, and (ii) manufacture materials in a scalable manner [71]. A complete series of topologically optimised architectures can exhibit nearly constant values of Poisson's ratio over large deformations across nine equally dispersed values ranging between -0.8 and 0.8 (Fig. 27). This investigation suggests that it is at least technically feasible to combine topological optimisation with additive manufacturing, further to create mechanical metamaterials with programmable negative/positive Poisson's ratios. Alternatively,

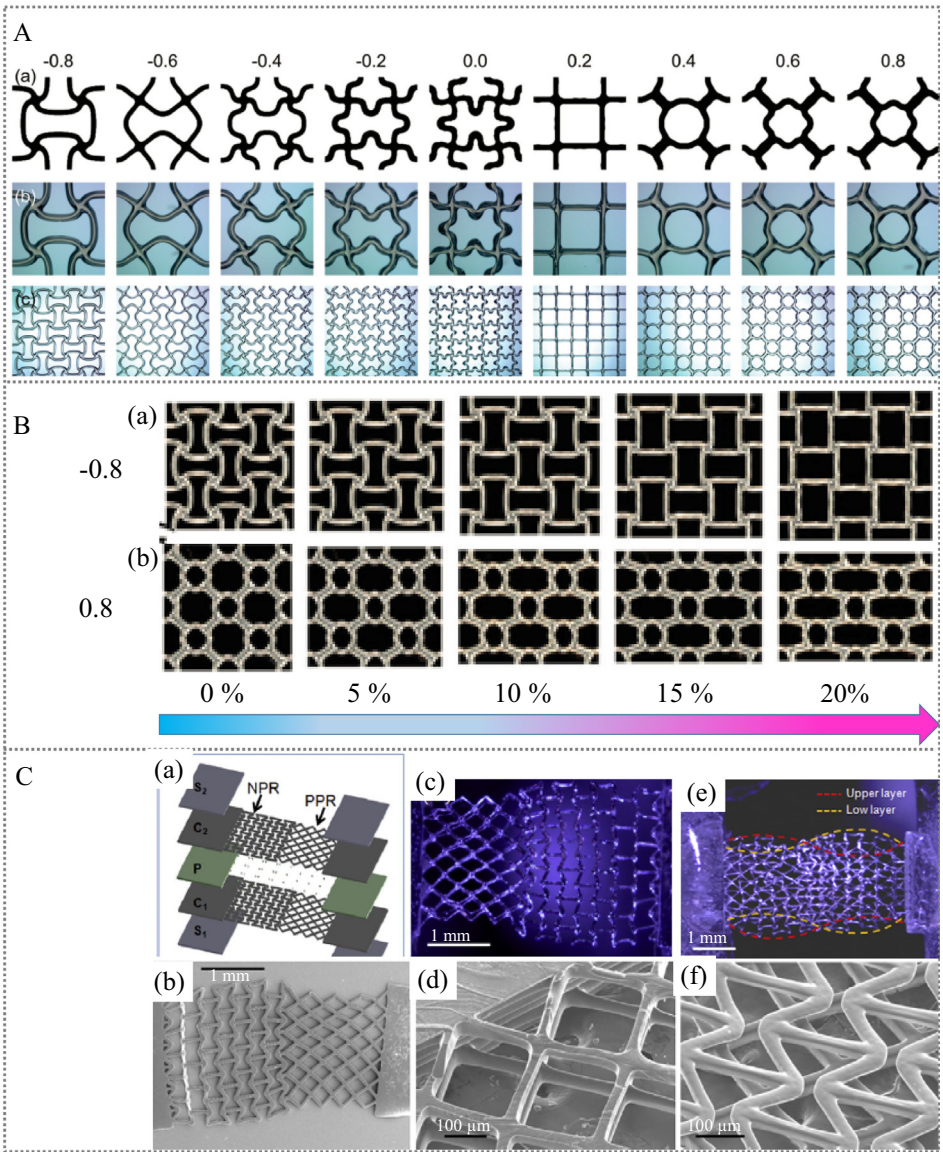

Fig. 27. (A) Topology and shape optimised architectures with programmable Poisson's ratio over large deformations [245]. (a) Designed and (b) printed unit cells for a programmable range of Poisson's ratio values. (c) 3 × 3 unit cells of the corresponding poly(dimethylsiloxane) (PDMS)-based architectures. (B) Deformation pattern of the 2 × 2 central unit cells corresponding to given longitudinal nominal strain values for (a) $\nu = -0.8$ and (b) $\nu = 0.8$. (C) Spatial tuning of negative and positive Poisson's ratio in a multi-layer scaffold constructed from polyethylene glycol (PEG) [366]. (a) Schematic of the two-layer scaffold assembled by stacking single-layer scaffolds with a connecting layer of vertical posts. SEM images of (b) single layer, (d) double layer hybrid scaffolds, (f) two-layer scaffolds with no supporting posts layer. Optical images of (c) double-layer scaffolds, (d) two-layer architecture showing negative Poisson's ratio behaviour on selective regions of top and bottom scaffolds, in their deformed strain states subjected to an applied axial strain.

if connecting square-shaped meta-atoms of a re-entrant structure (Fig. 27C), a spatially tunable mechanical metamaterial can be achieved with simultaneous negative and positive Poisson's ratio behaviour [366,367]. Scaffolds possessing a dual Poisson's ratio may be suitable for emulating the mechanical behaviour of native tissue for a variety of biomedical applications.

In summary, some Poisson's ratios in mechanical metamaterials can be greater than 1 [311], and some can be negative, or even be zero [367]. In advanced modern materials, the achievable Poisson's ratio can be any desired value. Some investigations [368] suggest that whole mechanical metamaterials are sensitive to hierarchical sub-structures, particularly the fraction of mass shared between the super-and sub-structures. Mechanical metamaterials having both positive and negative Poisson's ratios are especially significant to bioengineering and biomedical engineering [369,370]. This design concept is expected to extend into other fields, particularly for metallic and ceramic based materials.

8. Research translation and potential applications

The aim of this section is to describe various fabrication approaches to mechanical metamaterials, to research the translation of mechanical to optical or acoustic metamaterials, and to highlight some promising potential applications. Firstly, only the three main processing techniques are discussed, owing to restricted space. They are additive manufacturing via 3D printing for topological optimisation, interlocking assembly for auxetic metamaterials, and melt-electrospinning for micro-/nanolattice cellular metamaterials. Secondly, research translation can meet the application needs of optical, acoustic and thermal metamaterials. Finally, the application conditions associated with the application surroundings are discussed. Some specific applications are introduced, particularly bioengineering and biomedical engineering. This systematic analyse of application suggests that the combination of different types of lattice structures and existing metamaterials could be influential in the design of mechanical metamaterials.

8.1. Established fabrication techniques

Many advanced processing techniques have been used to fabricate various types of micro/nano mechanical metamaterials. They include additive manufacturing, i.e., 3D printing, for topological optimisation, folding/cutting approaches for origami/kirigami metamaterials, some interlocking assembly for auxetic metamaterials, and melt-electrospinning for micro-/nanolattice cellular metamaterials that are ultra-stiff and lightweight.

A general design route can be found in an example of pattern transformation [229]. For example, an elastomeric structure was fabricated that was capable of phase transition and of switching its state [229]. These structures can be fabricated by casting elastomers or using a 3D printer. A given programme can be created using computer aided design (CAD) software, and then the CAD file can be placed in a 3D printer to generate the required structure. This is a general fabrication approach. Different mechanical metamaterials have different steps in the fabrication and assembly. A blueprint is needed before processing and then an appropriate manufacturing techniques is applied to obtain the metamaterial. Folding or cutting approaches for origami-inspired metamaterials can consist of a series of design principles, which are described in detail in some referenced books [163]. Therefore, this subsection will concisely introduce additive manufacturing, interlocking assembly for auxetic metamaterials, and promising melt-electrospinning techniques.

8.1.1. Additive manufacturing

Additive manufacturing (AM) are commercially available fabrication techniques that allow nearly unlimited topological complexity [237]. These techniques include stereolithography (SLA), selective laser sintering (SLS), binder jetting, electron beam melting (EBM), and direct metal laser sintering (DMLS) [371]. Two significant benefits achieved from these techniques are that: (i) they allow the investigation and exploitation of beneficial size effects on plasticity and fracturing, with potential to dramatically increase the effective mechanical properties of the cellular material [106,372]; (ii) they allow interaction of the periodic structure with visible light, vastly simplifying the development of optical, acoustic, thermal and mechanical metamaterials.

Recent advances in additive manufacturing and topological optimisation techniques make it possible to design periodic lattice structures with controlled anisotropy (Fig. 6 [94,119]). In other words, 3D printing can be used to fabricate cellular metamaterials. For instance, selective laser melting (SLM) can be used to fabricate TiNi-based auxetic metamaterials [373]. A shortcoming of SLM is that the thermal footprint of the laser is usually large than the optical footprint, that is the laser spot size. The laser spot size must therefore be considered when calculating the tool path. Variations in heat transfer rate can lead to inhomogeneous distribution of solid metals in the conventional structures. It is therefore essential to tailor the NPR structure to be processable using the AM techniques, as shown in Fig. 28 [373]. Electron beam melting (EBM), one of the additive manufacturing processes, has been used to fabricate a 3D re-entrant NPR structure made from Ti-6Al-4V [374].

8.1.2. Interlocking assembly

Compared with the additive manufacturing methods, an alternative concept based on geometric interlocking assembly [207,375,376] has allowed the fabrication of periodic auxetic cellular structures. A two-dimensional auxetic model, shown in Fig. 29A, has been proposed by Ravirala et al. [375]. The assembly of interlocking hexagons deforms by particle translation to display auxetic behaviour. The geometric calculation of a hexagonally interlocked structure has shown an analytic solution for Young's moduli and Poisson's ratio,

$$E_x = k_h\left(\frac{2\cos^2\alpha+1}{\sin\alpha}\right)\left(\frac{l_1+l_2\cos\alpha+a}{l_2\sin^2\alpha+a\cos\alpha}\right) \tag{21}$$

$$E_y = k_h\left(\frac{2\cos^2\alpha+1}{\sin\alpha\cos^2\alpha}\right)\left(\frac{l_2\sin^2\alpha+a\cos\alpha}{l_1+l_2\cos\alpha+a}\right) \tag{22}$$

$$v_{xy} = -\frac{\cos\alpha(l_1+l_2\cos\alpha+a)}{l_2\sin^2\alpha+a\cos\alpha}, \quad v_{yx} = (v_{xy})^{-1} \tag{23}$$

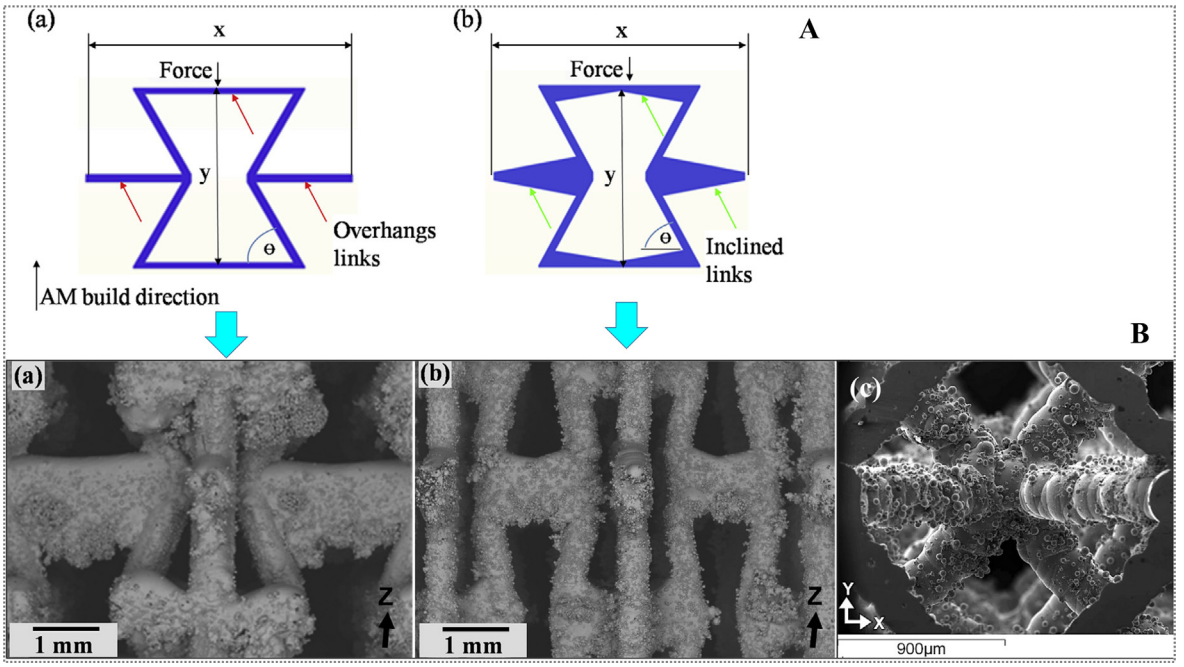

Fig. 28. (A) Re-entrant NPR (negative Poisson's ratio) unit cells (a) conventional unit cell, (b) modified AM (additive manufacturing) unit cell. (B) The morphology of TiNi-based NPR structures showing SEM micrographs for the (a) conventional re-entrant design, where the thickness of the struts changes due to the powder particles at its vicinity, (b) tailoring AM re-entrant design with relatively homogenous structures, and (c) a section through the struts showing the lack of cracks [373].

where E_x and E_y are the Young's modulus in the *x*- and *y*-directions, respectively, k_h, is connected to the stiffness of a spring of stiffness, l_1 and l_2 are the edge lengths of each hexagon, α is the angle between l_1 and l_2 aligned with the *x*-axis in Fig. 29A, *a* is the gap between adjoining hexagonal faces, and υ_{xy} and υ_{yx} are the Poisson's ratios for loading in the *x*- and *y*-directions, respectively [375].

Consequently, the fabrication of three-dimensional re-entrant auxetic structures [374] is emerging based on this interlocking assembly method. Auxeticity is attributed to the folding and unfolding of umbrella shaped elements in the 3D auxetic cellular structures, shown in Fig. 29B [376]. As seen in Fig. 29C, the Poisson's ratio υ_{yx} for a 3D interlocked structure is strongly dependent on the strut thickness, *t* [376].

8.1.3. Melt-electrospinning techniques

Melt-electrospinning is a direct writing mode [377], also considered by some to be a 3D printing method, which can be used to fabricate scaffold structures with honeycomb-like patterns for tissue engineering applications [378]. After nearly a decade of exploration, melt-electrospinning can be considered as initially coming from fused deposition modelling (FDM) [95,96,377–381]. This rapid prototyping (RP) technology (Fig. 30), also known as solid freeform fabrication (SFF), can make metamaterial structures much smaller and stronger. Tailoring the porosity of reinforced scaffolds can achieve a strong elastic component that can recover after physiological axial strains. Such structures are therefore expected to be a significant step towards developing biomechanically functional tissue constructs. A highly ordered arrangement of ultrafine fibres with distinctive surface topology can be used for encapsulating and sensing properties, opening new fields of application in areas such as textiles, filtration, environment, energy and biomedicine [378]. Currently, the melt electrospinning technique has been extended to an increasing range of synthetic polymers, composite systems, and other various materials including ceramics [377,381].

8.2. Research translation

Materials, both organic and inorganic, are found everywhere in nature. Material-parameter transformations have become an intuitive and powerful engineering tool in the design of inhomogeneous and anisotropic material distributions that perform desirable functions, e.g., invisibility cloaking. For example, a lattice of points from a discrete 2D lattice composed of a single constituent material can be transformed while keeping the properties of the elements connecting the lattice points the same [382]. A direct lattice-transformation approach can significantly alleviate and redistribute stress peaks in practical applications, such as tunnel walls in civil engineering. It is probable that we can obtain the materials we need, particularly by combining optical, acoustic and thermal metamaterials.

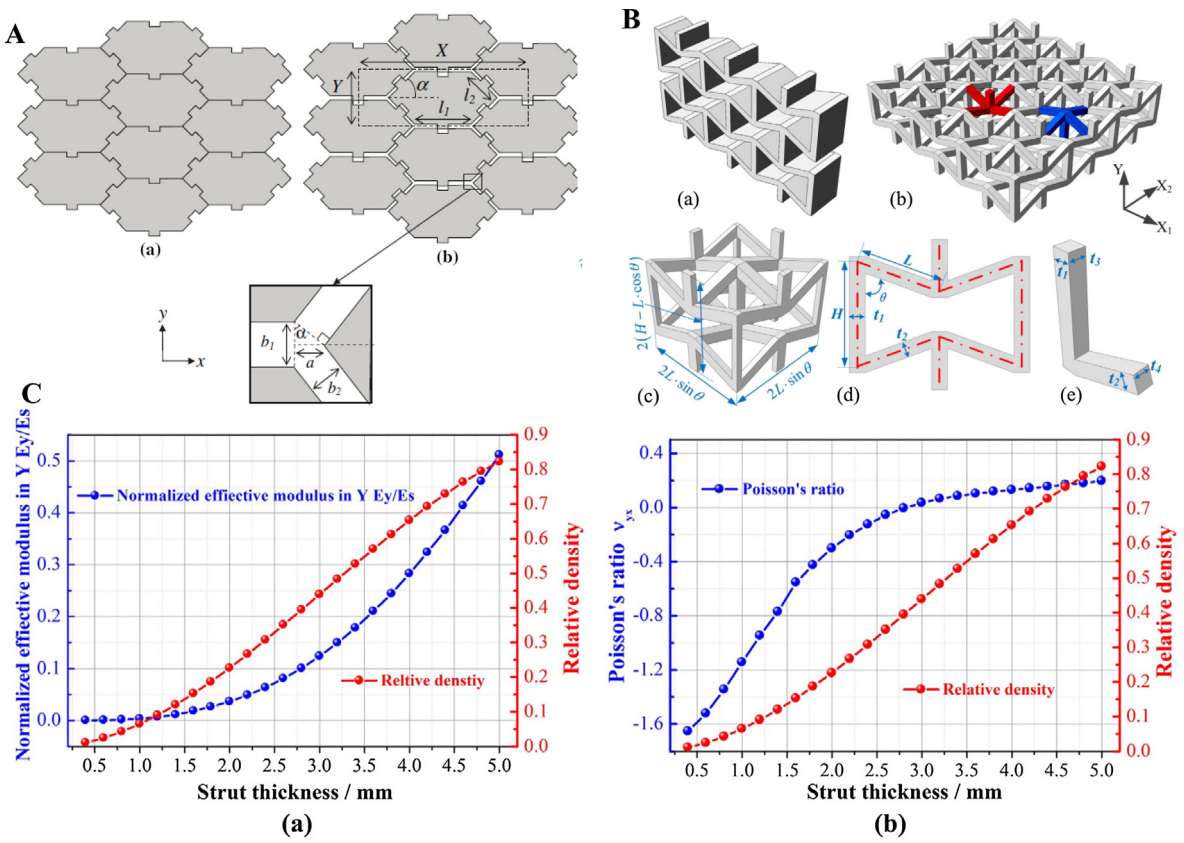

Fig. 29. (A) Interlocking two-dimensional hexagon structure for auxetic behaviour, (a) fully densified; (b) partially expanded [375]. The variable parameter is the gap parameter, a; a change in the interlock gap perpendicular to the adjoining hexagonal faces b_1, b_2, and each hexagon has edge lengths l_1 and l_2. The edges of length l_1 are aligned parallel to the x axis, and the edges of length l_2 are at an angle α to the x axis. (B) Interlocking assembled three-dimensional auxetic cellular structures [376]. (a) 2D re-entrant auxetic structure, (b) 3D re-entrant auxetic structure, and umbrella shaped elements, (c) the unit cell of the 3D auxetic structure and its dimensions, (d) in-plane parameters needed for describing 2D re-entrant auxetic structure, (e) more parameters needed for describing 3D re-entrant auxetic structure, the depth of the vertical strut t_3 and oblique strut t_4; where the length of the vertical struts (H), length of the oblique struts (L), the re-entrant angle (θ), width of the vertical struts (t_1) and width of the oblique struts (t_2). (C) The dependence of the (a) normalised compression Young's modulus, and (b) Poisson's ratio υ_{yx}, on the relative density of the structure in (B) [376].

8.3. Potential applications

Various applications can be found for mechanical metamaterials. First we will address the conditions associated with the application surroundings. Subsequently, one example from bioengineering and biomedical engineering will be introduced. Finally, some implications from the application are presented to solve conventional technical limitations. Combining different types of lattice metamaterials is proposed based upon the analysis of potential applications.

The elastic response of various mechanical metamaterials or biomaterials should be optimised for the intended application. Incorporating advanced lattice structures into mechanical metamaterials and non-Euclidean (fractal) geometries promotes novel methods to control the properties and performance of synthetic biomaterials for the biomedical field. The porous metamaterial obtained can be intersected with the geometry of a solid prosthesis to obtain a porous implant. These can also be specifically developed to promote the application of metamaterials to product development. A typical limitation of these applications is how to bridge their different conditions. The ideal application conditions are often constant and predictable, but sometimes the real conditions could be beyond what we predicted. Therefore, it is significant to clarify that various mechanical metamaterials, not only consequence of their special geometries, but also of interactions with external condition and constraints. That is to say, we need to know how conditions to entail in mechanical metamaterials. Sometimes they could be negative pressure or living tissues and their surroundings, and other possibilities describe the related research field.

In the case of bioengineering and biomedical engineering, auxetic metamaterials are expected to be designed with molecular scale control [370]. As such, this type of mechanical metamaterials can also be used in tissue engineering, with interactions at a cellular or even molecular level. The uniaxial excitations of an auxetic scaffold may lead to biaxial expansions and compressions of the growing tissue. This can promote growth and potentially control cell differentiation and tissue viability [366,369].

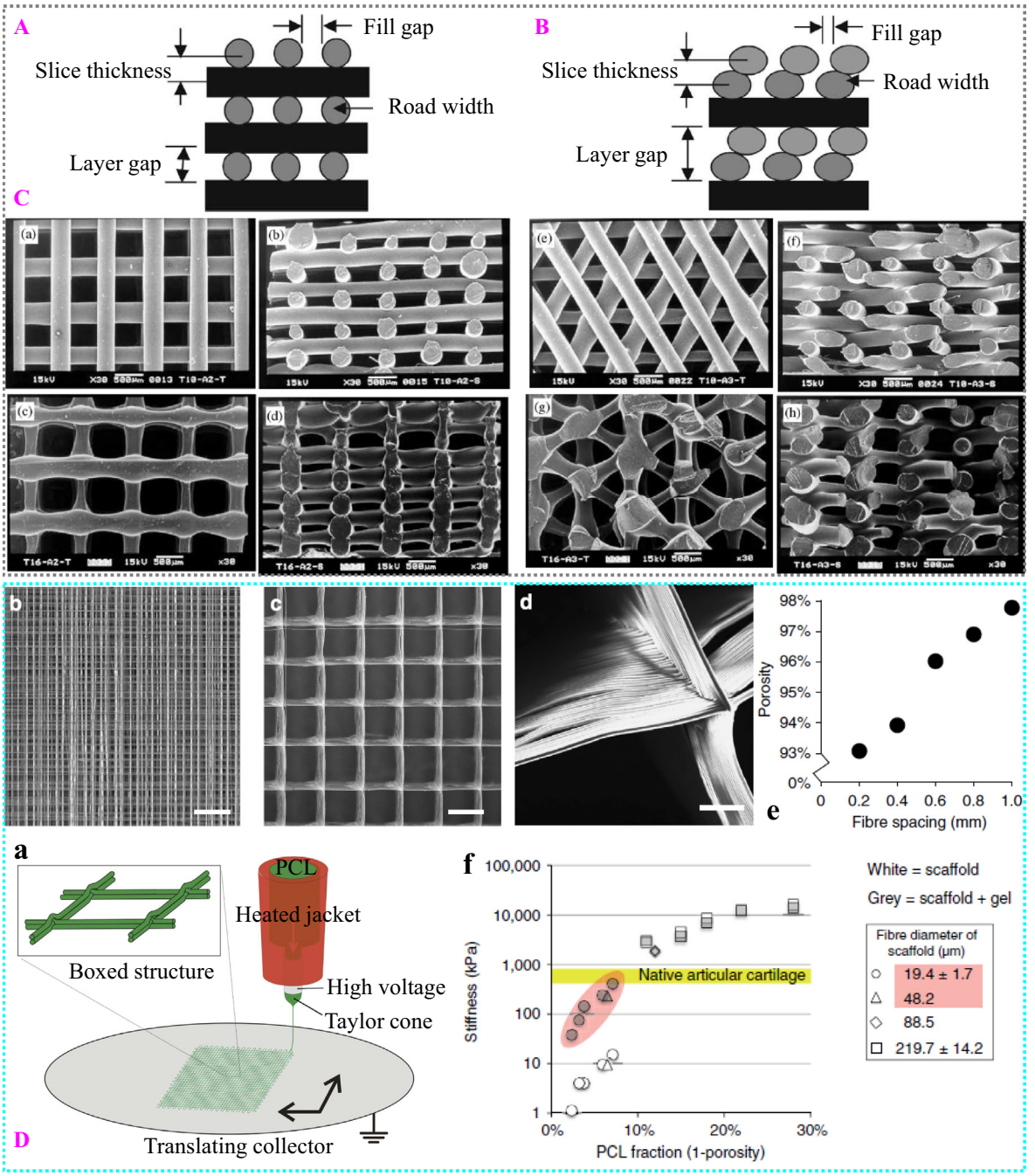

Fig. 30. Melt electrospinning writing for three-dimensionally printed microfibers. Lay-down pattern of (A) 0/90° forming square honeycomb pores, (B) 0/60/120° forming triangular honeycomb pores, in cross-section view during fused deposition modelling (FDM) building process. Polymer poly (ε-caprolactone) (PCL) scaffold fabricated (C) using the nozzle tip with the inner diameter 0.010 in, the target road width is approximately 0.254 mm, cut surface of lay-down pattern of (a) 0/90° in plan-view, (b) 0/90° in side-view, (e) 0/60/120° in plan-view, (f) 0/60/120° in side-view [95]; using the nozzle tip with the inner diameter 0.016 in, the target road width is approximately 0.406 mm, freeze-fractured surface of lay-down pattern of (c) 0/90° in plan-view, (d) 0/90° in side-view, (g) 0/60/120° in plan-view, (h) 0/60/120° in side-view [96]. (D) After nearly one decade, fabrication of PCL microfiber scaffolds [378] by 3D printing, here melt-electrospinning in a direct writing mode. (a) Thin PCL fibres were stacked in a 0–90° orientation through combined extrusion and an electrostatic field between the dispensing needle and the translating collector plate. Several fibre gaps were applied ranging from (b) 0.2 and (c) 1.0 mm as visualised with stereomicroscopy (scale bar, 1 mm). (d) Detailed image of the fibres that fused at the cross-sections (fibre spacing 1.0 mm, scale bar, 200 μm). (e) The porosity of the scaffolds varied between 93 and 98% depending on the set fibre spacing. (b) Moduli of scaffolds and scaffold/gel composites as a function of porosity, showing the synergistic increase in stiffness was only observed for thin-fibre scaffolds with a high porosity (polymer fraction 2–7% porosity 98–93% (highlighted in red)), fabricated with melt electrospinning writing (MEW). Fused deposition modelling (FDM) scaffolds were fabricated from 10-fold thicker fibres, resulting in a higher stiffness; however, no synergistic reinforcement was observed.

There is both a challenge and an opportunity for conventional photolithography or stereolithography techniques to fabricate two-dimensional auxetics. Generally, conventional techniques can yield a distance between lattices of around 50–100 μm. This range leaves significant clearances between the cells and prevents them from interacting at the single cellular level.

One complementary approach could be used to obtain novel metamaterials [321,383], such as pentamode mechanical metamaterials [33]. These mechanical metamaterials can be gradually tuned to provide fluid-like behaviour in spite of being a solid structure. They are expected to provide desired radial variations of mechanical properties within a scaffolding structure composed of a single material. In pentamode lattice metamaterials there are almost punctual contacts between trusses, thereby providing a remarkable flexibility. It is possible to combine pentamode metamaterials with micro-/nanolattices. The incorporation of geometrical gradients at contacts between trusses can lead to very rigid lattices in some parts of the scaffold and to very flexible lattices in other regions. Designable dual-material auxetic metamaterials can be fabricated using three-dimensional printing [384,385]. In addition, the combination of different types of lattice metamaterials and the use of conventional lattices, together with pentamode-based structures, can be used to control the mechanical properties of a single scaffold over a range of several orders of magnitude.

9. Conclusions and future directions

In this present work, mechanical metamaterials have been clearly recognised and systematically classified based on the fundamental material mechanics, i.e., the relationships among three elastic moduli and the Poisson's ratio. From the perspective of structure-fabrication-property relationships, this critical review covers the recent and rapidly advancing subject of mechanical metamaterials. Various counterintuitive mechanical properties can be achieved, providing a number of benefits which include: (i) a new variety of mechanical metamaterials that are ultra-lightweight and ultra-stiff, consisting of micro-/nanolattices, chiral/anti-chiral hierarchical, origami-inspired, and coupled cellular origami metamaterials; (ii) controllable and variable stiffness in various pattern transformations composed of various hole shapes set in different tessellations, confined by geometric constraints; (iii) vanishing shear modulus over a three-dimensional profile, metamaterials displaying two-dimensional properties similar to the behaviour of liquids, such as pentamode metamaterials; (iv) negative compressibility or negative thermal expansion, meaning metamaterial expansion under pressure, contraction under tension, and contraction upon warming; and (v) auxetics or negative Poisson's ratio materials yielding counterintuitive dilatational behaviour, that is, the occurrence of lateral expansion (negative transversal response) upon stretching. These anomalous mechanical responses are highly desired targets in the design of new modern materials with advanced properties.

Four current challenges dominate the design of mechanical metamaterials, based on the design principle, fabrication techniques and the application conditions of the mechanical metamaterials. First, combinations of various properties, such as a single mechanical metamaterial possessing ultra-stiffness, ultra-lightweight, and vanishing shear modulus, or combining tunable stiffness and positive/negative Poisson's ratio. Secondly, a combination of different motifs or structures, e.g. cellular origami, or cellular with chiral patterns [386], that can aid the topological optimisation of sophisticated, state-of-the-art geometrical configurations. The third challenge to extend to other parent materials, particularly metals or alloys, and thereby reduce the size effects of plasticity, fracture and large concentrations of stress. Finally, due to advanced research in nanostructures, particularly the dislocation of crystal defects with atomic scale resolution by virtue of three-dimensional characterisation techniques, it is widely expected that soon we can build intriguing structures atom by atom. These will not be limited to crystal defects as we move forward. Some implications from metal-organic frameworks (MOFs), and some technical hints for structural optimisation, will be shared.

9.1. Implications of metal-organic frameworks

Crystalline metal-organic frameworks can inspire future designs of mechanical metamaterials. MOFs are formed by reticular synthesis, which creates strong bonds between inorganic and organic units [321,387]. These materials are constructed by joining metal-containing units [secondary building units (SBUs)] with organic linkers, using strong bonds (reticular synthesis) to create open crystalline frameworks with permanent porosity [387]. MOFs have exceptional porosity and a wide range of potential uses, including gas storage, separations, catalysis, and applications in energy technologies such as fuel cells, supercapacitors, and catalytic converters [321]. The design concept of MOFs can be applied to new, advanced mechanical metamaterials, particularly to feasibly obtain the elegant properties of NLC/NAC, or NTE. If the natural MOF crystal structure can be simplified into struts and hinges, as shown in Fig. 31 [308,312,388], we can create new manmade structures, i.e., mechanical metamaterials, based on these frameworks. MOFs have various attractive mechanical behaviours, especially giant NLC/NAC and NTE effects [314,315,334]. By extending this analysis to other mechanical metamaterial topologies, it is possible to establish a generic predictive approach for the dimensionality of NTE or negative compressibility for a large range of different framework. The framework geometry can play a crucial role in determining the properties of metamaterials showing anisotropic responses via hinging.

9.2. Structural optimisation

In burgeoning negative compressibility, the range of the ratio of shear/bulk moduli, $-4/3G < K < 0$, can be another future direction. Ten years ago, Lakes et al. [67] proposed a range of negative compressibility, $-4/3G < K < 0$. This range setting

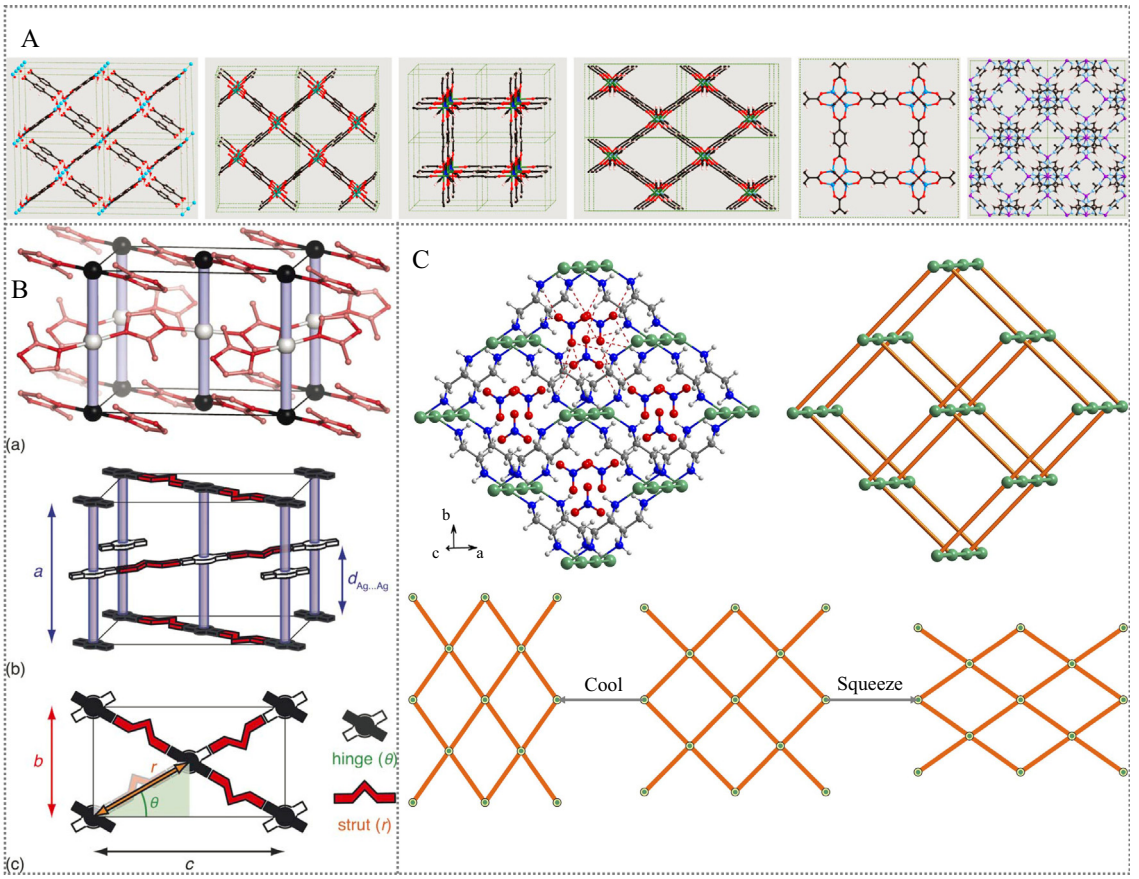

Fig. 31. Implications of metal-organic frameworks (MOFs). (A) Anisotropic elastic properties of Flexible MOFs [388]. (a) From left to right: MIL-53(Al) lp structure, MIL-47, DMOF1-sq, DMOF1-loz, MOF-5, and ZIF-8. (B) Supramolecular mechanics [308]. (a) Representation of the crystal structure of Ag(mim): Ag atoms shown as large black and white spheres and 2-methylimidazolate anions in red. Argentophilic interactions are shown as translucent cylinders. (b and c) Abstract representations of the same structure with atoms replaced by XBUs: argentophilic interactions, hinges and struts. Also indicated is the relationship between the XBU parameters $d_{Ag\cdots Ag}$, r, θ and the unitcell dimensions a, b, c. (C) Giant negative linear compression positively coupled to massive thermal expansion in [Ag(en)]NO_3-I [314]. (a) The framework of Ag^+ cations linked by $NH_2(CH_2)_2NH_2$ (en) ligands viewed approximately along the channels filled with anions NO_3^-. The NH···O and CH···O hydrogen bonds are indicated as red dashed lines. (b) The framework of $CdSO_4$ type topology. (c) The schematic illustration exaggerating the 'wine-rack' motif responses to temperature and pressure. Colour code: green balls and sticks represent Ag···Ag bonds, orange struts –en–Ag–en–, grey atoms C, red O, blue N, light grey H.

originated partly from the allowable range of Poisson's ratios for isotropic elastic solids, $-1 < \upsilon < 0.5$, and was further deduced by the strong ellipticity requirement. We then wondered how we can achieve-and even possibly extend-this focus range.

In emerging origami-inspired metamaterials, the next step is to continue to emulate the principles of paper folding and translating them into the design of new DNA origami metamaterials and advanced applications [389]. Formalising the rules of origami for use in computer modelling and simulation has been challenging [182]. This is because theoretical models tend to oversimplify, often erroneously classifying a foldable origami structure as unfoldable. Modelling or simulation is a simplified formalisation for the natural world. We can see the world use these tools, but not nature itself. If we believe some currently impossible thing can be derived by modelling or simulation, and if we provide some totally different boundary conditions, or use new fabrication methods, we can see the impossible made possible. This is what research is currently doing. This is the case for the square-twist crease pattern [179]. To achieve heuristic developments in constructing patterns with desirable qualities, the bridge between origami and physics is established. Following this route, we have sound reason to believe that geometric crystallography, for instance, the Bravais crystal lattice, Miller indices, and even preferred crystallographic orientation, i.e., microtexture in Euler space represented by three Eulerian angles in Bunge notation [199], can give the necessary theoretical underpinning to the structural design of mechanical metamaterials. Simultaneously, it is necessary for us to consider how to establish a new periodic of table physical properties [390] or gene engineering of materials, analogous to the periodic table of elements. Hence, it will be possible to design materials on demand, and thereby predict the mechanical properties of various materials.

One challenge is how to deal with substantial geometric complexity when studying three-dimensional mechanical metamaterials, such as three-dimensional pentamode structures [44,285] or plane pantographic metamaterials [391]. The metamaterial concept combined with such fabrication technologies might further enable interesting mechanical metamaterials in future studies. For example, even lighter metamaterials than the micro-/nanolattice cellular materials presented, with much smaller unit cells. Another interesting possibility could couple different types of metamaterials, e.g., Mechano-optical, mechano-acoustic, and mechano-thermal metamaterials. These explorations are coming into reach and no longer seem far off.

In conclusion, the integration of metamaterials and topological optimisation into customer-responsive microstructures allow for the development of novel cutting-edge and technologically relevant manmade materials. Mechanical metamaterials have various counterintuitive mechanical properties, some of which cannot be found in nature, and thereby have broad potential in applications across multiple areas of material research. Particularly recently, rapid advances have been made in fabrication technique. Different modes of additive manufacturing are reducing the structural size scale of the fabricated materials, the range of usable metamaterials, and most importantly, the unit cost. A relatively cheap additive process with nanometre resolution will emerge, and will thereby open the possibility of various truss-type nanolattices through a net-shape manufacturing process, to achieve negative thermal expansion. The broader the vision for metamaterials, the larger will be the number of opportunities for materials science. Therefore, mechanical metamaterials are expected to begin a new era of materials which are much lighter, stronger, tougher, and more durable. What we want new metamaterials to be, or to do, or to think, will be achieved through the design of new crystal-like structures, new constituents or new properties.

Acknowledgements

This work was supported by the China Postdoctoral Science Foundation under Grant No. 2015M580094, and the National Natural Science Foundation of China under Grant Nos. 11274198 and 51532004. The authors thank the support from Fundamental Research Funds for the Central Universities of China (WK2480000001, WK2090050040). The authors also thank corresponding publishers/authors for their kind permission to reproduce their figures. The authors gratefully acknowledge the persons who were contacted for their helpful discussions and inputs.

References

[1] Zheludev NI. The road ahead for metamaterials. Science 2010;328:582–3.
[2] Soukoulis CM, Wegener M. Past achievements and future challenges in the development of three-dimensional photonic metamaterials. Nat Photonics 2011;5:523–30.
[3] Pendry JB. Negative refraction makes a perfect lens. Phys Rev Lett 2000;85:3966.
[4] Shelby RA, Smith DR, Schultz S. Experimental verification of a negative index of refraction. Science 2001;292:77–9.
[5] Smith DR, Pendry JB, Wiltshire MC. Metamaterials and negative refractive index. Science 2004;305:788–92.
[6] Bose JC. On the rotation of plane of polarisation of electric waves by a twisted structure. P R Soc Lond 1898;63:146–52.
[7] Veselago VG. The electrodynamics of substances with simulaneously negative values of ε and μ. Phys-Usp+ 1968;10:509–14.
[8] Solymar L, Shamonina E. Waves in metamaterials. Oxford: Oxford University Press; 2009.
[9] Pendry JB, Schurig D, Smith DR. Controlling electromagnetic fields. Science 2006;312:1780–2.
[10] Cai W, Shalaev V. Optical metamaterials: fundamentals and applications. New York: Springer; 2010.
[11] Marqués R, Martín F, Sorolla M. Metamaterials with negative parameters: theory, design and microwave applications. New Jersey: John Wiley & Sons; 2011.
[12] Wegener M. Metamaterials beyond optics. Science 2013;342:939–40.
[13] Maldovan M. Sound and heat revolutions in phononics. Nature 2013;503:209–17.
[14] Liu Y, Zhang X. Metamaterials: a new frontier of science and technology. Chem Soc Rev 2011;40:2494–507.
[15] Zhao Q, Zhou J, Zhang F, Lippens D. Mie resonance-based dielectric metamaterials. Mater Today 2009;12:60–9.
[16] Li X, Gao H. Mechanical metamaterials: smaller and stronger. Nat Mater 2016;15:373–4.
[17] Pacchioni G. Mechanical metamaterials: the strength awakens. Nat Rev Mater 2016.
[18] Wang P, Shim J, Bertoldi K. Effects of geometric and material nonlinearities on tunable band gaps and low-frequency directionality of phononic crystals. Phys Rev B 2013;88:014304.
[19] Lee JB, Peng S, Yang D, Roh YH, Funabashi H, Park N, et al. A mechanical metamaterial made from a DNA hydrogel. Nat Nanotechnol 2012;7:816–20.
[20] Bückmann T, Thiel M, Kadic M, Schittny R, Wegener M. An elasto-mechanical unfeelability cloak made of pentamode metamaterials. Nat Commun 2014;5:4130.
[21] Kuzyk A, Schreiber R, Fan Z, Pardatscher G, Roller E-M, Högele A, et al. DNA-based self-assembly of chiral plasmonic nanostructures with tailored optical response. Nature 2012;483:311–4.
[22] Brûlé S, Javelaud EH, Enoch S, Guenneau S. Experiments on seismic metamaterials: molding surface waves. Phys Rev Lett 2014;112:133901.
[23] Shim J, Shan S, Košmrlj A, Kang SH, Chen ER, Weaver JC, et al. Harnessing instabilities for design of soft reconfigurable auxetic/chiral materials. Soft Matter 2013;9:8198–202.
[24] Zhang Y, Matsumoto EA, Peter A, Lin P-C, Kamien RD, Yang S. One-step nanoscale assembly of complex structures via harnessing of an elastic instability. Nano Lett 2008;8:1192–6.
[25] Matsumoto EA, Kamien RD. Elastic-instability triggered pattern formation. Phys Rev E 2009;80:021604.
[26] Bertoldi K, Reis PM, Willshaw S, Mullin T. Negative Poisson's ratio behavior induced by an elastic instability. Adv Mater 2010;22:361–6.
[27] Matsumoto EA, Kamien RD. Patterns on a roll: a method of continuous feed nanoprinting. Soft Matter 2012;8:11038–41.
[28] Lakes R. Foam structures with a negative Poisson's ratio. Science 1987;235:1038–40.
[29] Milton GW. Composite materials with Poisson's ratios close to −1. J Mech Phys Solids 1992;40:1105–37.
[30] Prall D, Lakes R. Properties of a chiral honeycomb with a Poisson's ratio of −1. Int J Mech Sci 1997;39:305–14.
[31] Evans KE, Alderson A. Auxetic materials: functional materials and structures from lateral thinking! Adv Mater 2000;12:617–28.
[32] Lim T-C. Auxetic materials and structures. Singapore: Springer; 2015.

[33] Kadic M, Bückmann T, Stenger N, Thiel M, Wegener M. On the practicability of pentamode mechanical metamaterials. Appl Phys Lett 2012;100:191901.
[34] Christensen J, Kadic M, Kraft OI, Wegener M. Vibrant times for mechanical metamaterials. MRS Commun 2015;5:453–62.
[35] Gatt R, Grima JN. Negative compressibility. Phys Status Solidi 2008;2:236–8.
[36] Lakes R, Lee T, Bersie A, Wang Y. Extreme damping in composite materials with negative-stiffness inclusions. Nature 2001;410:565–7.
[37] Nicolaou ZG, Motter AE. Mechanical metamaterials with negative compressibility transitions. Nat Mater 2012;11:608–13.
[38] Wyart M, Liang H, Kabla A, Mahadevan L. Elasticity of floppy and stiff random networks. Phys Rev Lett 2008;101:215501.
[39] Gómez LR, Turner AM, van Hecke M, Vitelli V. Shocks near jamming. Phys Rev Lett 2012;108:058001.
[40] Chen BG-G, Upadhyaya N, Vitelli V. Nonlinear conduction via solutions in a topological mechanical insulator. Proc Natl Acad Sci 2014;111:13004–9.
[41] Paulose J, Chen BG-G, Vitelli V. Topological modes bound to dislocations in mechanical metamaterials. Nat Phys 2015;11:153–6.
[42] Nash LM, Kleckner D, Read Al, Vitelli V, Turner AM, Irvine WTM. Topological mechanics of gyroscopic metamaterials. Proc Natl Acad Sci 2015;112:14495–500.
[43] Bauer J, Schroer A, Schwaiger R, Kraft O. Approaching theoretical strength in glassy carbon nanolattices. Nat Mater 2016;15:438–43.
[44] Kadic M, Bueckmann T, Schittny R, Wegener M. Metamaterials beyond electromagnetism. Rep Prog Phys 2013;76:126501.
[45] Fleury R, Monticone F, Alù A. Invisibility and cloaking: origins, present, and future perspectives. Phys Rev Appl 2015;4:037001.
[46] Sun J, Litchinitser NM. Metamaterials. In: Haus JW, editor. Fundamentals and applications of nanophotonics. Waltham: Woodhead Publishing; 2016. p. 253–307.
[47] dell'Isola F, Steigmann D, Corte AD. Synthesis of fibrous complex structures: designing microstructure to deliver targeted macroscale response. Appl Mech Rev 2016;67:060804.
[48] Lee JH, Singer JP, Thomas EL. Micro-/nanostructured mechanical metamaterials. Adv Mater 2012;24:4782–810.
[49] Vescovo DD, Giorgio I. Dynamic problems for metamaterials: review of existing models and ideas for further research. Int J Eng Sci 2014;80:153–72.
[50] Lee JH, Koh CY, Singer JP, Jeon SJ, Maldovan M, Stein O, et al. 25th anniversary article: ordered polymer structures for the engineering of photons and phonons. Adv Mater 2014;26:532–69.
[51] Lee SH, Park CM, Seo YM, Wang ZG, Kim CK. Acoustic metamaterial with negative modulus. J Phys-Condens Mater 2009;21:175704.
[52] Bažant ZP, Cedolin L. Stability of structures: elastic, inelastic, fracture and damage theories. London: World Scientific; 2010.
[53] Timoshenkgo S, Goodier J. Theory of elasticity. New York: McGraw-Hill; 1970.
[54] Ledbetter H, Reed RP. Elastic properties of metals and alloys, I. Iron, nickel, and iron-nickel alloys. J Phys Chem Ref Data 1973;2:531–618.
[55] Milton GW. The theory of composites. New York: Cambridge University Press; 2002.
[56] Newnham RE. Properties of materials: anisotropy, symmetry, structure. Oxford: Oxford University Press; 2004.
[57] Eisenstadt MM. Introduction to mechanical properties of materials. New York: Macmillan; 1971.
[58] Atkin RJ, Fox N. An introduction to the theory of elasticity. London: Courier Corporation; 2013.
[59] Fung Y. Foundations of solid mechanics. New Jersey: Upper Saddle River; 1965.
[60] Wang Y, Lakes R. Extreme stiffness systems due to negative stiffness elements. Am J Phys 2004;72:40–50.
[61] de Jong M, Chen W, Angsten T, Jain A, Notestine R, Gamst A, et al. Charting the complete elastic properties of inorganic crystalline compounds. Sci Data 2015;2:150009.
[62] Greaves GN, Greer A, Lakes R, Rouxel T. Poisson's ratio and modern materials. Nat Mater 2011;10:823–37.
[63] Milton GW, Cherkaev AV. Which elasticity tensors are realizable? J Eng Mater Technol 1995;117:483–93.
[64] Xie YM, Yang X, Shen J, Yan X, Ghaedizadeh A, Rong J, et al. Designing orthotropic materials for negative or zero compressibility. Int J Solids Struct 2014;51:4038–51.
[65] Ashby MF. Materials selection in mechanical design. 4th ed. Burlington, MA: Butterworth-Heinemann; 2011.
[66] Schaedler T, Jacobsen A, Torrents A, Sorensen A, Lian J, Greer J, et al. Ultralight metallic microlattices. Science 2011;334:962–5.
[67] Wang Y, Lakes R. Composites with inclusions of negative bulk modulus: extreme damping and negative Poisson's ratio. J Compos Mater 2005;39:1645–57.
[68] Xinchun S, Lakes RS. Stability of elastic material with negative stiffness and negative Poisson's ratio. Phys Status Solidi B 2007;244:1008–26.
[69] Lakes R, Wojciechowski K. Negative compressibility, negative Poisson's ratio, and stability. Phys Status Solidi B 2008;245:545–51.
[70] Nicolaou ZG, Motter AE. Longitudinal inverted compressibility in super-strained metamaterials. J Stat Phys 2013;151:1162–74.
[71] Cairns AB, Goodwin A. Negative linear compressibility. Phys Chem Chem Phys 2015;17:20449–65.
[72] Cairns AB, Catafesta J, Levelut C, Rouquette J, Van Der Lee A, Peters L, et al. Giant negative linear compressibility in zinc dicyanoaurate. Nat Mater 2013;12:212–6.
[73] Goodwin AL, Keen DA, Tucker MG. Large negative linear compressibility of $Ag_3[Co(CN)_6]$. Proc Natl Acad Sci 2008;105:18708–13.
[74] Haghpanah B, Papadopoulos J, Mousanezhad D, Nayeb-Hashemi H, Vaziri A. Buckling of regular, chiral and hierarchical honeycombs under a general macroscopic stress state. Proc R Soc A 2014;470:20130856.
[75] Zheng X, Lee H, Weisgraber TH, Shusteff M, DeOtte J, Duoss EB, et al. Ultralight, ultrastiff mechanical metamaterials. Science 2014;344:1373–7.
[76] Choi J, Lakes R. Nonlinear analysis of the Poisson's ratio of negative Poisson's ratio foams. J Compos Mater 1995;29:113–28.
[77] Celli P, Gonella S. Tunable directivity in metamaterials with reconfigurable cell symmetry. Appl Phys Lett 2015;106:091905.
[78] Silverberg JL, Evans AA, McLeod L, Hayward RC, Hull T, Santangelo CD, et al. Using origami design principles to fold reprogrammable mechanical metamaterials. Science 2014;345:647–50.
[79] Li S, Wang KW. Fluidic origami: a plant-inspired adaptive structure with shape morphing and stiffness tuning. Smart Mater Struct 2015;24:105031.
[80] Bertoldi K, Boyce M, Deschanel S, Prange S, Mullin T. Mechanics of deformation-triggered pattern transformations and superelastic behavior in periodic elastomeric structures. J Mech Phys Solids 2008;56:2642–68.
[81] Mullin T, Deschanel S, Bertoldi K, Boyce M. Pattern transformation triggered by deformation. Phys Rev Lett 2007;99:084301.
[82] Shan S, Kang SH, Wang P, Qu C, Shian S, Chen ER, et al. Harnessing multiple folding mechanisms in soft periodic structures for tunable control of elastic waves. Adv Funct Mater 2014;24:4935–42.
[83] Audoly B, Boudaoud A. Buckling of a stiff film bound to a compliant substrate—Part I: formulation, linear stability of cylindrical patterns, secondary bifurcations. J Mech Phys Solids 2008;56:2401–21.
[84] Fleck N, Deshpande V, Ashby M. Micro-architectured materials: past, present and future. Proc R Soc A 2010;466:2495–516.
[85] Neelakantan S, Bosbach W, Woodhouse J, Markaki A. Characterization and deformation response of orthotropic fibre networks with auxetic out-of-plane behaviour. Acta Mater 2014;66:326–39.
[86] Gibson LJ, Ashby MF. Cellular solids: structure and properties. New York: Cambridge University Press; 1997.
[87] Lakes R. Materials with structural hierarchy. Nature 1993;361:511–5.
[88] Queheillalt DT, Wadley HN. Cellular metal lattices with hollow trusses. Acta Mater 2005;53:303–13.
[89] Torrents A, Schaedler T, Jacobsen A, Carter W, Valdevit L. Characterization of nickel-based microlattice materials with structural hierarchy from the nanometer to the millimeter scale. Acta Mater 2012;60:3511–23.
[90] Cundy HM, Rollett AP. Mathematical models. Oxford: Clarendon Press Oxford; 1961.
[91] Lockwood EH, Macmillan RH. Geometric symmetry. Cambridge: CUP Archive; 1978.
[92] Frederickson GN. Dissections: plane and fancy. New York: Cambridge University Press; 2003.
[93] Hyun S, Torquato S. Optimal and manufacturable two-dimensional, Kagome-like cellular solids. J Mater Res 2002;17:137–44.
[94] Hedayati R, Sadighi M, Mohammadi-Aghdam M, Zadpoor AA. Mechanics of additively manufactured porous biomaterials based on the rhombicuboctahedron unit cell. J Mech Behav Biomed Mater 2016;53:272–94.

[95] Hutmacher DW, Schantz T, Zein I, Ng KW, Teoh SH, Tan KC. Mechanical properties and cell cultural response of polycaprolactone scaffolds designed and fabricated via fused deposition modeling. J Biomed Mater Res 2001;55:203–16.
[96] Zein I, Hutmacher DW, Tan KC, Teoh SH. Fused deposition modeling of novel scaffold architectures for tissue engineering applications. Biomaterials 2002;23:1169–85.
[97] Deshpande V, Fleck N, Ashby M. Effective properties of the octet-truss lattice material. J Mech Phys Solids 2001;49:1747–69.
[98] Ma HS, Prevost JH, Jullien R, Scherer GW. Computer simulation of mechanical structure-property relationship of aerogels. J Non-Cryst Solids 2001;285:216–21.
[99] Shen J, Zhou S, Huang X, Xie YM. Simple cubic three-dimensional auxetic metamaterials. Phys Status Solidi B 2014;251:1515–22.
[100] Maldovan M, Ullal CK, Jang JH, Thomas EL. Sub-micrometer scale periodic porous cellular structures: microframes prepared by holographic interference lithography. Adv Mater 2007;19:3809–13.
[101] Lee J-H, Wang L, Kooi S, Boyce MC, Thomas EL. Enhanced energy dissipation in periodic epoxy nanoframes. Nano Lett 2010;10:2592–7.
[102] Wang L, Boyce MC, Wen CY, Thomas EL. Plastic dissipation mechanisms in periodic microframe-structured polymers. Adv Funct Mater 2009;19:1343–50.
[103] Bückmann T, Stenger N, Kadic M, Kaschke J, Frölich A, Kennerknecht T, et al. Tailored 3D mechanical metamaterials made by dip-in direct-laser-writing optical lithography. Adv Mater 2012;24:2710–4.
[104] Evans A, Hutchinson J, Fleck N, Ashby M, Wadley H. The topological design of multifunctional cellular metals. Prog Mater Sci 2001;46:309–27.
[105] Ashby MF. Metal foams: a design guide. Woburn (MA): Butterworth-Heinemann; 2000.
[106] Meza LR, Das S, Greer JR. Strong, lightweight, and recoverable three-dimensional ceramic nanolattices. Science 2014;345:1322–6.
[107] Bell AG. The tetrahedral principle in kite structure. NGM 1903;14:6.
[108] Maloney KJ, Roper CS, Jacobsen AJ, Carter WB, Valdevit L, Schaedler TA. Microlattices as architected thin films: analysis of mechanical properties and high strain elastic recovery. APL Mater 2013;1:022106.
[109] Qiu L, Liu JZ, Chang SL, Wu Y, Li D. Biomimetic superelastic graphene-based cellular monoliths. Nat Commun 2012;3:1241.
[110] Worsley MA, Kucheyev SO, Satcher Jr JH, Hamza AV, Baumann TF. Mechanically robust and electrically conductive carbon nanotube foams. Appl Phys Lett 2009;94:073115.
[111] Davami K, Zhao L, Lu E, Cortes J, Lin C, Lilley DE, et al. Ultralight shape-recovering plate mechanical metamaterials. Nat Commun 2015;6:10019.
[112] Meza LR, Zelhofer AJ, Clarke N, Mateos AJ, Kochmann DM, Greer JR. Resilient 3D hierarchical architected metamaterials. Proc Natl Acad Sci 2015;112:11502–7.
[113] Deshpande VS, Ashby MF, Fleck NA. Foam topology: bending versus stretching dominated architectures. Acta Mater 2001;49:1035–40.
[114] Gurtner G, Durand M. Stiffest elastic networks. Proc R Soc A 2014;470:20130611.
[115] Norris AN. Mechanics of elastic networks. Proc R Soc Lond A 2014;470:20140522.
[116] Zhu C, Han TY-J, Duoss EB, Golobic AM, Kuntz JD, Spadaccini CM, et al. Highly compressible 3D periodic graphene aerogel microlattices. Nat Commun 2015;6:6962.
[117] Mecklenburg M, Schuchardt A, Mishra YK, Kaps S, Adelung R, Lotnyk A, et al. Aerographite: ultra lightweight, flexible nanowall, carbon microtube material with outstanding mechanical performance. Adv Mater 2012;24:3486–90.
[118] Jacobsen AJ, Mahoney S, Carter WB, Nutt S. Vitreous carbon micro-lattice structures. Carbon 2011;49:1025–32.
[119] Xu S, Shen J, Zhou S, Huang X, Xie Y. Design of lattice structures with controlled anisotropy. Mater Des 2016;93:443–7.
[120] Cabras L, Brun M. A class of auxetic three-dimensional lattices. J Mech Phys Solids 2016;91:56–72.
[121] Nguyen BD, Cho JS, Kang K. Optimal design of "Shellular", a micro-architectured material with ultralow density. Mater Des 2016;95:490–500.
[122] Lee MG, Lee JW, Han SC, Kang K. Mechanical analyses of "Shellular", an ultralow-density material. Acta Mater 2016;103:595–607.
[123] Han SC, Lee JW, Kang K. A new type of low density material: shellular. Adv Mater 2015;27:5506–11.
[124] Hyde S, Blum Z, Landh T, Lidin S, Ninham BW, Andersson S, et al. The language of shape. Danvers (MA, USA): Elsevier; 1996.
[125] Lee W, Kang DY, Song J, Moon JH, Kim D. Controlled unusual stiffness of mechanical metamaterials. Sci Rep 2016;6:20312.
[126] Wohlgemuth M, Yufa N, Hoffman J, Thomas EL. Triply periodic bicontinuous cubic microdomain morphologies by symmetries. Macromolecules 2001;34:6083–9.
[127] Schoen AH. Infinite periodic minimal surfaces without self-intersections. NASA technical report, TN D-5541, Washington DC; 1970.
[128] Miskin MZ, Jaeger HM. Adapting granular materials through artificial evolution. Nat Mater 2013;12:326–31.
[129] Salari-Sharif L, Schaedler TA, Valdevit L. Energy dissipation mechanisms in hollow metallic microlattices. J Mater Res 2014;29:1755–70.
[130] Khanoki S, Pasini D. Fatigue design of a mechanically biocompatible lattice for a proof-of-concept femoral stem. J Mech Behav Biomed Mater 2013;22:65–83.
[131] Liu Y, Schaedler TA, Chen X. Dynamic energy absorption characteristics of hollow microlattice structures. Mech Mater 2014;77:1–13.
[132] Zou JH, Liu JH, Karakoti AS, Kumar A, Joung D, Li QA, et al. Ultralight multiwalled carbon nanotube aerogel. ACS Nano 2010;4:7293–302.
[133] Montemayor LC, Greer JR. Mechanical response of hollow metallic nanolattices: combining structural and material size effects. J Appl Mech 2015;82:071012.
[134] Valdevit L, Jacobsen AJ, Greer JR, Carter WB. Protocols for the optimal design of multi-functional cellular structures: from hypersonics to micro-architected materials. J Am Ceram Soc 2011;94:15–34.
[135] Kang SH, Shan S, Košmrlj A, Noorduin WL, Shian S, Weaver JC, et al. Complex ordered patterns in mechanical instability induced geometrically frustrated triangular cellular structures. Phys Rev Lett 2014;112:098701.
[136] Meeussen AS, Paulose J, Vitelli V. Topological design of geared metamaterials; 2016. arXiv 1602:08769.
[137] Shan Z, Adesso G, Cabot A, Sherburne M, Asif SS, Warren O, et al. Ultrahigh stress and strain in hierarchically structured hollow nanoparticles. Nat Mater 2008;7:947–52.
[138] Grima JN, Gatt R, Farrugia P-S. On the properties of auxetic meta-tetrachiral structures. Phys Status Solidi B 2008;245:511–20.
[139] Wojciechowski KW. Two-dimensional isotropic system with a negative Poisson ratio. Phys Lett A 1989;137:60–4.
[140] Gatt R, Attard D, Farrugia P-S, Azzopardi KM, Mizzi L, Brincat J-P, et al. A realistic generic model for anti-tetrachiral systems. Phys Status Solidi B 2013;250:2012–9.
[141] Alderson A, Alderson K, Attard D, Evans K, Gatt R, Grima JN, et al. Elastic constants of 3-, 4-and 6-connected chiral and anti-chiral honeycombs subject to uniaxial in-plane loading. Compos Sci Technol 2010;70:1042–8.
[142] Spadoni A, Ruzzene M. Elasto-static micropolar behavior of a chiral auxetic lattice. J Mech Phys Solids 2012;60:156–71.
[143] Lorato A, Innocenti P, Scarpa F, Alderson A, Alderson KL, Zied KM, et al. The transverse elastic properties of chiral honeycombs. Compos Sci Technol 2010;70:1057–63.
[144] Chen Y, Scarpa F, Liu Y, Leng J. Elasticity of anti-tetrachiral anisotropic lattices. Int J Solids Struct 2013;50:996–1004.
[145] Sigmund O, Torquato S, Aksay IA. On the design of 1–3 piezocomposites using topology optimization. J Mater Res 1998;13:1038–48.
[146] Mousanezhad D, Haghpanah B, Ghosh R, Hamouda AS, Nayeb-Hashemi H, Vaziri A. Elastic properties of chiral, anti-chiral, and hierarchical honeycombs: a simple energy-based approach. Theor Appl Mech Lett 2016. https://doi.org/10.1016/j.taml.2016.02.004.
[147] Pozniak AA, Wojciechowski KW. Poisson's ratio of rectangular anti-chiral structures with size dispersion of circular nodes. Phys Status Solidi B 2014;251:367–74.
[148] Miller W, Smith CW, Scarpa F, Evans KE. Flatwise buckling optimization of hexachiral and tetrachiral honeycombs. Compos Sci Technol 2010;70:1049–56.
[149] Bacigalupo A, Gambarotta L. Simplified modelling of chiral lattice materials with local resonators. Int J Solids Struct 2016;83:126–41.
[150] Spadoni A, Ruzzene M, Gonella S, Scarpa F. Phononic properties of hexagonal chiral lattices. Wave Motion 2009;46:435–50.

[151] Abdeljaber O, Avci O, Inman DJ. Optimization of chiral lattice based metastructures for broadband vibration suppression using genetic algorithms. J Sound Vib 2016;369:50–62.
[152] Rossiter J, Takashima K, Scarpa F, Walters P, Mukai T. Shape memory polymer hexachiral auxetic structures with tunable stiffness. Smart Mater Struct 2014;23:045007.
[153] Bettini P, Airoldi A, Sala G, Di Landro L, Ruzzene M, Spadoni A. Composite chiral structures for morphing airfoils: numerical analyses and development of a manufacturing process. Compos Part B 2010;41:133–47.
[154] Zhang QC, Yang XH, Li P, Huang GY, Feng SS, Shen C, et al. Bioinspired engineering of honeycomb structure-using nature to inspire human innovation. Prog Mater Sci 2015;74:332–400.
[155] Lang RJ. The science of origami. Phys World 2007;20:30–1.
[156] Song J, Chen Y, Lu G. Axial crushing of thin-walled structures with origami patterns. Thin Wall Struct 2012;54:65–71.
[157] Schenk M, Guest SD. Geometry of miura-folded metamaterials. Proc Natl Acad Sci 2013;110:3276–81.
[158] Wei Z, Guo Z, Dudte L, Liang H, Mahadevan L. Geometric mechanics of periodic pleated origami. Phys Rev Lett 2013;110:215501.
[159] Waitukaitis S, Menaut R, Chen BG-g, van Hecke M. Origami multistability: from single vertices to metasheets. Phys Rev Lett 2015;114:055503.
[160] Lv C, Krishnaraju D, Konjevod G, Yu H, Jiang H. Origami based mechanical metamaterials. Sci Rep 2014;4:5979.
[161] Hanna BH, Lund JM, Lang RJ, Magleby SP, Howell LL. Waterbomb base: a symmetric single-vertex bistable origami mechanism. Smart Mater Struct 2014;23:094009.
[162] Demaine ED, O'Rourke J. Geometric folding algorithms. New York: Cambridge University Press; 2007.
[163] Lang RJ. Origami design secrets: mathematical methods for an ancient art. Boca Raton: AK Peters/CRC Press; 2011.
[164] Peraza-Hernandez EA, Hartl DJ, Malak Jr RJ, Lagoudas DC. Origami-inspired active structures: a synthesis and review. Smart Mater Struct 2014;23:094001.
[165] Bowen LA, Grames CL, Magleby SP, Howell LL, Lang RJ. A classification of action origami as systems of spherical mechanisms. J Mech Des 2013;135:111008.
[166] Silverberg JL, Na J-H, Evans AA, Liu B, Hull TC, Santangelo CD, et al. Origami structures with a critical transition to bistability arising from hidden degrees of freedom. Nat Mater 2015;14:389–93.
[167] Shafer J. Origami to astonish and amuse. New York: St. Martin's Griffin; 2001.
[168] Miura K. New structural form of sandwich core. J Aircraft 1975;12:437–41.
[169] Miura K. Method of packaging and deployment of large membranes in space. In: Proceedings of 31st congress international astronautical federation. p. 1–10.
[170] Papa A, Pellegrino S. Systematically creased thin-film membrane structures. J Spacecraft Rockets 2008;45:10–8.
[171] Kim J, Hanna JA, Byun M, Santangelo CD, Hayward RC. Designing responsive buckled surfaces by halftone gel lithography. Science 2012;335:1201–5.
[172] Jamal M, Kadam SS, Xiao R, Jivan F, Onn TM, Fernandes R, et al. Bio-origami hydrogel scaffolds composed of photocrosslinked PEG bilayers. Adv Healthc Mater 2013;2:1142–50.
[173] Mahadevan L, Rica S. Self-organized origami. Science 2005;307:1740.
[174] Amar MB, Jia F. Anisotropic growth shapes intestinal tissues during embryogenesis. Proc Natl Acad Sci 2013;110:10525–30.
[175] Shyer AE, Tallinen T, Nerurkar NL, Wei Z, Gil ES, Kaplan DL, et al. Villification: how the gut gets its villi. Science 2013;342:212–8.
[176] Yasuda H, Yang J. Reentrant origami-based metamaterials with negative Poisson's ratio and bistability. Phys Rev Lett 2015;114:185502.
[177] Landau L. Theory of elasticity. New Delhi: Butterworth Heinemann; 1986.
[178] Tachi T. Freeform variations of origami. J Geom Graph 2010;14:203–15.
[179] Demaine ED, Demaine ML, Hart V, Price GN, Tachi T. (Non) existence of pleated folds: how paper folds between creases. Graph Combinator 2011;27:377–97.
[180] Resch RD. Self-supporting structural unit having a series of repetitious geometrical modules. US patent no. 3407558; 1968.
[181] Tachi T. Designing freeform origami tessellations by generalizing Resch's patterns. J Mech Des 2013;135:111006.
[182] Al-Mulla T, Buehler MJ. Origami: folding creases through bending. Nat Mater 2015;14:366–8.
[183] Kim J, Hanna JA, Hayward RC, Santangelo CD. Thermally responsive rolling of thin gel strips with discrete variations in swelling. Soft Matter 2012;8:2375–81.
[184] Qi Z, Campbell DK, Park HS. Atomistic simulations of tension-induced large deformation and stretchability in graphene kirigami. Phys Rev B 2014;90:245437.
[185] Cho Y, Shin J-H, Costa A, Kim TA, Kunin V, Li J, et al. Engineering the shape and structure of materials by fractal cut. Proc Natl Acad Sci 2014;111:17390–5.
[186] Zhang Y, Yan Z, Nan K, Xiao D, Liu Y, Luan H, et al. A mechanically driven form of Kirigami as a route to 3D mesostructures in micro/nanomembranes. Proc Natl Acad Sci 2015;112:11757–64.
[187] Xu S, Yan Z, Jang K-I, Huang W, Fu H, Kim J, et al. Assembly of micro/nanomaterials into complex, three-dimensional architectures by compressive buckling. Science 2015;347:154–9.
[188] Castle T, Cho Y, Gong X, Jung E, Sussman DM, Yang S, et al. Making the cut: lattice kirigami rules. Phys Rev Lett 2014;113:245502.
[189] Sussman DM, Cho Y, Castle T, Gong X, Jung E, Yang S, et al. Algorithmic lattice kirigami: a route to pluripotent materials. Proc Natl Acad Sci 2015;112:7449–53.
[190] Chen BG-G, Liu B, Evans AA, Paulose J, Cohen I, Vitelli V, et al. Topological mechanics of origami and kirigami; 2016. arXiv:1508:00795.
[191] Eidini M. Zigzag-base folded sheet cellular mechanical metamaterials. Extreme Mech Lett 2016;6:96–102.
[192] Eidini M, Paulino GH. Unraveling metamaterial properties in zigzag-base folded sheets. Sci Adv 2015;1:1500224.
[193] Liu S, Lv W, Chen Y, Lu G. Deployable prismatic structures with rigid origami patterns. J Mech Robot 2016;8:031002.
[194] Brunck V, Lechenault F, Reid A, Adda-Bedia M. Elastic theory of origami-based metamaterials. Phys Rev E 2016;93:033005.
[195] Hanna BH, Magleby SP, Lang RJ, Howell LL. Force–deflection modeling for generalized origami waterbomb-base mechanisms. J Appl Mech 2015;82:081001.
[196] Waitukaitis S, van Hecke M. Origami building blocks: generic and special four-vertices. Phys Rev E 2016;93:023003.
[197] Huffman DA. Curvature and creases: a primer on paper. IEEE Trans Comput 1976;25:1010–9.
[198] Evans AA, Silverberg JL, Santangelo CD. Lattice mechanics of origami tessellations. Phys Rev E 2015;92:013205.
[199] Bunge H-J. Texture analysis in materials science: mathematical methods. Berlin: Butterworth; 1982.
[200] Bös F, Vouga E, Gottesman O, Wardetzky M. On the incompressibility of cylindrical origami patterns; 2016. arXiv:1507:08472.
[201] Overvelde JTB, de Jong TA, Shevchenko Y, Becerra SA, Whitesides GM, Weaver JC, et al. A three-dimensional actuated origami-inspired transformable metamaterial with multiple degrees of freedom. Nat Commun 2016;7:10929.
[202] Safsten C, Fillmore T, Logan A, Halverson D, Howell L. Analyzing the stability properties of kaleidocycles. J Appl Mech 2016;83:051001.
[203] Klett Y, Middendorf P. Kinematic analysis of congruent multilayer tessellations. J Mech Robot 2016;8:034501.
[204] Cheung KC, Tachi T, Calisch S, Miura K. Origami interleaved tube cellular materials. Smart Mater Struct 2014;23:094012.
[205] Tachi T, Miura K. Rigid-foldable cylinders and cells. J IASS 2012;53:217–26.
[206] Filipov ET, Tachi T, Paulino GH. Origami tubes assembled into stiff, yet reconfigurable structures and metamaterials. Proc Natl Acad Sci 2015;112:12321–6.
[207] Cheung KC, Gershenfeld N. Reversibly assembled cellular composite materials. Science 2013;341:1219–21.
[208] Genzer J, Groenewold J. Soft matter with hard skin: from skin wrinkles to templating and material characterization. Soft Matter 2006;2:310–23.

[209] Bende NP, Evans AA, Innes-Gold S, Marin LA, Cohen I, Hayward RC, et al. Geometrically controlled snapping transitions in shells with curved creases. Proc Natl Acad Sci 2015;112:11175–80.
[210] Rafsanjani A, Akbarzadeh A, Pasini D. Snapping mechanical metamaterials under tension. Adv Mater 2015;27:5931–5.
[211] Arora WJ, Nichol AJ, Smith HI, Barbastathis G. Membrane folding to achieve three-dimensional nanostructures: nanopatterned silicon nitride folded with stressed chromium hinges. Appl Phys Lett 2006;88:053108.
[212] Na JH, Evans AA, Bae J, Chiappelli MC, Santangelo CD, Lang RJ, et al. Programming reversibly self-folding origami with micropatterned photo-crosslinkable polymer trilayers. Adv Mater 2015;27:79–85.
[213] Dias MA, Dudte LH, Mahadevan L, Santangelo CD. Geometric mechanics of curved crease origami. Phys Rev Lett 2012;109:114301.
[214] Thiria B, Adda-Bedia M. Relaxation mechanisms in the unfolding of thin sheets. Phys Rev Lett 2011;107:025506.
[215] Lechenault F, Thiria B, Adda-Bedia M. Mechanical response of a creased sheet. Phys Rev Lett 2014;112:244301.
[216] Overvelde JTB, Shan S, Bertoldi K. Compaction through buckling in 2D periodic, soft and porous structures: effect of pore shape. Adv Mater 2012;24:2337–42.
[217] Singamaneni S, Bertoldi K, Chang S, Jang JH, Young SL, Thomas EL, et al. Bifurcated mechanical behavior of deformed periodic porous solids. Adv Funct Mater 2009;19:1426–36.
[218] Bendsoe MP, Sigmund O. Topology optimization: theory, methods and applications. New York: Springer; 2003.
[219] de Kruijf N, Zhou S, Li Q, Mai Y-W. Topological design of structures and composite materials with multiobjectives. Int J Solids Struct 2007;44:7092–109.
[220] Overvelde JTB, Bertoldi K. Relating pore shape to the non-linear response of periodic elastomeric structures. J Mech Phys Solids 2014;64:351–66.
[221] Florijn B, Coulais C, van Hecke M. Programmable mechanical metamaterials. Phys Rev Lett 2014;113:175503.
[222] Chung J, Waas AM. Compressive response of circular cell polycarbonate honeycombs under inplane biaxial static and dynamic loading, Part I: experiments. Int J Impact Eng 2002;27:729–54.
[223] Okumura D, Inagaki T, Ohno N. Effect of prestrains on swelling-induced buckling patterns in gel films with a square lattice of holes. Int J Solids Struct 2015;58:288–300.
[224] Jang J-H, Koh CY, Bertoldi K, Boyce MC, Thomas EL. Combining pattern instability and shape-memory hysteresis for phononic switching. Nano Lett 2009;9:2113–9.
[225] Karnessis N, Burriesci G. Uniaxial and buckling mechanical response of auxetic cellular tubes. Smart Mater Struct 2013;22:084008.
[226] Shan S, Kang SH, Zhao Z, Fang L, Bertoldi K. Design of planar isotropic negative Poisson's ratio structures. Extreme Mech Lett 2015;4:96–102.
[227] Krishnan D, Johnson H. Optical properties of two-dimensional polymer photonic crystals after deformation-induced pattern transformations. J Mech Phys Solids 2009;57:1500–13.
[228] Li J, Shim J, Deng J, Overvelde JT, Zhu X, Bertoldi K, et al. Switching periodic membranes via pattern transformation and shape memory effect. Soft Matter 2012;8:10322–8.
[229] Yang D, Jin L, Martinez RV, Bertoldi K, Whitesides GM, Suo Z. Phase-transforming and switchable metamaterials. Extreme Mech Lett 2016;6:1–9.
[230] Keplinger C, Li T, Baumgartner R, Suo Z, Bauer S. Harnessing snap-through instability in soft dielectrics to achieve giant voltage-triggered deformation. Soft Matter 2012;8:285–8.
[231] Jang J-H, Ullal CK, Gorishnyy T, Tsukruk VV, Thomas EL. Mechanically tunable three-dimensional elastomeric network/air structures via interference lithography. Nano Lett 2006;6:740–3.
[232] Singamaneni S, Tsukruk VV. Buckling instabilities in periodic composite polymeric materials. Soft Matter 2010;6:5681–92.
[233] Jaffe B. Piezoelectric ceramics. London: Academic Press; 1971.
[234] Grima JN, Mizzi L, Azzopardi KM, Gatt R. Auxetic perforated mechanical metamaterials with randomly oriented cuts. Adv Mater 2016;28:385–9.
[235] Carta G, Brun M, Baldi A. Design of a porous material with isotropic negative Poisson's ratio. Mech Mater 2016;97:67–75.
[236] Calladine CR. Buckminster Fuller's "tensegrity" structures and Clerk Maxwell's rules for the construction of stiff frames. Int J Solids Struct 1978;14:161–72.
[237] Valdevit L, Bauer J. Fabrication of 3D micro-architected/nano-architected materials. In: Baldacchini T, editor. Three-dimensional microfabrication using two-photon polymerization. Oxford: William Andrew Publishing; 2016. p. 345–73.
[238] Hall EO. The deformation and ageing of mild steel: III discussion of results. Proc Phys Soc 1951;64:747–53.
[239] Petch N. The cleavage strength of polycrystals. J Iron Steel Inst 1953;174:25–8.
[240] Schiotz J, Tolla FDD, Jacobsen KW. Softening of nanocrystalline metals at very small grain sizes. Nature 1998;391:561–3.
[241] Gazder AA, Sánchez-Araiza M, Jonas JJ, Pereloma EV. Evolution of recrystallization texture in a 0.78 wt.% Cr extra-low-carbon steel after warm and cold rolling. Acta Mater 2011;59:4847–65.
[242] Griffith A. The phenomena of rupture and flow in solids. Philos Trans R Soc Lond A 1921;221:163–98.
[243] Jang D, Meza LR, Greer F, Greer JR. Fabrication and deformation of three-dimensional hollow ceramic nanostructures. Nat Mater 2013;12:893–8.
[244] Rayneau-Kirkhope DJ, Dias MA. Designing recipes for auxetic behaviour of 2-d lattices; 2016. arXiv:1602:06105.
[245] Clausen A, Wang F, Jensen JS, Sigmund O, Lewis JA. Topology optimized architectures with programmable Poisson's ratio over large deformations. Adv Mater 2015;27:5523–7.
[246] Kaminakis NT, Stavroulakis GE. Topology optimization for compliant mechanisms, using evolutionary-hybrid algorithms and application to the design of auxetic materials. Composites Part B 2012;43:2655–68.
[247] Pickett GT. Self-folding origami membranes. Europhys Lett 2007;78:48003.
[248] Lebée A, Sab K. Transverse shear stiffness of a chevron folded core used in sandwich construction. Int J Solids Struct 2010;47:2620–9.
[249] Felton S, Tolley M, Demaine E, Rus D, Wood R. A method for building self-folding machines. Science 2014;345:644–6.
[250] Hawkes E, An B, Benbernou N, Tanaka H, Kim S, Demaine E, et al. Programmable matter by folding. Proc Natl Acad Sci 2010;107:12441–5.
[251] An B, Benbernou N, Demaine ED, Rus D. Planning to fold multiple objects from a single self-folding sheet. Robotica 2011;29:87–102.
[252] Kuribayashi K, Tsuchiya K, You Z, Tomus D, Umemoto M, Ito T, et al. Self-deployable origami stent grafts as a biomedical application of Ni-rich TiNi shape memory alloy foil. Mater Sci Eng A 2006;419:131–7.
[253] Elsayed E, Basily BB. A continuous folding process for sheet materials. Int J Mater Prod Technol 2004;21:217–38.
[254] Tang R, Huang H, Tu H, Liang H, Liang M, Song Z, et al. Origami-enabled deformable silicon solar cells. Appl Phys Lett 2014;104:083501.
[255] Song Z, Ma T, Tang R, Cheng Q, Wang X, Krishnaraju D, et al. Origami lithium-ion batteries. Nat Commun 2014;5:3140.
[256] Dias MA, Santangelo CD. The shape and mechanics of curved-fold origami structures. Europhys Lett 2012;100:54005.
[257] Py C, Reverdy P, Doppler L, Bico J, Roman B, Baroud CN. Capillary origami: spontaneous wrapping of a droplet with an elastic sheet. Phys Rev Lett 2007;98:156103.
[258] Bassik N, Stern GM, Gracias DH. Microassembly based on hands free origami with bidirectional curvature. Appl Phys Lett 2009;95:091901.
[259] Sadoc JFS, Mosseri R. Geometrical frustration. Cambridge (England): Cambridge University Press; 2006.
[260] Mao X, Souslov A, Mendoza CI, Lubensky TC. Mechanical instability at finite temperature. Nat Commun 2015;6:5968.
[261] Ellenbroek WG, Zeravcic Z, van Saarloos W, van Hecke M. Non-affine response: Jammed packings vs. spring networks. Europhys Lett 2009;87:34004.
[262] Katgert G, van Hecke M. Jamming and geometry of two-dimensional foams. Europhys Lett 2010;92:34002.
[263] Goodrich CP, Dagois-Bohy S, Tighe BP, van Hecke M, Liu AJ, Nagel SR. Jamming in finite systems: stability, anisotropy, fluctuations, and scaling. Phys Rev E 2014;90:022138.
[264] Ellenbroek WG, Hagh VF, Kumar A, Thorpe MF, van Hecke M. Rigidity loss in disordered systems: three scenarios. Phys Rev Lett 2015;114:135501.
[265] Coulais C, Overvelde JTB, Lubbers LA, Bertoldi K, van Hecke M. Discontinuous buckling of wide beams and metabeams. Phys Rev Lett 2015;115:044301.

[266] Haghpanah B, Papadopoulos J, Vaziri A. Plastic collapse of lattice structures under a general stress state. Mech Mater 2014;68:267–74.
[267] Jacobsen AJ, Carter WB, Nutt S. Compression behavior of micro-scale truss structures formed from self-propagating polymer waveguides. Acta Mater 2007;55:6724–33.
[268] Jacobsen AJ, Carter WB, Nutt S. Micro-scale truss structures formed from self-propagating photopolymer waveguides. Adv Mater 2007;19:3892–6.
[269] Jacobsen AJ, Carter WB, Nutt S. Micro-scale truss structures with three-fold and six-fold symmetry formed from self-propagating polymer waveguides. Acta Mater 2008;56:2540–8.
[270] Qian W, Yu Z, Wang X, Lai Y, Yellen BB. Elastic metamaterial beam with remotely tunable stiffness. J Appl Phys 2016;119:055102.
[271] Ding Y, Liu Z, Qiu C, Shi J. Metamaterial with simultaneously negative bulk modulus and mass density. Phys Rev Lett 2007;99:093904.
[272] Matthews J, Klatt T, Morris C, Seepersad CC, Haberman M, Shahan D. Hierarchical design of negative stiffness metamaterials using a bayesian network classifier. J Mech Des 2016;138:041404.
[273] Oh JH, Kwon YE, Lee HJ, Kim YY. Elastic metamaterials for independent realization of negativity in density and stiffness. Sci Rep 2016;6:23630.
[274] Oh JH, Seung HM, Kim YY. Adjoining of negative stiffness and negative density bands in an elastic metamaterial. Appl Phys Lett 2016;108:093501.
[275] Li P. Constitutive and failure behaviour in selective laser melted stainless steel for microlattice structures. Mater Sci Eng A 2015;622:114–20.
[276] Paulose J, Meeussen AS, Vitelli V. Selective buckling via states of self-stress in topological metamaterials. Proc Natl Acad Sci 2015;112:7639–44.
[277] Kadic M, Bückmann T, Schittny R, Wegener M. On anisotropic versions of three-dimensional pentamode metamaterials. New J Phys 2013;15:023029.
[278] Sigmund O. Tailoring materials with prescribed elastic properties. Mech Mater 1995;20:351–68.
[279] Milton GW, Briane M, Willis JR. On cloaking for elasticity and physical equations with a transformation invariant form. New J Phys 2006;8:248.
[280] Bückmann T, Kadic M, Schittny R, Wegener M. Mechanical metamaterials with anisotropic and negative effective mass-density tensor made from one constituent material. Phys Status Solidi B 2015;252:1671–4.
[281] Bückmann T, Schittny R, Thiel M, Kadic M, Milton GW, Wegener M. On three-dimensional dilational elastic metamaterials. New J of Phys 2014;16:033032.
[282] Schittny R, Bückmann T, Kadic M, Wegener M. Elastic measurements on macroscopic three-dimensional pentamode metamaterials. Appl Phys Lett 2013;103:231905.
[283] Martin A, Kadic M, Schittny R, Bückmann T, Wegener M. Phonon band structures of three-dimensional pentamode metamaterials. Phys Rev B 2012;86:155116.
[284] Huang Y, Lu X, Liang G, Xu Z. Pentamodal property and acoustic band gaps of pentamode metamaterials with different cross-section shapes. Phys Lett A 2016;380:1334–8.
[285] Méjica GF, Lantada AD. Comparative study of potential pentamodal metamaterials inspired by Bravais lattices. Smart Mater Struct 2013;22:115013.
[286] Kadic M, Bückmann T, Schittny R, Gumbsch P, Wegener M. Pentamode metamaterials with independently tailored bulk modulus and mass density. Phys Rev Appl 2014;2:054007.
[287] Layman CN, Naify CJ, Martin TP, Calvo DC, Orris GJ. Highly anisotropic elements for acoustic pentamode applications. Phys Rev Lett 2013;111:024302.
[288] Grima JN, Evans KE. Auxetic behavior from rotating triangles. J Mater Sci 2006;41:3193–6.
[289] Grima JN, Gatt R, Ellul B, Chetcuti E. Auxetic behaviour in non-crystalline materials having star or triangular shaped perforations. J Non-Cryst Solids 2010;356:1980–7.
[290] Grima JN, Chetcuti E, Manicaro E, Attard D, Camilleri M, Gatt R, et al. On the auxetic properties of generic rotating rigid triangles. Proc R Soc Lond A 2012;468:810–30.
[291] Chetcuti E, Ellul B, Manicaro E, Brincat JP, Attard D, Gatt R, et al. Modeling auxetic foams through semi-rigid rotating triangles. Phys Status Solidi B 2014;251:297–306.
[292] Wicks N, Hutchinson JW. Sandwich plates actuated by a Kagome planar truss. J Appl Mech-Trans ASME 2004;71:652–62.
[293] Wills A, Ballou R, Lacroix C. Model of localized highly frustrated ferromagnetism: the kagomé spin ice. Phys Rev B 2002;66:144407.
[294] Hutchinson RG, Wicks N, Evans AG, Fleck NA, Hutchinson JW. Kagorne plate structures for actuation. Int J Solids Struct 2003;40:6969–80.
[295] Wang J, Evans AG, Dharmasena K, Wadley HNG. On the performance of truss panels with Kagome cores. Int J Solids Struct 2003;40:6981–8.
[296] Lucato S, Wang J, Maxwell P, McMeeking RM, Evans AG. Design and demonstration of a high authority shape morphing structure. Int J Solids Struct 2004;41:3521–43.
[297] Mao X, Lubensky T. Coherent potential approximation of random nearly isostatic kagome lattice. Phys Rev E 2011;83:011111.
[298] Sun K, Souslov A, Mao X, Lubensky T. Surface phonons, elastic response, and conformal invariance in twisted kagome lattices. Proc Natl Acad Sci 2012;109:12369–74.
[299] Vitelli V. Topological soft matter: kagome lattices with a twist. Proc Natl Acad Sci 2012;109:12266–7.
[300] Kane C, Lubensky T. Topological boundary modes in isostatic lattices. Nat Phys 2014;10:39–45.
[301] Baughman RH, Stafström S, Cui C, Dantas SO. Materials with negative compressibilities in one or more dimensions. Science 1998;279:1522–4.
[302] Chen M, Karpov E. Bistability and thermal coupling in elastic metamaterials with negative compressibility. Phys Rev E. 2014;90:033201.
[303] Thompson J. Stability predictions through a succession of folds. Philos Trans R Soc-A 1979;292:1–23.
[304] Thompson J. 'Paradoxical'mechanics under fluid flow. Nature 1982;296:135–7.
[305] Lakes R, Drugan W. Dramatically stiffer elastic composite materials due to a negative stiffness phase? J Mech Phys Solids 2002;50:979–1009.
[306] Cai W, Gładysiak A, Anioła M, Smith VJ, Barbour LJ, Katrusiak A. Giant negative area compressibility tunable in a soft porous framework material. J Am Chem Soc 2015;137:9296–301.
[307] Munn R. Role of the elastic constants in negative thermal expansion of axial solids. J Phys C 1972;5:535.
[308] Ogborn JM, Collings IE, Moggach SA, Thompson AL, Goodwin AL. Supramolecular mechanics in a metal-organic framework. Chem Sci 2012;3:3011–7.
[309] Lakes R. Advances in negative Poisson's ratio materials. Adv Mater 1993;5:293–6.
[310] Babaee S, Shim J, Weaver JC, Chen ER, Patel N, Bertoldi K. 3D soft metamaterials with negative Poisson's ratio. Adv Mater 2013;25:5044–9.
[311] Lee T, Lakes R. Anisotropic polyurethane foam with Poisson'sratio greater than 1. J Mater Sci 1997;32:2397–401.
[312] Cai W, Katrusiak A. Giant negative linear compression positively coupled to massive thermal expansion in a metal–organic framework. Nat Commun 2014;5:4337.
[313] Hodgson SA, Adamson J, Hunt SJ, Cliffe MJ, Cairns AB, Thompson AL, et al. Negative area compressibility in silver (I) tricyanomethanide. Chem Commun 2014;50:5264–6.
[314] Li W, Probert MR, Kosa M, Bennett TD, Thirumurugan A, Burwood RP, et al. Negative linear compressibility of a metal–organic framework. J Am Chem Soc 2012;134:11940–3.
[315] Collings IE, Tucker MG, Keen DA, Goodwin AL. Geometric switching of linear to area negative thermal expansion in uniaxial metal–organic frameworks. CrystEngComm 2014;16:3498–506.
[316] Haines J, Chateau C, Leger J, Bogicevic C, Hull S, Klug D, et al. Collapsing cristobalitelike structures in silica analogues at high pressure. Phys Rev Lett 2003;91:015503.
[317] McCann D, Cartz L, Schmunk R, Harker Y. Compressibility of hexagonal selenium by X-ray and neutron diffraction. J Appl Phys 1972;43:1432–6.
[318] Cairns AB, Thompson AL, Tucker MG, Haines J, Goodwin AL. Rational design of materials with extreme negative compressibility: selective soft-mode frustration in KMn $[Ag(CN)_2]_3$. J Am Chem Soc 2011;134:4454–6.
[319] Ohwada K, Nakao H, Fujii Y, Isobe M, Ueda Y. Structural aspects of NaV_2O_5 under high pressure. J Phys Soc Jpn 1999;68:3286–91.
[320] Cliffe MJ, Goodwin AL. PASCal: a principal axis strain calculator for thermal expansion and compressibility determination. J Appl Crystallogr 2012;45:1321–9.
[321] Furukawa H, Cordova KE, O'Keeffe M, Yaghi OM. The chemistry and applications of metal-organic frameworks. Science 2013;341:974–86.
[322] Miller W, Smith C, Mackenzie D, Evans K. Negative thermal expansion: a review. J Mater Sci 2009;44:5441–51.

[323] Evans JSO. Negative thermal expansion materials. J Chem Soc Dalton 1999:3317–26.
[324] Bisquert J. Master equation approach to the non-equilibrium negative specific heat at the glass transition. Am J Phys 2005;73:735–41.
[325] Steeves CA, e Lucato SLS, He M, Antinucci E, Hutchinson JW, Evans AG. Concepts for structurally robust materials that combine low thermal expansion with high stiffness. J Mech Phys Solids 2007;55:1803–22.
[326] Lakes R. Cellular solids with tunable positive or negative thermal expansion of unbounded magnitude. Appl Phys Lett 2007;90:221905.
[327] Fortes AD, Suard E, Knight KS. Negative linear compressibility and massive anisotropic thermal expansion in methanol monohydrate. Science 2011;331:742–6.
[328] Azuma M, W-t Chen, Seki H, Czapski M, Oka K, Mizumaki M, et al. Colossal negative thermal expansion in $BiNiO_3$ induced by intermetallic charge transfer. Nat Commun 2011;2:347.
[329] Ha CS, Hestekin E, Li J, Plesha ME, Lakes RS. Controllable thermal expansion of large magnitude in chiral negative Poisson's ratio lattices. Phys Status Solidi B 2015;252:1431–4.
[330] Miller W, Mackenzie DS, Smith CW, Evans KE. A generalised scale-independent mechanism for tailoring of thermal expansivity: positive and negative. Mech Mater 2008;40:351–61.
[331] Grima JN, Ellul B, Attard D, Gatt R, Attard M. Composites with needle-like inclusions exhibiting negative thermal expansion: a preliminary investigation. Compos Sci Technol 2010;70:2248–52.
[332] Grima JN, Ellul B, Gatt R, Attard D. Negative thermal expansion from disc, cylindrical, and needle shaped inclusions. Phys Status Solidi B 2013;250:2051–6.
[333] Grima JN, Attard D, Caruana-Gauci R, Gatt R. Negative linear compressibility of hexagonal honeycombs and related systems. Scr Mater 2011;65:565–8.
[334] Wu Y, Kobayashi A, Halder GJ, Peterson VK, Chapman KW, Lock N, et al. Negative thermal expansion in the metal-organic framework material Cu_3(1, 3, 5-benzenetricarboxylate)$_2$. Angew Chem Int Ed 2008;120:9061–4.
[335] Prawoto Y. Seeing auxetic materials from the mechanics point of view: a structural review on the negative Poisson's ratio. Comput Mater Sci 2012;58:140–53.
[336] Evans KE. Auxetic polymers: a new range of materials. Endeavour 1991;15:170–4.
[337] Grima JN, Evans K. Auxetic behavior from rotating squares. J Mater Sci Lett 2000;19:1563–5.
[338] Grima JN, Jackson R, Alderson A, Evans KE. Do zeolites have negative Poisson's ratios? Adv Mater 2000;12:1912–8.
[339] Smith CW, Grima JN, Evans K. A novel mechanism for generating auxetic behaviour in reticulated foams: missing rib foam model. Acta Mater 2000;48:4349–56.
[340] Grima JN, Alderson A, Evans KE. Auxetic behaviour from rotating rigid units. Phys Status Solidi B 2005;242:561–75.
[341] Grima JN, Zammit V, Gatt R, Alderson A, Evans K. Auxetic behaviour from rotating semi-rigid units. Phys Status Solidi B 2007;244:866–82.
[342] Grima JN, Farrugia PS, Caruana C, Gatt R, Attard D. Auxetic behaviour from stretching connected squares. J Mater Sci 2008;43:5962–71.
[343] Grima JN, Oliveri L, Attard D, Ellul B, Gatt R, Cicala G, et al. Hexagonal honeycombs with zero Poisson's ratios and enhanced stiffness. Adv Eng Mater 2010;12:855–62.
[344] Grima JN, Caruana-Gauci R. Mechanical metamaterials: materials that push back. Nat Mater 2012;11:565–6.
[345] Grima JN, Caruana-Gauci R, Wojciechowski KW, Gatt R. Smart metamaterials with tunable auxetic and other properties. Smart Mater Struct 2013;22:084016.
[346] Mizzi L, Azzopardi KM, Attard D, Grima JN, Gatt R. Auxetic metamaterials exhibiting giant negative Poisson's ratios. Phys Status Solidi R 2015;9:425–30.
[347] Masters I, Evans K. Models for the elastic deformation of honeycombs. Compos Struct 1996;35:403–22.
[348] Rothenburg L, Berlin A, Bathurst RJ. Microstructure of isotropic materials with negative Poisson's ratio. Nature 1991;354:470–2.
[349] Pozniak A, Smardzewski J, Wojciechowski K. Computer simulations of auxetic foams in two dimensions. Smart Mater Struct 2013;22:084009.
[350] Yi Cho, Ahn T-H, Cho H-H, Shin J-H, Moon JH, Yang S, et al. Study of architectural responses of 3D periodic cellular materials. Modell Simul Mater Sci Eng 2013;21:065018.
[351] Grima JN, Williams JJ, Evans KE. Networked calix[4] arene polymers with unusual mechanical properties. Chem Commun 2005;32:4065–7.
[352] Silva SP, Sabino MA, Fernandes EM, Correlo VM, Boesel LF, Reis RL. Cork: properties, capabilities and applications. Int Mater Rev 2005;50:345–65.
[353] Carneiro V, Meireles J, Puga H. Auxetic materials—a review. Mater Sci-Poland 2013;31:561–71.
[354] Hou X, Silberschmidt VV. Metamaterials with negative Poisson's ratio: a review of mechanical properties and deformation mechanisms. In: Silberschmidt VV, Matveenko VP, editors. Mechanics of advanced materials. New York: Springer; 2015. p. 155–79.
[355] Critchley R, Corni I, Wharton JA, Walsh FC, Wood RJ, Stokes KR. A review of the manufacture, mechanical properties and potential applications of auxetic foams. Phys Status Solidi B 2013;250:1963–82.
[356] Goldstein R, Gorodtsov V, Lisovenko D, Volkov M. Negative Poisson's ratio for cubic crystals and nano/microtubes. Phys Mesomech 2014;17:97–115.
[357] Caddock B, Evans K. Microporous materials with negative Poisson's ratios. I. Microstructure and mechanical properties. J Phys D 1989;22:1877.
[358] Clarke J, Duckett R, Hine P, Hutchinson I, Ward I. Negative Poisson's ratios in angle-ply laminates: theory and experiment. Composites 1994;25:863–8.
[359] Neelakantan S, Tan J-C, Markaki AE. Out-of-plane auxeticity in sintered fibre network mats. Scr Mater 2015;106:30–3.
[360] Shim J, Perdigou C, Chen ER, Bertoldi K, Reis PM. Buckling-induced encapsulation of structured elastic shells under pressure. Proc Natl Acad Sci 2012;109:5978–83.
[361] Reis PM. A perspective on the revival of structural (In)stability with novel opportunities for function: from buckliphobia to buckliphilia. J Appl Mech 2015;82:111001.
[362] Gatt R, Mizzi L, Azzopardi JI, Azzopardi KM, Attard D, Casha A, et al. Hierarchical auxetic mechanical metamaterials. Sci Rep 2015;5:8395.
[363] Ting T, Barnett D. Negative Poisson's ratios in anisotropic linear elastic media. J Appl Mech 2005;72:929–31.
[364] Baughman RH, Shacklette JM, Zakhidov AA, Stafström S. Negative Poisson's ratios as a common feature of cubic metals. Nature 1998;392:362–5.
[365] Baughman RH, Dantas SO, Stafström S, Zakhidov AA, Mitchell TB, Dubin DH. Negative Poisson's ratios for extreme states of matter. Science 2000;288:2018–22.
[366] Soman P, Lee JW, Phadke A, Varghese S, Chen S. Spatial tuning of negative and positive Poisson's ratio in a multi-layer scaffold. Acta Biomater 2012;8:2587–94.
[367] Fozdar D, Soman P, Lee J, Han L, Chen S. Three-dimensional polymer constructs exhibiting a tunable negative Poisson's ratio. Adv Funct Mater 2011;21:2712–20.
[368] Taylor CM, Smith CW, Miller W, Evans KE. The effects of hierarchy on the in-plane elastic properties of honeycombs. Int J Solids Struct 2011;48:1330–9.
[369] Zhang W, Soman P, Meggs K, Qu X, Chen S. Tuning the Poisson's ratio of biomaterials for investigating cellular response. Adv Funct Mater 2013;23:3226–32.
[370] Ma Y, Zheng Y, Meng H, Song W, Yao X, Lv H. Heterogeneous PVA hydrogels with micro-cells of both positive and negative Poisson's ratios. J Mech Behav Biomed 2013;23:22–31.
[371] Gibson I, Rosen DW, Stucker B. Additive manufacturing technologies. New York: Springer; 2014.
[372] Bauer J, Hengsbach S, Tesari I, Schwaiger R, Kraft O. High-strength cellular ceramic composites with 3D microarchitecture. Proc Natl Acad Sci 2014;111:2453–8.
[373] Li S, Hassanin H, Attallah MM, Adkins NJE, Essa K. The development of TiNi-based negative Poisson's ratio structure using selective laser melting. Acta Mater 2016;105:75–83.

[374] Schwerdtfeger J, Heinl P, Singer RF, Körner C. Auxetic cellular structures through selective electron-beam melting. Phys Status Solidi B 2010;247:269–72.
[375] Ravirala N, Alderson A, Alderson KL. Interlocking hexagons model for auxetic behaviour. J Mater Sci 2007;42:7433–45.
[376] Wang XT, Li XW, Ma L. Interlocking assembled 3D auxetic cellular structures. Mater Des 2016;99:467–76.
[377] Brown TD, Dalton PD, Hutmacher DW. Melt electrospinning today: an opportune time for an emerging polymer process. Prog Polym Sci 2016. https://doi.org/10.1016/j.progpolymsci.2016.01.001.
[378] Visser J, Melchels FP, Jeon JE, van Bussel EM, Kimpton LS, Byrne HM, et al. Reinforcement of hydrogels using three-dimensionally printed microfibres. Nat Commun 2015;6:6933.
[379] Costa PF, Hutmacher DW, Theodoropoulos C, Gomes ME, Reis RL, Vaquette C. Additively manufactured device for dynamic culture of large arrays of 3D tissue engineered constructs. Adv Healthc Mater 2015;4:864–73.
[380] Brown TD, Edin F, Detta Ni, Skelton AD, Hutmacher DW, Dalton PD. Melt electrospinning of poly(ε-caprolactone) scaffolds: phenomenological observations associated with collection and direct writing. Mater Sci Eng C 2014;45:698–708.
[381] Muerza-Cascante ML, Haylock D, Hutmacher DW, Dalton PD. Melt electrospinning and its technologization in tissue engineering. Tissue Eng Part B Rev 2015;21:187–202.
[382] Bückmann T, Kadic M, Schittny R, Wegener M. Mechanical cloak design by direct lattice transformation. Proc Natl Acad Sci 2015;112:4930–4.
[383] Lantada AD, Elipe JCÁ. Porous and lattice structures for biodevices with advanced properties. In: Lantada AD, editor. Handbook on advanced design and manufacturing technologies for biomedical devices. New York: Springer; 2013. p. 121–36.
[384] Wang K, Chang Y-H, Chen Y, Zhang C, Wang B. Designable dual-material auxetic metamaterials using three-dimensional printing. Mater Des 2015;67:159–64.
[385] Schwerdtfeger J, Wein F, Leugering G, Singer RF, Körner C, Stingl M, et al. Design of auxetic structures via mathematical optimization. Adv Mater 2011;23:2650–4.
[386] Körner C, Liebold-Ribeiro Y. A systematic approach to identify cellular auxetic materials. Smart Mater Struct 2015;24:025013.
[387] Yaghi OM, Keeffe M, Ockwig NW, Chae HK, Eddaoudi M, Kim J. Reticular synthesis and the design of new materials. Nature 2003;423:705–14.
[388] Ortiz AU, Boutin A, Fuchs AH, Coudert F-X. Anisotropic elastic properties of flexible metal-organic frameworks: how soft are soft porous crystals? Phys Rev Lett 2012;109:195502.
[389] Rothemund PWK. Folding DNA to create nanoscale shapes and patterns. Nature 2006;440:297–302.
[390] Wang XL. The codes of matter and their applications. Sci Bull 2015;60:1661–73.
[391] dell'Isola F, Lekszycki T, Pawlikowski M, Grygoruk R, Greco L. Designing a light fabric metamaterial being highly macroscopically tough under directional extension: first experimental evidence. Z Angew Math Phys 2015;66:3473–98.